UNIVERSITY OF LJUBLJANA

Faculty of Mechanical Engineering

EXTENSION OF COLLISIONLESS DISCHARGE MODELS FOR APPLICATION TO FUSION-RELEVANT AND GENERAL PLASMAS

Dissertation

Submitted to the Faculty of Mechanical Engineering of the
University of Ljubljana
for the acquirement of a scientific degree of Doctor of Science

Leon Kos

Ljubljana, 2009

Dr/404 Leon Kos EXTENSION OF COLLISIONLESS DISCHARGE MODELS . . .

UNIVERSITY OF LJUBLJANA

Faculty of Mechanical Engineering

EXTENSION OF COLLISIONLESS DISCHARGE MODELS FOR APPLICATION TO FUSION-RELEVANT AND GENERAL PLASMAS

Dissertation

Submitted to the Faculty of Mechanical Engineering of the
University of Ljubljana
for the acquirement of a scientific degree of Doctor of Science

mag. Leon Kos

Mentor: Prof. dr. Jožef Duhovnik

Co-mentor: Prof. dr. Siegbert Kuhn
University of Innsbruck, Austria

Ljubljana, 2009

Univerza *v Ljubljani*
Fakulteta *za strojništvo*

Aškerčeva cesta 6
SI-1000 Ljubljana, Slovenija
telefon: (01) 47 71 200
faks: (01) 25 18 567
www.fs.uni-lj.si
dekanat@fs.uni-lj.si

Tekoča številka: DR/404

Datum: 26.5.2009

Na osnovi sklepa 21. seje Senata Univerze v Ljubljani z dne 14.5.2009 izdajam naslednjo

ODLOČBO

Senat Univerze v Ljubljani je na svoji seji dne 14.5.2009

kandidatu **mag.Leonu Kosu, univ.dipl.inž.**

1. sprejel temo doktorske disertacije z naslovom:

   Razširitev nekolozijskih razelektritvenih modelov za aplikacijo v fuzijsko relevantnih in splošnih plazmah

2. imenoval mentorja: prof.dr. Jožef Duhovnik
3. in somentorja: prof.dr. Siegbert Kuhn

4. odobril pisanje doktorske disertacije v angleškem jeziku

V skladu s členom 169 Statuta Univerze v Ljubljani z dne 21.12.2004 mora kandidat najpozneje v štirih letih od dneva, ko je bila sprejeta tema disertacije, predložiti izdelano doktorsko disertacijo.

Prof.dr. Jožef Duhovnik,
dekan

Pravni pouk:
Zoper to odločbo je dopusten ugovor na Senat Univerze v Ljubljajni v roku 15 dni od prejema odločbe.

Dostavljeno:
mag.L.Kos
dr.J.Duhovnik
dr.S.Kuhn (Avstrija)

Acknowledgments

This work would not have been possible without the support and encouragement of my colleague and friend, Dr. Nikola Jelić on whose suggestion I chose this topic and began writing the thesis. He has also been abundantly helpful, and has assisted me in numerous ways, including suggestion on code development and evaluating the numbers that resulted in many figures throughout the thesis. My supervisor Prof. Jožef Duhovnik lead my research interests through many projects that finally resulted in this thesis. His wisdom and interdisciplinary work within EU FP7 projects like EUFORIA [42, 28] introduced me to many open computational problems in fusion and plasma physics. My co-mentor Prof. Siegbert Kuhn advised me on theoretical aspects and checked nearly every sentence when writing a topic-related article. I am grateful to Prof. D. D. Tskhakaya, my advisor in the final stages of the work, for checking out the derivations of formulas and many valuable discussions on physical theoretical points. I am indebted to Prof. K.-U Riemann for his early advices on computational and theoretical aspects, as well as for using his software in order to obtain the results in the limit of zero ion temperature. This work was supported by the European Commission under (i) the Contract of Association between The European Atomic Energy Community (EURATOM) and the Ministry of Higher Education, Science and Technology of the Republic of Slovenia No. FU06-CT-2007-00065 (ii) the Contract of Association between EURATOM and the Austrian Academy of Sciences and, by (iii) the Austrian Science Fund (FWF) under project P19333-N16. It was carried out within the framework of the European Fusion Development Agreement. The views and opinions expressed herein do not necessarily reflect those of the European Commission. Numerical calculations associated with this work were supported by the Austrian Ministry of Science and research (BMWF) as part of the UniInfrastrukturprogramm of the Forschungsplattform Scientific Computing at the Leopold-Franzens Universität (LFU) Innsbruck.

I cannot end without thanking my wife and children, on whose constant encouragement, patience and love I relied as I sat at the computer. Their smiles and hugs when returning home will always inspire me, and I hope to continue, in my own small way, to show them my gratitude. It is to them that I dedicate this work.

koda: Dr 404

UDK 517.968.21(043.3)
UDK 52.726(043.3)
UDK 539.175.3(043.3)

Leon Kos

RAZŠIRITEV NEKOLIZIJSKIH RAZELEKTRITVENIH MODELOV ZA APLIKACIJO V FUZIJSKO RELEVANTNIH IN SPLOŠNIH PLAZMAH

Ključne besede: plazemski plašč, nekolizijski razelektritveni modeli, integro-diferencialne enačbe, fuzija, numerične metode

PACS: 52.25.Dg, 02.60.Nm, 52.40.Kh, 52.65.-y, 94.20.Fg, 95.75.Pq, 02.70.-c, 52.58.-c

Izvleček: Doktorsko delo predstavlja matematično-numerično razširitev nekolizijskih razelektritvenih modelov v široka temperaturna območja in za primere končne debeline plazemskega plašča, ki omogočajo izpopoljnene aplikacije v fuzijsko relevantnih in splošnih plazmah. Prispevke dela lahko strnemo na: (i) Obstoječi model je razširjen s tako imenovanim končnim $\varepsilon \equiv \lambda_D/L$, kar pomeni, da kvazi-nevtralnost ni striktno zagotovljena, temveč se uporablja kompletna Poissonova enačba namesto pogoja kvazinevtralnosti. (ii) Določanje jedra je bilo izvedeno z neposredno z uporabo splošnih programskih knjižnic. Profil potenciala je določen z zgoščeno mrežo na samo ob steni, temveč tudi v središču simetrije tako, da se bo uporabila adaptivna metoda. (iii) Osnovne hidrodinamske količine, kot so ionska gostota, ionski fluks, ionska energija in temperatura, so bili izpeljani neposredno iz porazdelitve hitrosti na mreži z integracijo, ki je samoadaptivna v bližini singularnosti jedra integrala, kot tudi v bližini singularnosti električnega polja oz. inverzne vrednosti. (iv) Izvedena sta dva izračuna, in sicer v širokem spektru ionskih temperatur z upoštevanjem končne vrednosti ε in v limitnem primeru $\varepsilon = 0$.

Code nr: Dr 404

UDC 517.968.21(043.2)
UDC 52.726(043.3)
UDC 539.175.3(043.3)

Leon Kos

EXTENSION OF COLLISIONLESS DISCHARGE MODELS FOR APPLICATION TO FUSION-RELEVANT AND GENERAL PLASMAS

Keywords:
plasma sheath, collisionless discharge, integro-differential equations, fusion, numerical methods

PACS: 52.25.Dg, 02.60.Nm, 52.40.Kh, 52.65.-y, 94.20.Fg, 95.75.Pq, 02.70.-c, 52.58.-c

Abstract: Thesis presents an analytic-numerical approach extension of collisionless dicharge models into wide ion-source temperature ranges and for finite $\epsilon = \lambda_D/L$. The results of this computational model will extend the validity of the solution to both fusion-relevant and general plasmas. The author's approach is as follows: (i) Existing models are extended to the so-called "finite-$\varepsilon \equiv \lambda_D/L$" case. This means that strict quasineutrality is not strictly satisfied unless ε is strictly zero. (ii) In this approach, the kernel is not approximated but calculated exactly. The grid for calculating potential profile is refined not only at the wall of the system but also in the center of symmetry. (iii) The basic hydrodynamic quantities like ion density, in outflux, directional energy and temperature are derived directly from the velocity distribution on a grid which is self-adaptive near the singularities of the integral kernel as well as near the singularities of the electric field. (iv) Two types of results are obtained, namely for a wide spectrum of ion temperatures with $\varepsilon = 0$ and for several temperatures with ε finite.

Contents

Acknowledgments v

Izvleček vii

Abstract ix

Notation xv

1 Introduction 1
- 1.1 Motivation and thesis aims . . . 4
- 1.2 Thesis overview . . . 6

2 Physical background of the problem 7
- 2.1 Plasma definition . . . 7
- 2.2 Plasma modelling . . . 10
- 2.3 Theoretical backgrounds . . . 12
- 2.4 The trajectory method . . . 15
- 2.5 Moments of the velocity distribution function . . . 18

3 Overview of existing models 21
- 3.1 Basic considerations on the two-scale model . . . 21
- 3.2 Tonks-Langmuir model . . . 22
- 3.3 Emmert et al.'s model . . . 24
- 3.4 Bissell-Johnson model . . . 25
- 3.5 Scheuer-Emmert model . . . 29

4 Analytic-Numerical method 31
- 4.1 Implementation aspects . . . 37

5 Extension of the theoretical model **41**
5.1 Basic considerations . . . 41
5.2 Theoretical backgrounds . . . 45
5.3 Maxwellian distribution of neutrals . . . 50
5.4 Numerical method . . . 52

6 Results **53**
6.1 The two-scale limit $\varepsilon = 0$ . . . 53
6.2 Unified plasma and sheath solution $\varepsilon > 0$ . . . 67
    6.2.1 Particle In Cell method . . . 75

7 Discussion and Conclusion **79**
7.1 Contributions to science . . . 81

Bibliography **82**

A Ion source of the „Water bag" type **91**

B Code description **93**
B.1 XML definition . . . 93
B.2 Parameters . . . 95
    B.2.1 Global Parameters . . . 95
    B.2.2 Numerical Parameters . . . 97
    B.2.3 Grid Parameters . . . 99
    B.2.4 Code Parameters . . . 99
    B.2.5 Diagnostic Parameters . . . 101

C Slovenski povzetek **103**
C.1 Uvod . . . 103
    C.1.1 Motivacija in namen disertacije . . . 106
    C.1.2 Pregled disertacije . . . 108
C.2 Izvleček vsebine . . . 108
    C.2.1 Fizikalno ozadje problema . . . 108
    C.2.2 Pregled stanja in obstoječih modelov . . . 110
    C.2.3 Analitično numerična metoda . . . 111
    C.2.4 Razširitev teoretičnega modela . . . 111
    C.2.5 Rezultati . . . 112

C.3 Sklepi 113
C.3.1 Prispevki k znanosti 115

Vita **117**

Notation

Symbols and abbreviations

DC	Direct current
E	Strength of the electric field
ε_0	Vacuum dielectric constant
$\varepsilon = \lambda_D/L$	
$f_i,\ f$	Ion distribution function
$\Gamma_{i,e}$	Ion, electron flux
γ_i	Ion polytropic coefficient
$H(x)$	Heaviside step function
$\mathrm{K}_0(x)$	Modified Bessel function
k	Boltzmann constant
L	Half length of the system
λ_D	Debye length
$m_{i,e}$	Ion, electron mass
$n_{i,e}$	Ion, electron number density
Φ, ψ	Electrostatic potential
R	Ionization rate
SOL	Scrape off layer
SE	Sheath edge
$\tau = T_e/T_i$	Electron/Ion temperature ratio
$T_{i,e}$	Ion, electron temperature
T_n	Temperature of the neutral gas
VDF	Velocity distribution function
x	Coordinate of the observation

Chapter 1

Introduction

For simplicity's sake, the plasma-wall transition layer is usually split into two sublayers - the sheath with the width of the order of the Debye length λ_D and the presheath with the characteristic length of the order of relevant collision or ionization length L. Usually

$$\lambda_D \ll L \; , \tag{1.1}$$

that allows to consider these two sublayers separately. This approximation is known as the two-scale approximation. Under condition (1.1) the presheath can be considered to be quasi-neutral, while the Debye sheath is characterized by the charge separation.

Defining the edge of quasi-neutral plasma, i.e., the sheath boundary (or sheath edge) is an old but still not definitely solved problem which is of high relevance for fusion, laboratory and space plasmas. The sheath boundary is a surface up to which plasma can be considered as quasi-neutral, and the presheath can be modeled by using fluid approximation (instead of employing a demanding kinetic model), with relevant boundary conditions of the sheath entrance. However, this surface is still impossible to find with high accuracy. The sheath boundary can be rather precisely defined only in the asymptotic two-scale limit. In such approximation the sheath boundary can be identified either from the plasma side (infinitely thin sheath) as the point of electric field singularity (the famous Tonks-Langmuir model [70] from 1929), or from the sheath side (infinitely large sheath) as the point of the vanishing electric field (the famous Bohm model [12] from 1949). Both models were originally developed for the case of cold ion sources (ions created in plasma with *negligible velocities* in comparison with electron velocities) and were later generalized in a commonly adopted expression saying that the sheath edge is a place at which the ion average velocity in the x-direction, normal to the wall is larger or equal to the local ion sound velocity.

$$u_i \geq \sqrt{k(T_e^* + \gamma T_i)/m_i} \ , \tag{1.2}$$

where k is Boltzmann's constant, m_i is the ion mass, T_e^* is the so-called electron "screening" temperature ($T_e^* = en_e/(kdn_e/d\Phi)$), T_i is the ion effective temperature, Φ is the local plasma potential, and γ is the ion "polytropic" coefficient (defined by $dp_i/dx = \gamma kT_i dn_i/dx$), with all quantities taken at the plasma-sheath boundary. In fact the expression (1.2) is obtained in the hydrodynamic approximation for the ion gas.

While over the last half-century γ was assumed to be constant in all fluid plasma models, it has been recognized only recently that γ is a spatially varying quantity (depending on position x in the one-dimensional case) rather than a global constant. Kuhn et al. (2006) [40] showed by predominantly analytical means that in the asymptotic two-scale limit γ_i (subscript i means ions) exhibits a sharp peak exactly at the plasma-sheath boundary. Jelić at al. (2007) [32], performed both analytic calculations and numerical particle-in-cell (PIC) simulations in the finite $\varepsilon(= \lambda_D/L)$ plasmas confirming the results of Kuhn et al. for the "cold" ion velocity distribution ($T_i \ll T_e$). However, the analytic results obtained for cold ion-sources are only of limited importance to fusion plasmas.

In order to extend the validity of the Tonks-Langmuir model to the case of the finite ion temperature source Bissell and Johnson [10] in 1987 developed an appropriate model. However, their solution to the model was not enough reliable i.e., fails for small ion-source temperatures as a consequence of their choice of the kernel approximation in the integral equation. Secondly, Bissell and Johnson imposed the boundary condition at the presheath boundary *in advance*, based on the so-called "marginal generalized Bohm criterion". This assumption has been recently explicitly disproved to be valid in general (see Riemann [53] and references therein).

On the other hand, in 1988 Scheuer and Emmert [61] used a better kernel approximation enabling them to extend the validity of the Bissell-Johnson model also for negligible ion-source temperatures, thus fitting excellently the original Tonks-Langmuir model. Secondly, they did not impose the presheath boundary in advance but instead they calculated it a posteriori.

However due to *kernel approximations*, both above solutions remain limited either for small or for large temperatures. In the present work we present the method how to obtain the results for arbitrary T_n/T_e in an arbitrary wide range. This is done by employing the exact kernel of the integral equation and solving it numerically. In addition, we present the results of our PIC simulations as a highly reliable reference investigation.

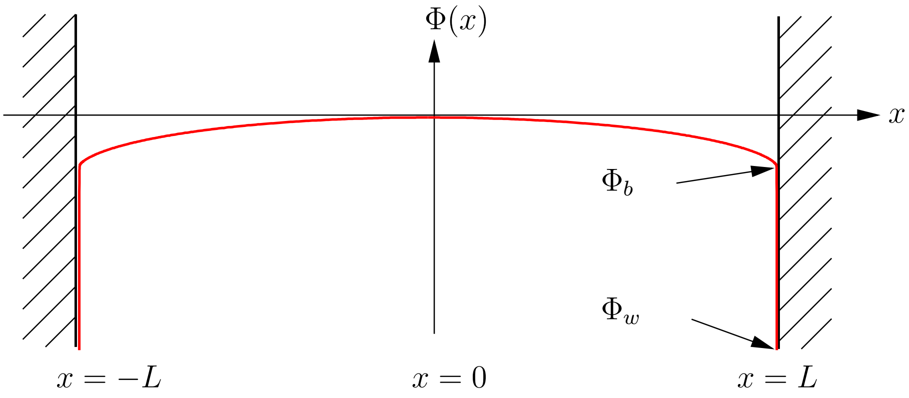

Figure 1.1: Schematic diagram for the collisionless discharge analysis in one-dimensional (plane) geometry with potential $\Phi(x)$ after formation of sheaths. The plasma center at $x=0$, walls at $x=\pm L$.

The geometry of the problem is a symmetric one-dimensional plane-parallel as illustrated in Fig. 1.1.

For the case of the *"cold ion-source velocity distribution"* the final ion velocity distribution was calculated analytically. The term "cold" as mentioned above, refers to the case when ions in the plasma are born with a negligible temperature in comparison with that of electrons. In the model, once the equation for plasma in the presheath is solved the sheath equation (there is a strong electric field localized in the sheath) is solved by using the boundary condition emerged from the solution of the plasma equation.

Towards the end of the last century attempts were made on solving two-scale problem for the case of the *"warm ion-source velocity distribution"*, i.e., for the case when the ion-source temperature is comparable with the prescribed electron temperature. In such a scenario the model's Fredholm equation cannot be solved unless a special ion source distribution shape is prescribed in advance so as to yield an analytic result. Therefore a numerical computation method was applied. The original derivation by Bissell and Johnson [10] of the physical problem yields an equation of the type

$$\exp\left((1+\frac{\tau}{2})\Phi\right) = B\int_0^{\Phi_b} \Psi(\Phi')\exp\left((1+\frac{\tau}{2})\Phi'\right) \mathrm{K}_0\left(\frac{\tau}{2}|\Phi-\Phi'|\right) d\Phi' \ , \tag{1.3}$$

where the unknown function to be found is $\Psi(\Phi)$, Φ_b is the potential at the presheath edge, $\mathrm{K}_0(z)$ it the modified Bessel function. This is a Fredholm-type integral equation of the first kind. However, even in the two-scale approximation the final ion velocity distribution was not calculated for an arbitrary ion source temperature, because the singular kernel of the integral equation appeared to be inconvenient for numerical computations. In this thesis we intend to solve this equation exactly and, moreover, to solve the extended problem that we formulated, i.e., a more "stiff" integro-differential equation of the form

$$\begin{aligned}\exp\left((1+\frac{\tau}{2})\Phi\right)\left[1+\varepsilon^2\frac{\exp(-\Phi)}{\Psi^3(\Phi)}\frac{d^2\Psi(\Phi)}{d^2\Phi}\right]\\ = B\int_0^{\Phi_b} \Psi(\Phi')\exp\left((1+\frac{\tau}{2})\Phi'\right) \mathrm{K}_0\left(\frac{\tau}{2}|\Phi'-\Phi|\right) d\Phi' \ ,\end{aligned} \tag{1.4}$$

which is based on the full Poisson equation instead of the quasi-neutrality condition. This is an integro-differential equation which might be considered as a generalization of the Fredholm type equations, but it is neither of first or second kind but, obviously a non-linear one not classified in literature at all. In the above formulas B is an eigenvalue of the problem while ε and τ are free parameters.

1.1 Motivation and thesis aims

The author was engaged for a long period of time on exploitation of parallel computing related to fusion research with a task to optimize European resources. His participation in the EUFORIA project [42, 28] required his deep involvement in benchmarking some demanding plasma problems. Since the Bissell and Johnson [10] integral equation was a great challenge for this purpose, he started making his program packages for tackling this problem and we expect the present thesis to contribute considerably to fusion community in upgrading existing available results.

The problem described above is of high importance to fusion and general plasmas. In order to employ the fluid codes like SOLPS [15] and EDGE-2D e.g., designed for simulations of the Scrape-Off Layer (SOL) [18] region in TOKAMAK devices [64] one has to determine the computational region boundaries. The boundary condition, however, could not be precisely found on the basis of fluid theory but kinetic theory should be employed as well. The results from kinetic theory, which assumes a warm ion population, require demanding computational resources.

Our examination of the problems with the existing models showed that approximations taken are not sufficiently accurate as they present somewhat different results.

We focus our research aims to achieve the following goals:

- The kernel should not be approximated but calculated exactly by using generic program packages.

- The grid for calculating a potential profile should be refined not only at the wall of the system, but also in the center of symmetry and a self-adaptivity of the grid integration should be considered.

- The basic hydrodynamic quantities like ion density, ion out-flux, ion total energy and temperature should be derived directly from velocity distribution on a grid which is self-adaptive near the singularities of the integral kernel as well as near the singularities of the electric field.

- The existing numerical models should be extended to the so-called "finite-$\varepsilon \equiv \lambda_D/L$" case. This means that quasi-neutrality is not strictly satisfied unless ε is strictly zero.

- Two types of result should be obtained, namely one for a wide spectrum of ion temperatures with $\varepsilon = 0$ and one for several temperatures with finite ε.

Thesis statement.

The problem of a special Fredholm-type integro-differential equation should be solved numerically without approximations to achieve an extended solution range applicable to fusion-relevant and general plasmas for an arbitrary ion temperature and arbitrary finite ε.

1.2 Thesis overview

In this thesis the author presents investigations and results with the following assumptions:

- The Poisson equation is employed in the whole discharge region.
- A two-scale approximation is obtained just within the limit of the infinitely small Debye length in comparison with the system length.
- The ion source-temperature can take an arbitrary value.
- The electron-neutral impact is considered as a ionization mechanism.

Chapter 2 describes physical and theoretical backgrounds of the plasma and its modeling. Relevant existing collisionless models and their limitations are discussed in Chapter 3. We extend the hot ion source temperature range of existing models by our analytic-numerical method described in Chapter 4. The generalization of the existing theoretical models to the finite Debye length and the extension of our analytic-numerical method are elaborated in Chapter 5. Results obtained by our analytic-numerical method and our PIC simulations as references are presented in Chapter 6. We conclude with a discussion in Chapter 7. Supplementary information that aids the reader or the user our code as well as a Slovenian translation are given in the appendices.

Chapter 2

Physical background of the problem

2.1 Plasma definition

In the terminology of Ancient Greek philosophy there is the fourth state of the occurrence of the world, i.e. - fire (besides solid, liquid, and gas occurrences). The term *plasma*, coined almost a century ago by Irvin Langmuir, corresponds to this philosophy. A plasma is a quasi-neutral gas of charged and neutral particles which exhibits collective behavior [17]. Ordinary fire is indeed a plasma but with a very low degree of ionization. Today we are interested in plasmas in which the degree of ionization is much higher than in the past (in the range from several to a hundred percent of the degree of ionization).

In nature plasma occupies the most (more than 99 %) of stellar and interstellar space of universe [26]. In laboratory plasmas can be produced at a wide range of pressures and temperatures. This is achieved by transferring some external energy to the gas leading to its ionization and resulting in plasmas known as e.g., DC (Townsend) [21] or microwave discharges, diode plasmas [41], neutral or non-neutral beam produced plasmas etc.

Experience with laboratory plasmas is substantially applied to scientific, technological and industrial application such as plasma-based lighting devices, electron beam-driven electrostatic fuel and paint injectors, plasma surface- cleaning and etching, material surface hardening, synthetic diamond production and plasma thin film deposition for e.g., thin-panel television systems, high-temperature super-conducting film deposition, plasma cutting, plasma welding, synthesis of materials, toxic waste treatment, water treatment systems, meat pasteurization, medical instrument sterilization, production of fullerenes, plasma polymerization, heavy ion extraction from mixed-mass gas flows, high voltage switches, ceramic powders production, plasma jet reactive engines, etc...

Qualitatively plasma is the ionized gas consisting of equal number of ions and electrons the motion of which is determined by collective effects.

The degree of ionization in a gas can be estimated on the basis of *Saha equation*

$$\frac{n_i^2}{n_0} = \left(\frac{2\pi m_e kT}{h^2}\right)^{\frac{3}{2}} \exp\left(-\frac{W}{kT}\right) .$$

where $k = 1.38\times10^{-23}$ J/K is the Boltzmann constant, $h = 6.62\times10^{-34}$ Js is the Planck constant, $m_e = 9.109\times10^{-31}$ is the electron mass, n_i is the number density of ionized atoms or molecules, n_0 is the number density of neutral particles, T is the absolute temperature of the gas, W is the ionization energy (e.g., the ionization energy is 24.59 eV for He, 15.76 eV for Ar, 14.53 eV for N, 13.62 eV for O and 13.60 eV for H and only 3.89 for Cs). At the room temperature this gives an estimation of $n_i/n_0 \sim 10^{-123}$. Obviously, plasma should be characterized by much higher temperatures, e.g., of the order of $1eV$ ($1eV$ corresponds to $T = 11600K$) and higher. Extreme examples are Cs, where substantial ionization can be obtained even at 0.1 eV ($\sim 1000K$) and fusion plasmas with temperatures of the order of 10 KeV, (hundreds of millions of K).

Quantitatively plasma is the ionized gas with properties as follows.

1. The macroscopic neutrality

   $$n_e = n_i \ , \tag{2.1}$$

   is satisfied. In laboratory plasmas, some reference density for a nice experiment of basic plasma phenomena could be kept e.g., at the order of $10^{16} \div 10^{18} m^{-3}$, while in fusion devices is almost for three orders of magnitude higher.

2. Any strong electric field is localized to distance λ_D, which is short compared with the characteristic system dimension L, i.e,

   $$\lambda_D \ll L \ , \tag{2.2}$$

   where

   $$\lambda_D = \sqrt{\frac{\epsilon_0 k T_e}{n_0 e^2}} \ , \tag{2.3}$$

   is the Debye radius. It follows that $\lambda_D = 7.43 \times 10^{-3}\sqrt{T_e/n}$ where T_e is in eV and n is in m^{-3}, so it can be quickly estimated that λ_D in both laboratory and fusion plasmas is of the order of tenths of a millimeter.

3. The density of the particles in the Debye sphere is high

   $$n \gg 1/\lambda_D^3 \ . \tag{2.4}$$

4. The characteristic frequency of collective processes i.e., electron oscillations ω_{ep}, is higher than the characteristic frequency of binary processes ω_{en} with neutrals and ions

   $$\omega_{ep} > \omega_{en}, \quad \omega_{ep} > \omega_{ei} \ , \tag{2.5}$$

   $$\omega_{ep} = \sqrt{\frac{n_e e^2}{m_e \epsilon_0}} \ , \tag{2.6}$$

   is the electron plasma frequency. With numerical values of the constant calculated, this is equivalent to $\omega_{ep} = 1.32\sqrt{n}$, and in laboratory plasmas this is with reference densities obviously of the order of a tenth GHz, while in fusion plasmas it is of the order of ten GHz.

   $$\nu_{en} = n_n \langle \sigma_{en}(v_r) v_r \rangle \tag{2.7}$$

   is the electron-neutral collision frequency. ν_{en} is given as an average value of the product of collision cross-section $\sigma_{en}(v_r)$ and relative velocity v_r. The electron–ion collision frequency is

   $$\nu_{ei} = \frac{Z^2 n e^4 \Lambda}{\epsilon_0 \sqrt{m_e}(kT_e)^{3/2}} \ , \tag{2.8}$$

   with Z the number of the ion charges and $\Lambda = \ln 4\pi n \lambda_D^3$ the Coloumb logarithm.

   $$\Lambda = \ln \frac{\lambda_D}{e^2/kT_e} \tag{2.9}$$

Practically plasma is always in contact with the surface – wall. In front of the wall a special properties of plasmas are established. This region is called “plasma–wall transition” (PWT) layer.

The problem of the PWT layer is one of the oldest in plasma physics [70, 12]. It plays an important role in various fields of plasma physics and technology such as fusion devices [64, 17], plasma diagnostics [31] and plasma processing [41]. However, the physical basis of the PWT is still the subject of numerous recent investigations. This is due to extreme dificulties of the problem connected with the nonlinearities and boundary conditions.

2.2 Plasma modelling

Plasma can be described by several theoretical approaches, each of which gives insight into physical pictures characterizing various particular plasma phenomena. These models are *Single particle* motion approximation, *fluid* approximation (single fluid and multi-fluid approaches) and *kinetic* description.

The single particle motion model is limited to particularly rare ionized gases when we can follow the single particle due to negligibly small interaction energy, whereas fluid approximation is applicable only in the case of a local thermodynamic equilibrium. At the plasma boundaries, fluid approximation breaks since the velocity distribution function is far from the equilibrium. The only way to describe plasma near boundaries is to use a kinetic approximation.

Kinetic approximation can be employed via computer simulations which calculate iteratively the positions of all particles and self-consistent electric and magnetic fields originated from particle positions and velocities. This is an expensive approach which suffers many technical limitations, primarily originated from a huge number of Newton equations to be solved together with Maxwell equations. Therefore the numerical calculation method based on solving the problem without going into details of motion of each particle may be considered of high interest.

A great benefit to plasma community is to resolve the plasma and sheath boundary as a transition from plasma quasi-neutrality (plasma region) to the strong electric field region (sheath region). This can be done via results of the kinetic codes where description of the sheath can be used as reliable boundary conditions for the fluid codes.

This is especially important for fusion plasmas where ion temperatures are comparable with electron temperatures. However, up to date there has been no satisfactory solution to this problem in a wide range of ion temperatures and no solution for non-negligible sheath thickness. The main task of this thesis is to resolve this problem for arbitrary value of these parameters.

2.3 Theoretical backgrounds

Kinetic Boltzmann equation states

$$v\frac{\partial f_i}{\partial x} - \frac{e}{m_i}\frac{d\Phi}{dx}\frac{\partial f_i}{\partial v} = S_i(x,v) \ , \tag{2.10}$$

where the ion source term $S_i(x,v)$ on the right-hand side is an intricate function reflecting the relevant microscopic physics involved in the model of interest, with x the Cartesian space coordinate, v the particle velocity, e the positive elementary charge, m_i the ion mass, and $\Phi(x)$ the electrostatic potential at position x. Considering the electron-neutral impact ionization, we further present the ion source term as follows

$$S_i(x,v) = Rn_n n_e(x) f_n(v) \ , \tag{2.11}$$

where R is the ionization rate and $f_N(v)$ denotes the velocity dependence of the neutral VDF.

A formal solution of the Boltzmann equation can be found along the characteristics in the form

$$-\frac{e}{m_i}\frac{\partial\Phi}{\partial x}\frac{1}{v} = \frac{dv}{dx} \ , \tag{2.12}$$

where the characteristics are

$$\begin{aligned} x' &= x \ , \\ {v'}^2 &= v^2 - \frac{2e}{m_i}(\Phi' - \Phi) \ . \end{aligned} \tag{2.13}$$

Consequently, the Boltzmann equation is transformed into

$$\frac{df_i}{dx'} = \frac{1}{v'(x')} S_i\left(x', v'\right)) \ , \tag{2.14}$$

with a formal solution in the form

$$f_i(x, v(x)) = \int\limits_0^x \frac{S_i(x', v^2 - \frac{2e}{m_i}(\Phi'(x') - \Phi))}{\sqrt{v^2 - \frac{2e}{m_i}(\Phi'(x') - \Phi)}} dx' \ . \tag{2.15}$$

This can be written in the form independent of the local coordinate x

$$\begin{aligned} f_i(\Phi(x), v) &= \int^{x} \frac{dx'}{d\Phi'} \frac{S_i(\Phi', v^2 - \frac{2e}{m_i}(\Phi' - \Phi))}{\sqrt{v^2 - \frac{2e}{m_i}(\Phi' - \Phi)}} d\Phi' \\ &\equiv \int_{\Phi} \frac{1}{E'(\Phi')} \frac{S_i(\Phi', v^2 - \frac{2e}{m_i}(\Phi' - \Phi))}{\sqrt{v^2 - \frac{2e}{m_i}(\Phi' - \Phi)}} d\Phi' \\ &\equiv \int_{\Phi} \text{Integrand}(\Phi, \Phi', v) \cdot d\Phi' \ , \end{aligned} \tag{2.16}$$

where

$$E = -\frac{d\Phi}{dx} \geq 0 \tag{2.17}$$

is electric field. Once we know $\Phi(x)$ we can calculate $E(x)$ and consequently $E(\Phi)$ providing the potential profile Φ is a monotonic function of coordinate x. Secondly, it is necessary to know the source function $S(v, x)$ at each point. There are three areas of interest.

In real experiment we can *measure* the potential profile and *assume* the source function based on a supposed physical scenario. In (PIC) simulation experiment we *obtain* the potential profile after simulating particle motion based on a Newtonian motion of particles in an electric and magnetic fields (superposition of both external and self-generated fields due to the particle position and velocities), providing we *assume* the source distribution according to our taste. Finally, in numerical calculation approach, we also *assume* the source distribution according to our taste (see Tonks Langmuir, Emmert at al. and Bissell and Johnson models in Chapter 3) and then *solve analytically or numerically* an integro-differential equation for an unknown potential or an electric field based on additional assumptions.

Nevertheless, regardless of the procedure how we obtain the data about the potential profile calculation of the velocity distribution that we present here is a rather universal one. The essential point is to find the region of integration of Integrand(Φ, Φ', v)

In Fig. 2.1 we show the potential profile and the corresponding characteristic trajectories of various population of particles obtained by a simulation "experiment" via BIT1 PIC code [74, 38] . This particular example corresponds to ions.

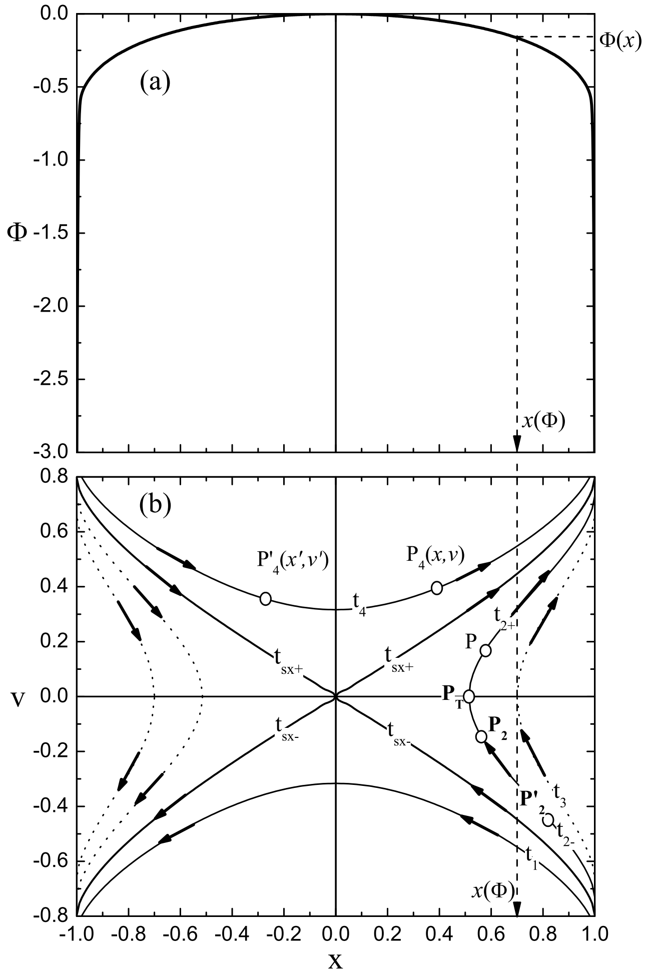

Figure 2.1: A randomly chosen potential profile calculated in our PIC simulations (a) with corresponding particle trajectory diagram (b).

The method is to "count" the particles with each particular velocity at any particular place $x(\Phi)$ with corresponding potential $\Phi(x)$. This is possible providing the places and velocities of particles originated from the whole space are known. Then, at any observation place, we know the number of particles with particular velocity distribution at that place. This is in fact the *final* or *actual* velocity distribution function (VDF) at the observation place.

First of all, we distinguish between the left and right hand sides of the system. Depending on the place of their birth and their directional velocity, ions created on one side of the system can overcome the potential barrier in the center of the system and be absorbed on the opposite side, otherwise they will be reflected and accelerated back within their originating half-side of the system. We plot a separatrix $t_{sx\pm}$ which is a boundary separating enough energetic particles from slow ones with a so-called "X-point" at $x = 0$, $v = 0$.

2.4 The trajectory method

The velocity distribution at any observation point of the discharge for a general ion source up to the wall can be obtained by performing an analysis of the phase space trajectories crossing the observation point from either its right or its left side, based on the energy conservation $v^2 + \Phi = v'^2 + \Phi' = Const.$

Let us now look at Fig. 2.1(a), where the place of the observation is an arbitrary point, the ion birth places are denoted with prime ($'$), so an integration of all the birth places should be carried out.

$$f_i(x, v) = \int_{\Phi_{start}}^{\Phi(x)} \frac{d\Phi'}{-E(\Phi')} \frac{S(x', v')}{v'} \tag{2.18}$$

1. First, we look at the trajectories of particles which pass point $x(\Phi)$ from its right to its left side, i.e., the trajectories of the type between t_1 and t_2 (including separatrix t_{sx-} and excluding all the particles of type t_3 and other trajectories with insufficient energy to pass from the right to the left side of the observation point). The contribution of these particles to the ion velocity distribution is thus

   $$f_i(x, v) = H(-v) \int_{\Phi_w}^{\Phi(x)} \frac{d\Phi'}{-E(\Phi')} \frac{S(x', v')}{v'} , \tag{2.19}$$

   where $H(x)$ is the Heaviside step function

   $$H(z) = \begin{cases} 1 \ , & x \geq 0 \\ 0 \ , & x < 0 \end{cases} . \tag{2.20}$$

2. Secondly, we look at the particles passing point $x(\Phi)$ from its left to its right, whose place of birth is at the right side of the plane of symmetry

between separatrices t_{sx-} and t_{sx+}:

$$\begin{aligned} f_i(x,v) = &\left[H(v)H(\sqrt{-\Phi}-v)\right] \\ &\times \left[\int_{\Phi_w}^{\Phi(x)+v^2} \frac{d\Phi'}{-E(\Phi')}\frac{S(x',v')}{v'} \right. \\ &\left. - \int_{\Phi(x)+v^2}^{\Phi(x)} \frac{d\Phi'}{-E(\Phi')}\frac{S(x',v')}{v'}\right] . \end{aligned} \tag{2.21}$$

Here the first integral belongs to those ions which are born at either side of point $x(\Phi)$ and have a turning point P_T, i.e., are born with negative velocities (the bottom part of the trajectory of type t_2), while the second integral belongs to the ions born with positive velocities (the upper part of the trajectory of type t_2).

3. Finally, we look at the particles passing point $x(\Phi)$ from its left to its right side, whose place of birth is above separatrix t_{sx+} (type t_4)

$$\begin{aligned} f_i(x,v) = &\left[H(v-\sqrt{-\Phi})\right] \\ &\times \left[\int_{\Phi_w}^{0} \frac{d\Phi'}{-E(\Phi')}\frac{S(x',v')}{v'} \right. \\ &\left. - \int_{0}^{\Phi(x)} \frac{d\Phi'}{-E(\Phi')}\frac{S(x',v')}{v'}\right] , \end{aligned} \tag{2.22}$$

   where the first integral belongs to those ions which are born at the left hand side of the plane of symmetry (with enough energy to overcome the potential maximum) and the second integral considers those particles which are born with positive velocities in the region between the plane of symmetry and observation point $x(\Phi)$ (no turning point).

Thus we obtain the velocity distribution as a composition of three parts, i.e., for negative velocities, for velocities between 0 and $\sqrt{-\Phi}$ and for those greater than $\sqrt{-\Phi}$. The illustration of the method is shown in Fig. 2.2.

With an explicit source distribution, which, in this work, is assumed to be Maxwellian, the non-dimensional form of ion VDF is

$$f(\Phi(x),v) = n_0 B \int_0^1 ds' \exp(\Phi') \frac{\exp\left[-(v^2-(\Phi'-\Phi))/T_i\right]}{\sqrt{v^2-(\Phi'-\Phi)}} , \tag{2.23}$$

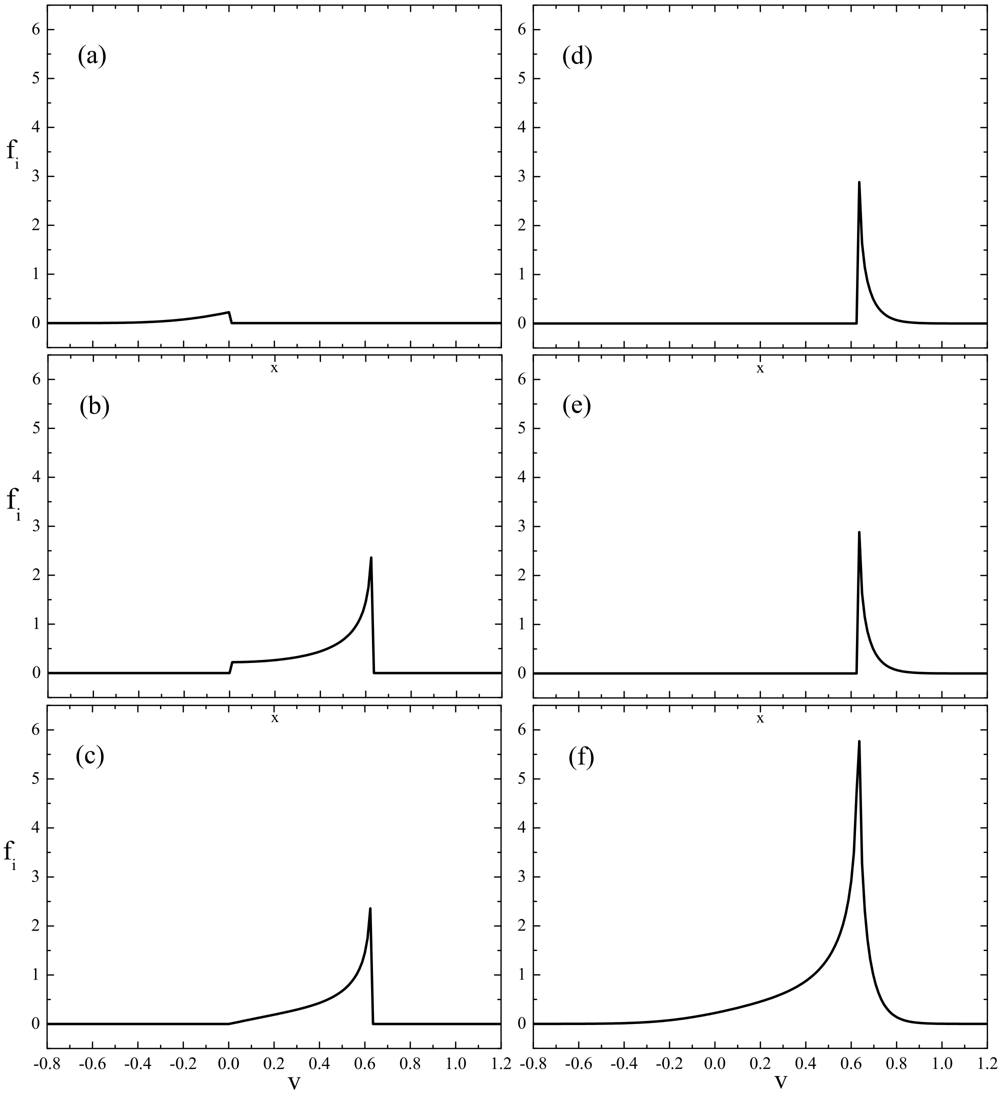

Figure 2.2: Velocity distribution function f_i for the ion source temperature $T_n = 1.0$ at potential position $\Phi = -0.4$ is a sum of 5 integrals. (a) in the first region $H(-v)$ as described by Eq. (2.19). Secondly, in the bounded region $H(v)H(\sqrt(-\Phi) - v)$ with (b) the first integral and (c) being athe second integral of Eq. (2.21). Finally, the remaining region $H(\sqrt(-\Phi) - v)$ shows: (d) the first population, and (e) the second population of Eq. (2.22). The sum of all integrals (2.19-2.22) smoothly combines (f) the complete ion velocity distribution function f_i.

where

$$s' = x'/L \ , \tag{2.24}$$

$$f = \frac{f_i}{\sqrt{m_i/2kTe}} \quad \text{and} \tag{2.25}$$

$$B = \frac{1}{2\pi}\sqrt{\frac{T_e m_i}{T_i m_e}}\frac{n_0}{n_{e,\mathrm{av}}}\exp(\Phi_w) \ . \tag{2.26}$$

The velocity distributions at various points $x(\Phi)$ for the cases of an analytically solved problem of the zero ion source temperature, a very small ion source temperature and a rather high source temperature $T_i = T_e$ will be shown in Results.

2.5 Moments of the velocity distribution function

The moments of velocity distribution are fluid quantities which are obtained as an infinite series of integrals $\int_{-\infty}^{\infty} v^j f_i(v)dv$, where $j = 0, 1, 2, \ldots$. Such quantities are e.g.: the ion density

$$n_i(\Phi(x)) = \int_{-\infty}^{\infty} f_i(v)dv \ , \tag{2.27}$$

the ion flux

$$\Gamma_i(\Phi(x)) = \int_{-\infty}^{\infty} v f_i(v)dv \ , \tag{2.28}$$

the ion total energy

$$K_i(\Phi(x))) = \frac{1}{n_i(\Phi)}\int_{-\infty}^{\infty} v^2 f_i(v)dv \ , \tag{2.29}$$

ion directional velocity

$$u_i(\Phi(x)) = \frac{1}{n_i(\Phi)}\Gamma_i(\Phi) \ , \tag{2.30}$$

and the ion temperature

$$T_i(\Phi(x)) = K_i(\Phi) - u_i^2(\Phi) \ , \tag{2.31}$$

as well as all higher moments like heat flux, energy flux etc at any location.

On the other hand, the Poisson equation states:

$$-\frac{d^2\Phi}{dx^2} = \frac{e}{\varepsilon_0}(n_i - n_e) \ , \tag{2.32}$$

where ε_0 is the vacuum dielectric constant and n_i, n_e are the ion and electron densities, respectively.

In non-dimensional form the space coordinate is normalized to a suitable characteristic length ℓ of the plasma, i.e., the physical extension L of the system or the ionization lengthℓ. In the present investigation, we are interested primarily in fusion plasmas, where ℓ or L is much larger than the Debye length λ_D.

At this point we introduce the normalized quantities of interest as follows:

$$\begin{gathered}\frac{e\Phi}{kT_e} \rightarrow \Phi \ , \quad \frac{m_i v^2}{2kT_e} \rightarrow v^2 \ , \quad \frac{x}{L} \rightarrow x \ , \quad \frac{n_{i,e}}{n_{e0}} \rightarrow n_{i,e} \ , \\ \frac{T_n}{T_e} \rightarrow T_n \ , \quad \frac{T_{i,src}}{T_e} \rightarrow T_{i,src} \ , \quad \frac{T_i}{T_e} \rightarrow T_i \ , \\ \frac{\sqrt{2}c_{s0}f_i}{n_{e0}} \rightarrow f_i \ , \quad S_i L \rightarrow S_i \ . \end{gathered} \tag{2.33}$$

where $c_{s0} \equiv \sqrt{kT_e/m_i}$ and L is any characteristic length of the system, (usually, the half-length of the plane-parallel discharge). Let us note that in the articles by B&J and S&E both normalized quantities T_i and $\tau \equiv 1/T_i$ are used in parallel, while we prefer to avoid τ wherever possible. Moreover, in our notation T_n is the neutral temperature, which is identical to the ion-source temperature $T_{i,\mathrm{src}}$. In the work of B&J, this temperature was denoted as T_i leading to serious confusion. In fact, the final ion velocity distribution function (VDF) turns out to be very different from the initial one. As an obvious example of such confusion, B&J defined in their work [Eq. (8)] the ion-sound velocity containing in fact the neutral temperature instead of the real (effective) ion temperature as should be calculated from the ion velocity distribution. So their Eq. (8) turns out to be inappropriate emerging from confusion notation only. To avoid such problems we use the notation $T_{i,src} \equiv T_n$ for the ion source temperature, and T_i will be *exclusively reserved* for the final effective ion temperature as calculated from the final velocity distribution function.

Throughout the text we will use either non-normalized or normalized quantities. To avoid any possible confusion we will state explicitly in each case which of them is used in a given context. Additional normalized quantities will appear later in a natural way.

Since we assume that the potential profile $\Phi(x)$ is monotonic, so that the inverse function $x(\Phi)$ is monotonic as well, the mathematical rule: $d^2y/dx^2 = -(d^2x/dy^2)/(dx/dy)^3$ holds. The Poisson equation [Eq. (2.32)] in normalized variables thus reads

$$\int f_i(\Phi, v)dv = n_e + \varepsilon^2 \frac{d^2x/d\Phi^2}{(dx/d\Phi)^3}. \tag{2.34}$$

Esq. (2.34) and (2.16) provide a complete description of the finite-ε discharge. The central quantity of interest is obviously inverse electric field$dx/d\Phi$. Once this quantity is found, the ion VDF can be calculated self-consistently from Eqs.(2.34) and Eq (2.16), depending on the assumption of vanishing or non-vanishing ε respectively. Then, the moments of the VDF can be calculated as functions of the potential Φ or, equivalently, of the position x.

Once a numerical solution of the system (2.34) and (2.16) is obtained, it is straightforward to calculate the ion velocity distribution and all their moments i.e. density ($n = \int f(v)dv$), directional velocity ($u = \frac{1}{n}\int f(v)vdv$), and ion temperature $T = \int \frac{1}{n} f(v)(v-u)^2 dv$ and all higher moments like heat flux, energy flux etc. at any location.

The special quantity of our interest is the polytropic coefficient $\gamma_i(x)$ (or equivalently$\gamma_i(\Phi)$), which can be found by using the expression

$$\gamma_i = 1 + \frac{n_i}{T_i}\frac{dT_i}{dn_i} \equiv 1 + \frac{n_i}{T_i}\frac{dT_i/d\Phi}{dn_i/d\Phi} \tag{2.35}$$

with previously calculated moments of the ion VDF.

Chapter 3

Overview of existing models

3.1 Basic considerations on the two-scale model

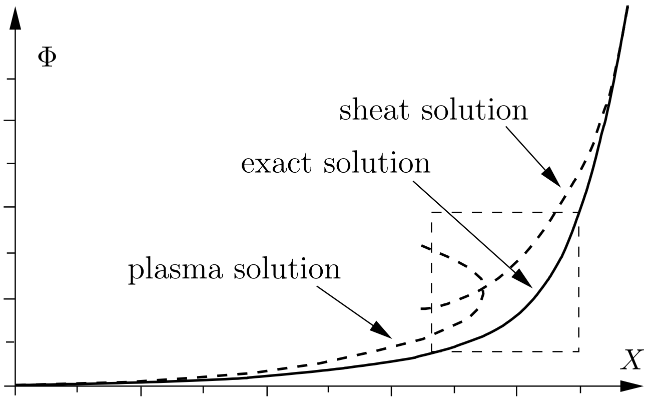

Figure 3.1: Symbolic picture illustrating the two-scale approximation.

The quasi-neutrality condition assumes the exact equality of ion (n_i) and electron (n_e) densities in a defined region of interest. The most common assumption is that the electrons are Boltzmann distributed, i.e., their velocity distribution is implicitly assumed to be Maxwellian. The ion velocity distribution is unknown and can be calculated from the quasi-neutrality condition

$$\int f_i(x, v)dv = n_0 \exp\left(\frac{e\phi}{kT_{e2}}\right) \tag{3.1}$$

This is an integral equation for unknown ion velocity distribution $f_{x,v}$. Finding a solution requires additional considerations and assumptions which are based on the Boltzmann equation (2.10).

3.2 Tonks-Langmuir model

Tonks and Langmuir started out with assumptions that the ions are born at rest, i.e., with zero initial velocity at any point of discharge (cold ion-source case). Under this assumption the source term can be written in the form

$$S_i(x,v) = s_i(x)\delta(v) \ , \tag{3.2}$$

where $\delta(v)$ is Dirac's delta-function. Considering $\delta(v^2) = \frac{\delta(v)}{2v}$ in this case the solution takes the form

$$f_i(x,v) = 2\int s_i(x')\delta\left(v'^2 - \frac{2e}{m_i}(\phi' - \phi)\right)\frac{dx'}{d\phi'}d\phi' \ . \tag{3.3}$$

Since only monotonic potential profiles were of interest the last equation takes form

$$\begin{aligned} f_i(\phi,v) &= 2\int s_i(\phi')\delta\left(v'^2 - \frac{2e}{m_i}(\phi' - \phi)\right)\frac{dx'}{d\phi'}d\phi' = \\ &= \frac{m_i}{e}s_i(\phi')\left|\frac{dx'}{d\phi'}\right|_{e\phi' = e\phi + \frac{m_i v^2}{2}} \ , \end{aligned} \tag{3.4}$$

wherefrom we conclude that the ion distribution function at the place of observation depends only on the place of their generation. That means that the ion energy at the place of observation is equal to the potential at that place

$$e\phi' = \frac{m_i v^2}{2} + e\phi = \mathcal{E}_i \ , \tag{3.5}$$

so the velocity distribution function

$$f_i(\phi,v) = \frac{m_i}{e}s_i(\mathcal{E}_i)\left|\frac{dx'}{d\phi'}\right| = f_i(\mathcal{E}_i) \tag{3.6}$$

depends only on the ion energy

$$f_i(\phi,v) = f_i(\mathcal{E}_i) \ . \tag{3.7}$$

Due to the cold-neutral assumption ions move exclusively in the positive direction of the x-axis (in the electric field direction). The ion with the kinetic energy $mv^2/2$ and the potential energy $e\phi(x)$ at point x is originated from the ionization process at x' with the potential $\phi' = \phi(x')$. For the velocity interval necessary for the integration of the distribution function and to find the ion density we thus have

$$0 \leq v \leq \sqrt{-\frac{2e\phi}{m_i}} \ . \tag{3.8}$$

Further we have to introduce energy $\mathcal{E}_i$

$$\mathcal{E}_i = \frac{m_i v^2}{2} + e\phi(x) \tag{3.9}$$

as a new variable, then the quasi-neutrality condition $n_i = n_e(x)$ can be represented in the form

$$\int\limits_{e\phi(x)}^{0} \frac{f_i(\mathcal{E}_i) d\mathcal{E}_i}{\sqrt{2m_i(\mathcal{E}_i - e\phi)}} = n_0 \exp\left(\frac{e\phi(x)}{kT_e}\right) \ . \tag{3.10}$$

This is and integral equation for the ion distribution function of the form

$$\int\limits_{0}^{x} \frac{S(x')}{\sqrt{x - x'}} dx = g(x) \ . \tag{3.11}$$

From (3.11) it follows

$$\int\limits_{0}^{x} \frac{dx'}{\sqrt{x - x'}} \int\limits_{0}^{x'} \frac{S(x'')dx''}{\sqrt{x' - x''}} = \int\limits_{0}^{x} \frac{g(x')dx'}{\sqrt{x - x'}} \ . \tag{3.12}$$

Changing the ordering of the integration by means of equality

$$\int\limits_{x''}^{x} \frac{dx'}{\sqrt{(x - x')(x' - x'')}} = \pi \ , \tag{3.13}$$

we find

$$f(x) = \frac{1}{\pi} \frac{d}{dx} \int\limits_{0}^{x} \frac{g(x')dx'}{\sqrt{x - x'}} \ . \tag{3.14}$$

Hence according to (3.13) and (3.14) we have

$$f_i(\mathcal{E}_i) = \frac{1}{\pi} \sqrt{2m_i} n_0 \frac{d}{d|\mathcal{E}_i|} \int\limits_{0}^{|\mathcal{E}_i|} \frac{e^{-\frac{|\mathcal{E}_i| - z}{kT_e}} dz}{\sqrt{s}} \ , \tag{3.15}$$

which yields definitely

$$f_i(\mathcal{E}_i) = \frac{n_0}{\pi}\sqrt{\frac{2m_i}{kT_e}}\left[\sqrt{-\frac{kT_e}{\mathcal{E}_i}} - 2F\left(\sqrt{-\frac{\mathcal{E}_i}{kT_e}}\right)\right] \ , \tag{3.16}$$

where $F(y)$ denotes the Dawson function:

$$F(y) = exp(-y^2)\int_o^y exp(y'^2)dy' \ . \tag{3.17}$$

Since the ion velocity distribution function is always positive the total energy is restricted to

$$-\mathcal{E}_i < \mathcal{E}_o \approx 0.854\,kT_e \ , \tag{3.18}$$

where $\mathcal{E}_o$ is solution for the case $f_i(\mathcal{E}_i) = 0$. In the most restrictive case of the spectrum of ion velocities $v = 0$ the condition

$$\frac{e\phi}{kT_e} > \frac{e\Delta\phi_b}{kT_e} = -0.854 \tag{3.19}$$

emerges. According to (3.6) the limiting case $\Delta\phi_b$ is the point where quasi-neutrality breaks, i.e., the electric field for this value becomes infinite.

The potential profile now becomes

$$x(\phi) = \frac{n_0}{\pi}\sqrt{\frac{2kT_e}{m_i}}\int\limits_0^{-\frac{e\phi}{kT_e}} \frac{1}{s_i(y)}\left[\frac{1}{\sqrt{y}} - 2F(\sqrt{y})\right]dy \ . \tag{3.20}$$

In the case when ionization is homogeneous the last expression is simple

$$x(\phi) = \frac{2n_0}{s_i\pi}\sqrt{\frac{2kT_e}{m_i}}F\left(\sqrt{-\frac{e\phi}{kT_{e2}}}\right) \ . \tag{3.21}$$

3.3 Emmert et al.'s model

Instead of using the Dirac function for the ion source Emmert et al. [22] constructed such an artificial warm ion source that the solution of plasma equation yields the desired form of Maxwellian. With their ion source they were able to solve this rather exotic case analytically.

3.4 Bissell-Johnson model

Bissell and Johnson [10] (B&J) started from a realistic Maxwellian ion source velocity distribution. In this case there is only hope of reasonable approximations to obtain an analytic solution. With this in view, they used the numerical computational method. The problem appears to be very daunting. They approximated the kernel of the integral equation and obtained the solution in a limited range of ion temperatures.

The procedure of Bissell and Johnson model is to apply the strict quasi-neutrality $n_i = n_e$, where

$$n_i = \int\limits_{-\infty}^{+\infty} f_i(x(\Phi), v) dv = \sum_I \int\limits_{v_1}^{v_2} dv \int\limits_a^b \frac{S_i\left(v^2 - \frac{2e}{m_i}(\Phi(x') - \Phi(x))\right)}{\sqrt{v^2 - \frac{2e}{m_i}(\Phi(x') - \Phi(x))}} dx' \tag{3.22}$$

and the electron velocity distribution is Boltzmannian, i.e.,

$$n_e(x) = n_{e0} \exp\left(\frac{e\Phi(x)}{kT_e}\right) . \tag{3.23}$$

The summation on the right-hand side of (3.22) describes the contributions to $n_i(x)$ from sources in different regions of the plasma – the limits of integration vary with the position and speed of the source particles. A similar procedure has already been used in the Section 2.3.

Bissell and Johnson also supposed that the source distribution is Maxwellian, i.e.,

$$S(x, v) = R n_n n_e(x) \sqrt{\frac{m_i}{2\pi k T_i}} \exp\left(-\frac{m_i v^2}{2kT_i}\right) , \tag{3.24}$$

where T_i is the ion source temperature.

The B&J model physically means that they supposed that ions are created from single electron-neutral impact ionization. Other models will be presented below.

With the above supposed ion source in [10] an integration over the velocity and the summation of sources in different regions of plasma are performed. The result is

$$\begin{aligned} n_i(x) = & \sqrt{\frac{m_i}{2\pi k T_i}} L R n_n n_e(x) \\ & \times \int\limits_0^{\psi_b} d\psi' \frac{dx'}{d\psi'} \exp(\psi' - \psi) \exp\left[\frac{\tau}{2}(\psi' - \psi)\right] \mathrm{K}_0\left[\frac{\tau}{2}|\psi' - \psi|\right] , \end{aligned} \tag{3.25}$$

where

$$\psi = \frac{e\Phi}{kT_e} \ , \quad \psi_b = \frac{e\Phi_b}{kT_e} \ , \quad \tau = \frac{T_e}{T_i} \ , \tag{3.26}$$

$\mathrm{K}_0(z)$ is the modified (hyperbolic) Bessel function [2] and Φ_b is the potential at the presheath boubdary.

The ion flux is given by the continuity equation

$$\frac{d\Gamma_i}{dx} = Rn_n n_e(x) \ , \tag{3.27}$$

which after athe integration takes the form

$$\Gamma_i = Rn_n \int_0^L n_e dx \equiv Rn_n n_{e,av} \ , \tag{3.28}$$

at the presheath boundary ($\lambda_D << L$). In (3.28) $n_{e,av}$ represent the mean value of the electron density over the system.

The electron flux for Maxwellian distribution at a wall is given by

$$\Gamma_e = \sqrt{\frac{kT_e}{2\pi m_e}} \exp(\Phi_w) \ . \tag{3.29}$$

The most "standard" assumption in collisionless discharge models is that the ion and electron fluxes at the wall are equal, so there is no electric current ($\Gamma_i = \Gamma_e$). In the present case, this "floating wall" condition yields

$$LRn_n = \frac{n_0}{n_{e,av}} \sqrt{\frac{kT_e}{2\pi m_e}} \exp(\Phi_e) \ . \tag{3.30}$$

With this condition the ion density becomes

$$\begin{aligned} n_i =& n_e(x) \sqrt{\frac{m_i}{2\pi kT_i}} \frac{n_0}{n_{e,av}} \sqrt{\frac{kT_e}{2\pi m_e}} \exp(\psi_w) \\ & \times \int\limits_0^{\psi_b} d\psi' \frac{dx'}{d\psi'} \exp(\psi' - \psi) \exp\left[\frac{\tau}{2}(\psi' - \psi)\right] \mathrm{K}_0\left[\frac{\tau}{2}|\psi' - \psi|\right] \ . \end{aligned} \tag{3.31}$$

Since quasi-neutrality condition $n_i = n_e$ is assumed this expression reduces to

$$\frac{1}{B} = \int_0^{\psi_b} d\psi' \frac{dx'}{d\psi'} \exp(\psi' - \psi) \exp\left[\frac{\tau}{2}(\psi' - \psi)\right] \mathrm{K}_0\left[\frac{\tau}{2}|\psi' - \psi|\right] \ . \tag{3.32}$$

where for shortness' sake B&J denoted

$$B = \frac{1}{2\pi}\sqrt{\frac{\tau m_i}{m_e}}\frac{n_0}{n_{av}}\exp(\phi_w)\ . \tag{3.33}$$

With above assumptions the only unknown quantity is the electric field

$$E = -\left(\frac{dx}{d\psi}\right)^{-1}\ . \tag{3.34}$$

Eq.(3.32) is a singular integral equation with a logarithmic singularity. Solving the above defined problem is very demanding from both theoretical and numerical points of view. B&J made next steps:

- The Bohm criterion is used as the boundary condition to the quasi-neutrality equation.
- The kernel of the integral equation is approximated in a limited range of validity.
- Value B is calculated self-consistently as an unknown.
- The wall potential and moments of the velocity distribution at the plasma-sheath boundary are calculated.

B&J used a switch function

$$J(\Phi'-\Phi) = \exp[\tau(\Phi'-\Phi)]\{1-\tanh[(\Phi'-\Phi)/\epsilon]\}/2+\{1+\tanh[(\Phi'-\Phi)/\epsilon]\}/2\ , \tag{3.35}$$

reduced the main equation to the form

$$\frac{1}{B} = \int\limits_0^{\Phi_b} d\Phi'\Psi(\Phi')F(\Phi'-\Phi) \tag{3.36}$$

with

$$F(\theta) = J(\theta)\exp(\theta)\exp(\frac{\tau}{2}|\theta|)\,\mathrm{K}_0(\frac{\tau}{2}|\theta|)\ , \tag{3.37}$$

and applied an intricate mathematical procedure which assumes an approximation of such a kernel via a Chebyshev polynomial series yielding a system of linear equations. They claimed that their approximation is more or less valid in the narrow range of T_i between 0.5 and 4. We repeated their derivations and in Fig. 3.2 we plot their kernel approximation with our repeated

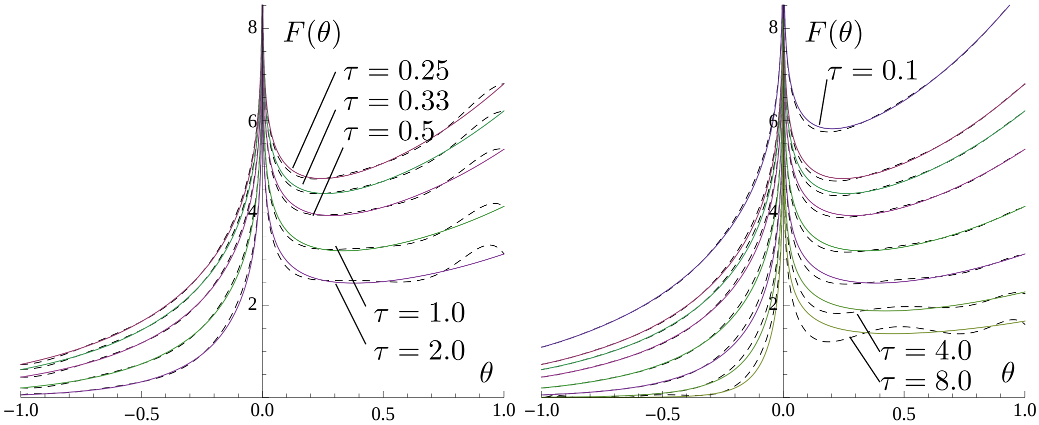

Figure 3.2: A comparison of the kernel $F(\theta)$ approximation of the B&J equation (left, dashed), our approximation (right, dashed) and the exact kernel (solid) for various values of $\tau = T_e/T_i$. The approximation error increases with higher τ's. While our approximation is better near $\theta = \Phi' - \Phi = 1$ it is still evident that errors at the center are significant and cannot be lowered with a polynomial approximation of order 8. In the left figure we show the comparison of the results obtained for $\tau = 0.25$, 0.33, 0.5, 1.0, 2.0, while in the right figure we also added results for $\tau = 0.1$, 4.0, and 8.0

results where we have taken into account that there were certain mistakes in polynomial coefficients.

The kernel of the B&J equation is shown in Fig. 3.2 for various values of parameter τ. Following their approach we calculated a tighter kernel approximation. Nevertheless, one can notice differences between either approximation and the exact kernel. Their approach is a specific one and the system of linear equations to be solved is closely related to the approximation that they used.

B&J concluded from derived quantities that the approximation to the kernel of the plasma equation for $T_e/T_i > 2$ was too poor to be used. However, the range of validity of the kernel is too narrow for both plasmas characterized with small and high enough ion source temperatures for, e.g., fusion application.

3.5 Scheuer-Emmert model

Scheuer and Emmert [61] (S&E) used a better kernel and another numerical computational approach. They extended the range of validity of solution but it still remains constrained up to certain ion temperatures.

The model by Emmert et.al. [22] is a full solution of both plasma and sheath regions. Their solution is analytic and it is valid for arbitrary ion temperatures. Unfortunately, their ion source is an artificial one arranged in advance to be integrable with the analytic method and to give the desired result. Nevertheless, this approach is not meaningless. As they wanted to have the final Maxwellian distribution only at the center of the system and to obtain its shape towards boundaries. This is close to the physical scenario where the ions move towards the divertor plate in the tokamak SOL. Far from the divertors their velocity distribution probably can be regarded as Maxwellian irrespective of the ion source distribution, which is anyhow a rather uncertain unknown in real experiments: during the observation in the SOL region one could perhaps measure the final velocity distribution, but its source can be only a matter of speculations.

As discussed with the B&J model, the ion source velocity distribution is Maxwellian and the final velocity distribution is to be calculated with the numerical method since any analytic attempt is not expected to yield results. In addition, unlike the Emmert et al. model, which is valid in both sheath and quasi-neutral regions, in the B&J model strict quasi-neutrality is assumed, and the sheath potential profile is not calculated.

Scheuer and Emmert started out from the B&J model, rewriting their result (3.32) in the form

$$\frac{1}{B} = \int_0^1 \exp\left[1 + \frac{\tau}{2}(\Phi - \Phi')\right] \mathrm{K}_0\left[\frac{\tau}{2}|\Phi - \Phi'|\right] ds' \tag{3.38}$$

with

$$\psi = -\frac{e\Phi(s)}{kT_e} \ , \quad \psi' = -\frac{e\Phi'(s')}{kT_e} \ , \tag{3.39}$$

$$B = \frac{1}{2\pi}\sqrt{\frac{\tau m_i}{m_e}\frac{n_0}{n_{av}}} \exp(\Phi_b) \ , \quad s = \frac{x}{L} \ , \tag{3.40}$$

The differences between the S&E and B&J approaches are as follows

- Quantity B appears to be a free parameter to be changed depending on, e.g., the ion to electron mass ratio for the fixed ion temperature.
- S&E made a better approximation of the kernel in the integral equation, which covers the cases of arbitrary high τ (or equivalently, arbitrary small ion temperatures). The new kernel approximation still remains valid for small τ (high enough ion temperatures as compared with electron temperatures).
- S&E (unlike B&J) calculated the plasma potential a posteriori and did not apply any kind of Bohm criterion in advance but they have demonstrated that this criterion indeed holds with a high degree of accuracy.
- S&E used different normalization [Eq. (3.39)] that reverses the sign of the potential profile in comparison with that of B&J (see Fig. 6.2).

Chapter 4

Analytic-Numerical method

In our work we follow the approach adopted by S&E, we have, however, improved it using

- the exact kernel,
- with a much better resolution of the computational grid,
- employing high grid refinements on both the zero and the infinite electric field side of the discharge,
- with implementation of additional stabilizing terms that improve convergence.

Following the "trick" applied by Scheuer and Emmert we introduce identity

$$1/B \equiv \exp(\phi_0) \tag{4.1}$$

so Eq. (3.38) takes the form

$$\exp(\phi_0) = \int_0^1 \exp\left[\left(1 + \frac{1}{2T_n}\right)(\phi - \phi')\right] \mathrm{K}_0\left(\left|\frac{\phi - \phi'}{2T_n}\right|\right) dx' \ , \tag{4.2}$$

where a simple formal identity $\phi - \phi' = \Phi - \Phi' = (\Phi - \phi_0) - (\Phi' - \phi_0)$ is introduced. Equation (3.38) can be rewritten into

$$\exp\left[-\left(1 + \frac{1}{2T_n}\right)\phi\right] = \exp(-\phi_0) \int_0^1 \exp\left[-\left(1 + \frac{1}{2T_n}\right)\phi'\right] \mathrm{K}_0\left(\left|\frac{\phi - \phi'}{2T_n}\right|\right) dx \tag{4.3}$$

or, after taking logarithms of both sides into a form conducive to a numerical procedure

$$\left(1+\frac{1}{2T_n}\right)\phi=\phi_0-\ln\left[\int_0^1\exp\left[-\left(1+\frac{1}{2T_n}\right)\phi'\right]\mathrm{K}_0\left(\left|\frac{\phi-\phi'}{2T_n}\right|\right)dx'\right]\ , \tag{4.4}$$

with K_0 being the zeroth order modified Bessel function of the second kind which is singular at every $x' \doteq x$. The unknown function of interest $\phi(x)$, which is integrated over a normalized interval, also includes a known high gradient at $x = 1$, while at $x = 0$, due to symmetry it is expected to have a zero gradient.

We can first look for a solution of Eq. 4.4 without the unknown additive constant ϕ_0. Once this solution is found, the additive constant is simply calculated from the vertical shift of the solution. Quantity B (related to the source strength) in our algorithm is calculated and iterated at each loop.

We start from Eq. (3.38) that is discretized over interval $x = [0, 1]$ with a varying density of sample points x_i. For a subsequent purpose of derived quantities like $dx/d\Phi$ a dense grid near zero is needed. The location of the i-th position at the grid is given by

$$x_i=\left[1-\left[1-\frac{i}{N-1}\right]^{\lambda_2}\right]^{\lambda_1}\ , \tag{4.5}$$

for index range $i = 0, 1, \ldots, N-1$, which covers x range of interest for N points. The grid density near zero is controlled via λ_1, while λ_2 controls the density near $x = 1$. Practical values for λ_1 and λ_2 range from 2 to 3 for grids with $N \geq 1000$ points. It should be noted that the grid density approaching $x = 1$ is extremely high and that an equivalent interval density can be as high as 10^8 points. Fig. 4.1 shows a zoom-in on the right hand side of Fig. 6.1 for $T_n = 1.0$

For function $\Phi(x)$ discretized at points x_i and break into $N-1$ intervals piecewise-linear profiles are assumed. The interpolating function $V(x')$ over each interval can be evaluated with

$$V(x')=V_i+\frac{V_{i+1}-V_i}{x_{i+1}-x_i}(x'-x_i)\ ,\quad x_i\leq x'\leq x_{i+1}\ , \tag{4.6}$$

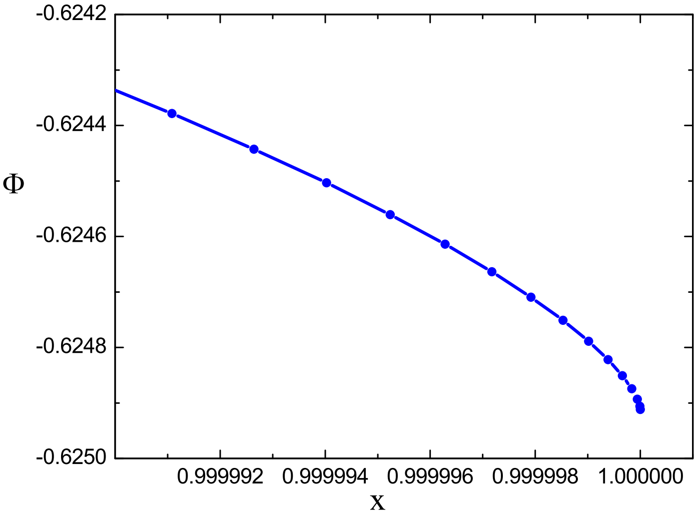

Figure 4.1: Zoom-in of the potential profile $\Phi(x)$ of the high density grid for $T_n = 1$ shows numerical approximation of the infinite potential when approaching $x = 1$. See Fig 6.1 for a complete potential profile for $\varepsilon = 0$ case.

where V_i represents discrete function value $V_i = \Phi(x_i)$. In a discrete form Eq. (4.4) is rewritten into

$$\begin{aligned} &\exp[(1+\frac{1}{2T_n})V_k] = \\ &B\sum_{i=0}^{N-1}\int_{x_i}^{x_{i+1}} dx' \exp[(1+\frac{1}{2T_n})V(x')]\,\mathrm{K}_0\left(\frac{1}{2T_n}|V_k - V(x')|\right) \ . \end{aligned} \tag{4.7}$$

The right-hand side of Eq.(4.7) can be abbreviated and formulated in the iterative form as

$$V_k = \frac{1}{1+\frac{1}{2T_n}}\ln(B\sum_{i=0}^{N-1} L_i), \tag{4.8}$$

where L_i represents the integral over each interval that should be evaluated for every index i at position k. The method applied can be considered as a *fixed-point* iterative method [19] with N nonlinear equations.

A careful investigation of plasma equation (4.7) that has the property of monotonicity reveals that for each position k there are at the most two neighboring intervals that lead to the singularity of the Bessel function. These singular intervals with integrable singularity at the boundary can be numerically solved with adaptive quadrature integration algorithms [23, 24]. The remaining intervals should not impose any numerical difficulties and can be solved with a non-singular quadrature formula over each interval. Note that this is not completely true and that observing Eq.(4.6) one can see that on condition $V_{i+1} - V_i \equiv 0$ additional singularity might arise, if monotonicity is not strictly maintained over the whole interval $[0, 1]$. Especially intervals near zero are prone for such singularities. Another observation of a numerical nature that might arise in Eq.(4.6) can be observed with high gradients approaching $x = 1$ and dense intervals that can lead to unstable discrete derivate $c_i = (V_{i+1} - V_i)/(x_{i+1} - x_i)$ found in Eq. (4.6).

These observations should be carefully considered when integrating Eq. (4.7) fully numerically at every k. One can also conclude that the chosen λ_1 and λ_2 as grid parameters have indirect influence on the presence of numerical instabilities and the presence of singularities that should be avoided as much as possible.

The formula (4.8) where the right-hand side of equation evaluates to new V_k is mathematically exact, but can only be applied when all V_k are perfectly accurate. With $V_k \to V_l$ on the left-hand side of Eq.(4.8) and additional soft-step parameter α one can get an iterative algorithm for new V_k values with

$$V_k^{new} = V_k + \alpha(V_l - V_k) \tag{4.9}$$

While the method (4.9) converges, it does so very slowly. The practical values for α are from 0.0001 to 0.1 and are dependent on initial solution and grid parameters. Large α's are prone to oscillatory behavior that starts at points near $x = 0$.

To speed up the computation, one can first compute an approximation on a coarser grid and gradually lower α when interpolating to the dense grid. An alternative approach when changing T_n is to start with an already converged solution for nearby T_n. The initial solution is recommended, although not required, to be as close as possible to the final solution. We suggest the following monotonous initialization function

$$V_k = 0.5(1 - \exp(k/N)) \ , \quad k = 0, 1, \ldots, N-1 \ , \tag{4.10}$$

disregarding λ_1 and λ_2.

To stabilize the convergence we introduced two additional vanishing a posteriori regularization operations on Eq.(4.9) that are based on the known solution smoothness. A simple Laplacian-like smoothing technique with smooth-step parameter β similar to Eq.(4.9) is employed as

$$V_k^{new} = V_k + \beta \left[\frac{V_{k-1} + V_{k+1}}{2} - V_k \right] , \quad k = N-1, N-2, \ldots, 1 \quad . \tag{4.11}$$

Choosing $\beta \leq 1$ stabilizes the convergence and should be gradually lowered to zero when the solution stabilizes. After observing the nature of instabilities, we found out that oscillatory behavior starting at $x = 0$ propagates throughout the mesh. To prevent this, we enforced a parabolic interpolation for the first m points that are rewritten with

$$\begin{aligned} V_k &= a x_k^2 + b x_k + c \ , \quad k = 0, 1, \ldots, m \\ a &= \frac{V_l - V_m}{x_l^2 - x_m^2} \ , \quad b = 0 \ , \quad c = \frac{x_l^2 V_m - x_m^2 V_l}{x_l^2 - x_m^2} \ , \end{aligned} \tag{4.12}$$

where mesh point x_l is chosen at $l = 3/4m$. The length of the rewritten profile can be up to $x_m < 0.1$ and gradually lowered when approaching the final solution. Constant B is unknown during the iterative procedure and as shown in Eq.(4.4) influences the shift of the solution. From Eq. (4.7) B can be expressed as

$$B = \frac{\exp[(1 + \frac{1}{2T_n})V_k]}{\sum_{i=0}^{N-1} L_i} \ , \tag{4.13}$$

with V_k being the old value, while L_i are next iteration zone integrals. Constant B should hold at every grid point. As an eigenvalue, B does not have a major impact on convergence. Similarly to other smooth step parameters, B should also be adjusted with soft-step of 0.005, calculated from the central grid point. Our experiments shown that initial $B = 0.3$ can be used for all cases.

The iterative process can be summarized through the following steps:

1. Set up B and grid positions using Eq.(4.5).

2. Create the initial solution with Eq.(4.10) or initialize the function profile with the nearest previous solution, if existent.

3. For every grid position calculate the sum of integrals V_k using equation (4.8).

4. Move function values V_k into a new position with a soft-step strategy (4.9) using step size α in the range $[0.0001, 0.1]$.

5. Stabilize the convergence with additional smoothing of the curve with (4.11) that prevents the oscillatory behavior of the solution. Similarly to Eq.(4.9) the step size should vanish as the solution approaches a stable form.

6. Prevent oscillations near $x = 0$ with a parabolic rewrite of the potential profile for all points with $x_m < 0.1$. Use Eq.(4.12) for the coefficients of the parabolic interpolation.

7. Calculate B using Eq.(4.13) and correct its value for 0.005 of the difference between new and old B.

8. Repeat the iteration from Step 3 following the solution quality criterions while gradually lowering the smooth-step and the parabolic interpolation range.

The stopping criteria for the iteration procedure cannot be simply expressed with a measure like the quadrature norm between the iterations. One of the most important convergence indicators is a potential at $x = 1$. During the convergence one should observe the curve properties near $x = 0$, where the parabolic interpolation ends. Potential V_{N-1} at $x = 1$ can also behave oscillatorily, with a convergent amplitude.

The number of iteration steps depends on a number of factors and can range from 2000 to 100000. The most influential is the soft-step size that should be as high as possible. Setting the soft-step too high produces undesirable oscillations at the beginning of the potential curve that cannot be easily rescued once they appear. The strategy for lowering smooth-step β and the parabolic interpolation is that, firstly, one should have a convergent solution and then smoothly lowering both parameters that should vanish for the final solution. Fig. 4.2 shows the described scenario with both parameters lowered, while monitoring the convergence, i.e. without the oscillatory nature through all computational area.

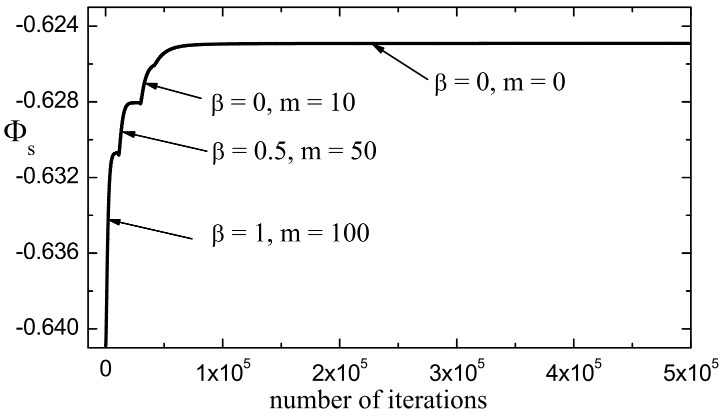

Figure 4.2: Convergence for $T_n = 1$ showing the last point of grid Φ_s. Gradually lowering smooth step and parabolic rewrite took about 500000 iterations and nearly 1 week of 8 core Intel Xeon 2GHz CPU time.

4.1 Implementation aspects

The implementation of the above-described approach was verified and coded in Mathematica and the C language using the GSL [25] scientific library for special functions and integrations. Most notable here is the Bessel K_0 function with a relative error under $\eta < 10^{-10}$ in a wide range as shown in Fig. 4.4. The upper limit for double machine precision K_0 obtained with this experiment is approximately 600 which is an imposed limit of our code in C on commodity computer architectures. For the numerical integration in zones we used our `long double` extension of QAG and QAGS quadrature algorithms that adaptively bisects the integration into subintervals until the given relative error limit is achieved. The integration of non-singular zones applies the Gauss-Kronrod 21-point integration rule while for singular zones results are extrapolated using the epsilon-algorithm. For more details consult Ref. [45].

While Mathematica was our first choice to prove some convergence experiments, it was soon clear that the problem would be time-consuming and that C code would require parallelization for reasonable proof of the concept. The number of integral evaluations is directly connected to the number of grid points N. We estimate a practical limit for Mathematica up to 200 points.

Our C code uses shared memory model parallelization with OpenMP [16,

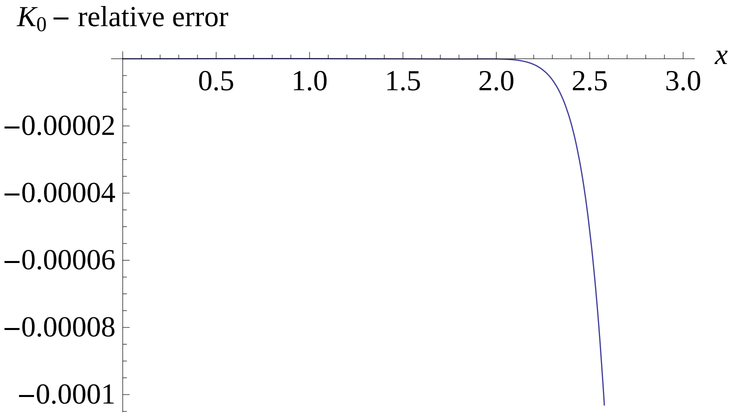

Figure 4.3: Relative error of the Modified Bessel function with polynomial approximation used in the S&E approach is minimized within range $[0, 2]$ while using such approximation for $x > 2$ is not viable.

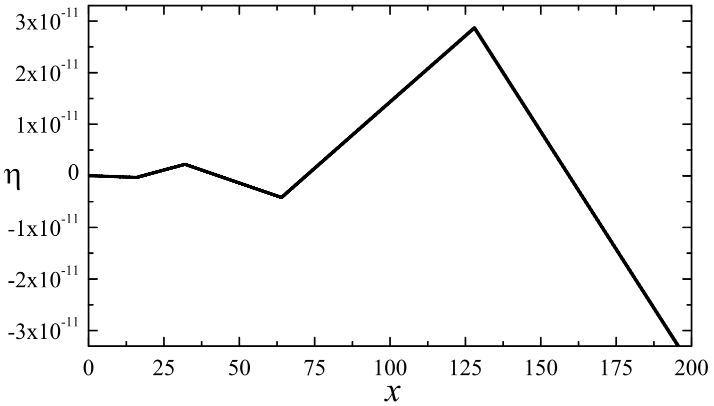

Figure 4.4: Relative error of the Bessel K_0 in the GLS library used in our approach shows relative error $\eta < 10^{-10}$ in a wide range.

47] approach. It seems that it is not practically time-bound by a number of intervals, but rather by precision limits that are imposed with a numeric model and machine precision.

We used `long double` precision for the numeric model wherever possible. Due to high gradients and the desired high grid we extended GSL library integration routines that exist only for `double` precision to `long double`. The upgrade consists of the modification of 43 source code files. As this can also be considered as a contribution to the Open source community, we submitted this patch for consideration in the future versions of GSL.

The practical number of points that enabled us to derive results was 1600. The required extremely high refinements on both sides of the domain are also sources of instabilities that need a special treatment with regard to precision. One must take care that the overall precision of the zone integration results within the high grid density is not violated. The relative error for QAG and QAGS algorithms was set to 10^{-6} with a maximum number 20000 of workspace for adaptive subintervals.

In our code, we implemented result caching mechanism that enabled us to experiment with parameters, so we could roll back in the presence of instabilities. Once a case is evaluated it is relatively fast to move to the nearby temperature. Depending on the solution criteria, the computational time on 8 core dual Xeon 2GHz CPU can range from one hour to one week. A helpful time-saving approach can be re-grid from/to low/high grid density.

Most of our computations as presented in the following chapters were obtained utilizing resources of the supercomputing center at the University of Innsbruck. Cluster consists of 48 Opteron machines (a total of 232 cores) with 2 to 16 cores with CentOS.

A careful study of loops that can be parallelized and their balancing improved overall scalability from 80% to nearly 100% according to Amdahl's law as shown within `systat` in Fig. 4.5 and `top` in Fig. 4.6.

The GSL library for QAG(S) integration routines requires one to preallocate sufficient `workspace` for adaptive refinement of the quadrature rules. Allocation of this temporarily space should be taken out of the loops to prevent cyclic allocation/deallocation, whereas taking into account that each thread will receive separate workspace.

Details on the code input parameters with the XML schema are elaborated in Appendix B.

```
                 /0   /1   /2   /3   /4   /5   /6   /7   /8   /9   /10
  Load Average   ||||||||||||||||||||||||||||||||||||

                 /0%  /10  /20  /30  /40  /50  /60  /70  /80  /90  /100
leon   ppgplasma XXXXXXXXXXXXXXXXXXXXXXXXXXXXXXXXXXXXXXXXX
leon   ppgplasma XXXXXXXXXXXXXXXXXXXXXXXXXXXXXXXXXXXXXXXXX
leon   ppgplasma XXXXXXXXXXXXXXXXXXXXXXXXXXXXXXXXXXXXXXXXX
leon   ppgplasma XXXXXXXXXXXXXXXXXXXXXXXXXXXXXXXXXXXXXXXX
leon   ppgplasma XXXXXXXXXXXXXXXXXXXXXXXXXXXXXXXXXXXXXXX
leon   ppgplasma XXXXXXXXXXXXXXXXXXXXXXXXXXXXXXXXXXXXX
leon   ppgplasma XXXXXXXXXXXXXXXXXXXXXXXXXXXXXXXXXXXXX
leon   ppgplasma XXXXXXXXXXXXXXXXXXXXXXXXXXXXXXXXXXXX
root  idle: cpu1 XXXXXXXXXXXXXXXXXXXXXXXXXXXX
root  idle: cpu0 XXXXXXXXXXXX
root  idle: cpu4 XXXXXXXXXXXX
root  idle: cpu3 XXXXXXXXXXXX
root  idle: cpu5 XXXXXXXXXXX
root  idle: cpu6 XXXXXXXXXX
root  idle: cpu2 XXXXXXXX
leon         sed X
```

Figure 4.5: Utilization of 8 core dual Intel Xeon(tm) 2GHz CPU on the FreeBSD OS. Up to 80% were achieved in the early versions of the code.

```
top - 01:46:01 up 3 days,  8:23,  1 user,  load average: 15.84, 10.29, 4.53
Tasks: 181 total,   2 running, 179 sleeping,   0 stopped,   0 zombie
Cpu0  :100.0% us,  0.0% sy,  0.0% ni,  0.0% id,  0.0% wa,  0.0% hi,  0.0% si
Cpu1  : 99.8% us,  0.2% sy,  0.0% ni,  0.0% id,  0.0% wa,  0.0% hi,  0.0% si
Cpu2  : 99.8% us,  0.2% sy,  0.0% ni,  0.0% id,  0.0% wa,  0.0% hi,  0.0% si
Cpu3  : 99.8% us,  0.0% sy,  0.0% ni,  0.2% id,  0.0% wa,  0.0% hi,  0.0% si
Cpu4  : 99.8% us,  0.0% sy,  0.0% ni,  0.2% id,  0.0% wa,  0.0% hi,  0.0% si
Cpu5  : 99.8% us,  0.0% sy,  0.0% ni,  0.2% id,  0.0% wa,  0.0% hi,  0.0% si
Cpu6  : 99.8% us,  0.2% sy,  0.0% ni,  0.0% id,  0.0% wa,  0.0% hi,  0.0% si
Cpu7  : 99.8% us,  0.0% sy,  0.0% ni,  0.2% id,  0.0% wa,  0.0% hi,  0.0% si
Cpu8  : 99.5% us,  0.5% sy,  0.0% ni,  0.0% id,  0.0% wa,  0.0% hi,  0.0% si
Cpu9  : 99.8% us,  0.0% sy,  0.0% ni,  0.2% id,  0.0% wa,  0.0% hi,  0.0% si
Cpu10 : 99.5% us,  0.2% sy,  0.0% ni,  0.2% id,  0.0% wa,  0.0% hi,  0.0% si
Cpu11 : 99.8% us,  0.0% sy,  0.0% ni,  0.2% id,  0.0% wa,  0.0% hi,  0.0% si
Cpu12 : 88.9% us,  0.5% sy,  0.0% ni, 10.6% id,  0.0% wa,  0.0% hi,  0.0% si
Cpu13 :100.0% us,  0.0% sy,  0.0% ni,  0.0% id,  0.0% wa,  0.0% hi,  0.0% si
Cpu14 : 99.5% us,  0.2% sy,  0.0% ni,  0.2% id,  0.0% wa,  0.0% hi,  0.0% si
Cpu15 : 99.8% us,  0.0% sy,  0.0% ni,  0.2% id,  0.0% wa,  0.0% hi,  0.0% si
Mem:  32912464k total,   352616k used, 32559848k free,   102496k buffers
Swap:  8385888k total,        0k used,  8385888k free,   134864k cached

  PID USER      PR  NI  VIRT  RES  SHR S %CPU %MEM    TIME+  COMMAND
 2827 c705185   15   0 77108 3236 2108 S    0  0.0   0:00.18 xterm
 3838 sgeadmin  16   0 59608 3236 1640 S    0  0.0  25:55.90 sge_execd
 2981 c705185   18   0  121m 3100 1532 R 1586  0.0  79:19.08 ppgplasma
 3967 root      16   0 15416 2684 1252 S    0  0.0   1:27.61 hald
```

Figure 4.6: Utilization of 4 × Quad-Core AMD Opteron(tm) 8356 @2.3GHz node with the CentOS shows that optimized code achieved nearly linear scalability.

Chapter 5

Extension of the theoretical model

Here we present a new approach how to solve the equation for the plasma-wall transition layer with the arbitrary function for the ion source. This problem is an old one which assumes solving an integral equation of the Fredholm type or, alternatively, the Volterra type with a particular bell-shaped kernel. Due to mathematical difficulties with such physically very important kernel choice its shape was in the past approximated in several ways yielding approximate numerical solutions. Unfortunately, these solutions are valid only in limited ranges of ion temperatures. In our approach we work with the *exact* kernel, so we can obtain results which are, in principle, of arbitrary precision within an arbitrary range of the ion source temperatures. A precise solution of the plasma equation with a finite temperature ion-source is extremely important in determining the plasma parameters at the plasma sheath boundary. We obtain the ion velocity distribution at an arbitrary point in a plane-parallel discharge, which also allows for the calculation of its moments (density, temperature and higher order moments) at the edge of the system, where boundary conditions for a discharge should be known with a high degree of accuracy.

5.1 Basic considerations

The Tonks-Langmuir [70] problem of collisionless discharges is a rather old and particularly basic one but, unfortunately, solved only under various assumptions which facilitate getting the solution but restricting its range of validity to particular types of application. A general mathematical formulation of the problem can be expressed as a task to find function $\Psi(\Phi)$. Our mathematical formulation of the problem can be expressed in the form of a rather general integro-differential equation

$$\varepsilon^2 n(\Phi) \frac{1}{\Psi^3} \frac{d\Psi}{d\Phi} = 1 - \lambda \int_0^{\Phi} \Psi(\Phi') \mathcal{K} \left(\tau (\Phi' - \Phi) \right) d\Phi' \tag{5.1}$$

with a prescribed singular kernel $\mathcal{K}$, prescribed function $n(\Phi)$, arbitrary parameters ε and τ and the eigenvalue of the problem λ (Physical backgrounds and derivations will be elaborated in detail in the next sections). Due to mathematical difficulties and lack of numerical and computational resources during the last 80 years the problem has been tackled either for one or for both vanishing ε and τ. In a series of works the author of the present thesis is making attempts to obtain a reliable solution of the problem without any limitations mentioned above.

Tonks and Langmuir recognized that plasma and sheath problem can be split into so-called “plasma approximation,” with strict quasi-neutrality assumed, and “sheath approximation,” with the electric field taking the role. The corresponding two regions of the plasma-wall transition layer are often called as “the presheath” and “the Debye sheath”. They found approximate solutions for these two regions for plane, cylindrical and spherical geometries. Their “intuitive” approach of splitting the plasma-sheath equation into two parts was later put into a rigorous mathematical context by Caruso and Cavaliere [14], who employed for this purpose van Dyke’s boundary layer theory. This approach to plasma physics is now well known as the “two-scale” approximation. Following this approach Harrison and Thompson (H&T) [29] upgraded Tonks and Langmuir approximate solutions to the exact analytic one, however, holding for cold ion source distribution under the assumption of strict quasi-neutrality ($\varepsilon \to 0$). Soon after H&T publication Self [62], however, announced a complete numerical solution, i.e., with the quasi-neutrality assumption removed, but still with a singular (cold) ion source ($T_n = 0$). Emmert et al. [22] tackled the plasma solution ($\varepsilon = 0$) with a regular (warm) ($T_n \neq 0$) but artificial ion source, prepared in advance to yield a Maxwellian ion distribution function. Bissell and Johnson [10], however, decided to start from a more realistic, i.e., Maxwellian ion source and found a numerical solution within a limited range of ion source temperatures. Their model was constrained by their choice of the kernel approximation. Soon after their work Scheuer and Emmert (S&E) [61] used a better kernel approximation enabling them to find a solution holding also in the range of small ion source temperatures, but, unfortunately, not for relatively 'warm' ion sources, which is of high importance for fusion application. A number of years after S&E's work the numerical method, libraries and computing resources dramatically increased. Kos [39] with collaborators became able to employ the exact kernel instead of an approximate one. Kos et al. solved the plasma problem with a Maxwellian source without any restriction regarding the ion temperature, however, for limiting $\varepsilon \rightarrow 0$ case. For many purposes the results by Kos et al. are sufficient, but for some refined purposes they are not enough exhaustive.

From a theoretical point of view, a complete plasma and sheath equation for a regular ion source without quasi-neutrality assumption is needed primarily in order to find a reasonably acceptable definition of the plasma-sheath boundary surface. Theoretical backgrounds underlying the definition started with the famous Bohm criterion [12], formulated for the case of a negligible ion temperature which was later upgraded in fluid approximations and the kinetic approach with various physical interpretations. In the kinetic interpretation it turns out that the plasma-sheath boundary is a surface at which *slow* perturbations originated from the sheath region are completely reflective (Allen [5]). Unfortunately, the definition of 'slow' perturbations is not enough precisely defined to be of practical use, e.g., in a laboratory experiment. A more explicit alternative definition by Stangeby and Allen [65] is based on fluid theory. They showed by analyzing both plasma and sheath sides that the plasma-sheath boundary is a Mach surface, so *none* ion-sound can penetrate this surface from the sheath to the plasma side. Allen and Stangeby's arguments are essentially based on a plasma dispersion relation in comparison with the Harrison and Thompson kinetic plasma sheath criterion.

On the other hand, there is an alternative approach to identify the plasma-sheath boundary as a region of finite thickness, *rather than a surface*. This approach is based on bridging the plasma and sheath solutions via a mathematical formulation of the intermediate scale, enabling matching plasma and sheath solutions via a uniformly valid approximate solution. While this approach is well established in fluid model and kinetic model for a cold ion source (see e.g., articles of Riemann [49, 53] and references therein) the scaling rules for warm ion sources are still under consideration. A highly reliable solution of the complete plasma-wall transition equation is needed for the confirmation of these rules.

In addition to the academic question of a reasonable definition of the sheath boundary being either an infinitely thin surface or a finite-width region, there is a strong need to have a practical definition for plasma-engineering purposes. For example, fluid codes in fusion research (SOLPS, EDGE2D) are not apt to deal with sheath region, so the computational domain should be limited to quasi-neutral plasma. Attempts towards linking hydrodynamic and kinetic parameters at the plasma edge were made by Kuhn et al. [40] employing a theoretical method and further elaborated via PIC simulations by Jelić et al. [32], however, for *singular* ion sources. PIC simulations for regular ion sources were performed by Jelić et al. (to be published).

However, in addition to PIC simulations, which in fact yield somehow 'experimental' i.e., 'empirical' data, the results of PIC simulation also require their analytic and/or numerical counterpart of the results. This is the main topic of the present chapter. In this chapter we shall present the method and results obtained for arbitrary T_n for arbitrary ion-source velocity distribution and for arbitrary ε. The procedure to get such a solution of such a problem essentially consists of several steps. The electron *density distribution* over the system should be prescribed in advance (usually Boltzmann distribution). Secondly, the ion source *velocity distribution* has to be prescribed. Based on these assumptions the rigorous solution of the kinetic equation for ions is found. The potential profile (or equivalently the Ψ, which physically presents the inverse electric field) should be found from Eq. (5.1) as a function of the place of observation. The potential profile obtained from Eq. (5.1) is a 'fingerprint' for any particular choice of ion-source velocity distribution from which the resulting ion velocity distribution and furthermore its moments can be calculated, providing the boundary conditions are well defined.

5.2 Theoretical backgrounds

The general formulation of the problem in plane-parallel symmetric discharge consists in simultaneously solving Boltzmann's kinetic equation for the ion velocity distribution function (VDF) $f_i(x, v)$,

$$v\frac{\partial f_i}{\partial x} - \frac{e}{m_i}\frac{d\Phi}{dx}\frac{\partial f_i}{\partial v} = S_i(x, v) \ , \tag{5.2}$$

and the Poisson's equation

$$-\frac{d^2\Phi}{dx^2} = \frac{e}{\varepsilon_0}(n_i - n_e) \ , \tag{5.3}$$

The source term $S_i(x, v)$ on the right-hand side of Eq. (5.2) describes microscopic processes assumed for a particular scenario of interest, x is the Cartesian space coordinate, v is the particle velocity, e is the positive elementary charge, m_i is the ion mass, $\Phi(x)$ the electrostatic potential at position x, ε_0 is the vacuum dielectric constant and $n_{i,e}$ are the ion and electron densities, respectively.

The schematic diagram of the geometry of the problem is shown in Fig. 5.1. The plates at $x \pm L$ are assumed to be perfectly absorbing and electrically floating. The electrostatic potential $\Phi(x)$ is assumed to be monotonic decreasing (for $x > 0$) and is defined to be zero at $x = 0$. Below we give a comprehensive analysis of the Tonks-Langmuir model starting from the general solution of the kinetic Eq. (5.2). In the expression of the source

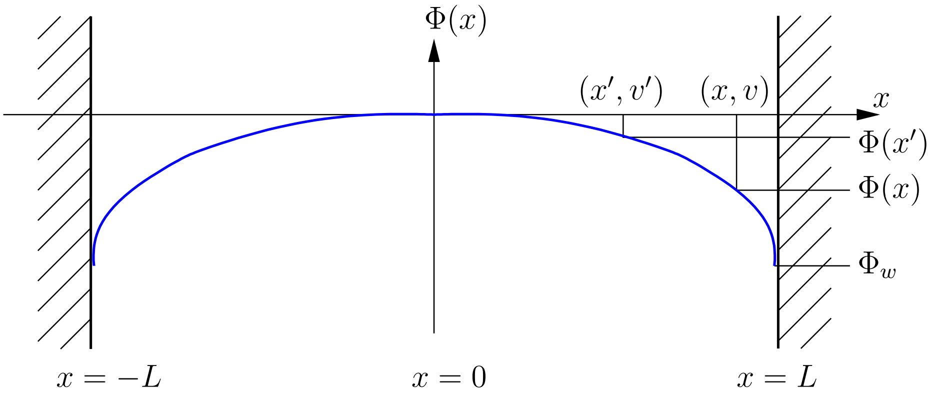

Figure 5.1: The geometry and coordinate system.

term $S_i(x, v)$, describing the ion birth due to the electron-neutral impact, the distribution function of neutrals is assumed to be quite general (this distribution function will be specified later on for specific cases).

$$S_i(v, x) = R n_n n_e(x) f_n \left(\frac{v}{v_{T_i}}\right) H \left(\frac{m_i v^2}{2}\right) , \tag{5.4}$$

where R is the ionization rate, n_n is the uniform number density of neutrals. The electrons follow the Boltzmann distribution to give the electron number density

$$n_e(x) = n_0 \exp \left\{ \frac{e\Phi(x)}{kT_e} \right\} . \tag{5.5}$$

Here n_0 is the electron density at $x = 0$. We introduce the Heaviside step function (see (2.20)) to satisfy the positiveness of the kinetic energy of the born ion. The term $f_n(v/v_{T_i})$ represents the velocity distribution function of the neutrals normalized as

$$\int_{\infty}^{\infty} f_n \left(\frac{v}{v_{T_i}}\right) dv = 1 , \tag{5.6}$$

where $v_{T_i} = \sqrt{kT_i/m_i}$ is the thermal velocity of the born ions defined by the temperature T_n of the neutral gas, $T_i \equiv T_n$. Due to the symmetry we further consider the right-hand half of the discharge, $x \geq 0$.

For the ion flux onto the wall from Eqs. (5.2), (5.4) and (5.6) we find

$$\Gamma_i = R n_n L n_{e,av} , \tag{5.7}$$

where $n_{e,av}$ represents the average value of the electron density over the system,

$$n_{e,av} = \frac{1}{L} \int_0^L n_e(x) dx . \tag{5.8}$$

The requirement that the ion current must be equal to the electron current at the wall enables us to write

$$\Gamma_i = \Gamma_e , \tag{5.9}$$

$$L R n_n n_{e,av} = \frac{1}{\sqrt{2\pi}} v_{T_e} n_0 \exp \left\{ \frac{e\Phi_w}{kT_e} \right\} , \tag{5.10}$$

where $v_{T_e} = \sqrt{kT_e/m_e}$, and m_e, T_e are the electron mass and temperature respectively, Φ_w is the wall potential. Introducing an auxiliary function

$$F_n\left(\frac{v}{v_{T_i}}\right) = \sqrt{2\pi} \cdot v_{T_i} f_n\left(\frac{v}{v_{T_i}}\right) \tag{5.11}$$

The source term (5.4) acquires the form

$$S_i(x,v) = \frac{1}{L} B n_e(x) F_n\left(\frac{v}{v_{T_i}}\right) H\left(\frac{m_i v^2}{2}\right) \ , \tag{5.12}$$

$$B = \frac{1}{2\pi}\sqrt{\frac{T_e}{T_i}\frac{m_i}{m_e}\frac{n_0}{n_{e,av}}} \exp\left\{\frac{e\Phi_w}{kT_e}\right\} \ . \tag{5.13}$$

The parameter B definers the ionization frequency ν_i and the characteristic ionization length λ_i as follows:

$$\nu_i = B\frac{\sqrt{2\pi}}{L} v_{T_i} \ , \tag{5.14}$$

and

$$\lambda_i = \frac{c_s}{\nu_i} = \frac{L}{B}\sqrt{\frac{T_e}{2\pi T_i}} \ . \tag{5.15}$$

The general solution of Eq. (5.2) with the source term (5.12) found by means of characteristics has the form

$$\begin{aligned} f_i^{\pm}(x,v) = & \pm \frac{B}{L} n_0 \int^x \frac{dx'}{\sqrt{v'^2}} \exp\left(\frac{e\Phi(x')}{kT_e}\right) F_n\left(\pm\frac{\sqrt{v'^2}}{v_{T_i}}\right) H(v'^2) \\ & + \bar{f}_i^{\pm}\left(v'^2 + \frac{2e}{m_i}\Phi(x')\right) \ , \end{aligned} \tag{5.16}$$

$$v'^2 = v^2 - \frac{2e}{m_i}\left\{\Phi(x') - \Phi(x)\right\} \tag{5.17}$$

In Eq. (5.16) $f_i^{\pm}$ denotes the distribution function of the ions moving in the positive („+”) and negative („-”) directions of the x-axis. The point (x', v') in the phase-space (see Fig. 5.1) is the point of the ion birth. The velocity v of the ion at the observation point x we find from the energy conservation law (5.17). Functions $\bar{f}_i^{\pm}(x,v)$ are the arbitrary functions corresponding to the homogeneous part of Eq. (5.2). These two arbitrary functions should be found by means of the following boundary conditions:

(a) At the center of the system, $x = 0$, the distribution function must be symmetric in the velocity space

$$f_i^+(0,v) = f_i^-(0,v) \ . \tag{5.18}$$

(b) Due to perfect absorption there are no ions on the wall surface, $x = L$, moving with a negative velocity (it means from the wall):

$$f_i^-(L,v) = 0 \ . \tag{5.19}$$

On the realization of condition (a) one has to shift the ion velocity in the form

$$v^2 \Rightarrow v^2 + \frac{2e}{m_i}\Phi(x) \ , \tag{5.20}$$

while with condition (b) we need the shifting

$$v^2 \Rightarrow v^2 - \frac{2e}{m_i}\left\{\Phi_w - \Phi(x)\right\} \ . \tag{5.21}$$

Straightforward calculations lead to the following solution of the Boltzmann kinetic equation for the arbitrary distribution function of neutrals.

$$\begin{aligned} f_i^+(x,v) = B\frac{n_0}{L}&\left\{\int_0^x dx' F_n\left(\frac{\sqrt{v'^2}}{v_{T_i}}\right) + \int_0^L dx' F_n\left(-\frac{\sqrt{v'^2}}{v_{T_i}}\right)\right\} \\ &\times \frac{1}{\sqrt{v'^2}}\exp\left\{\frac{e\Phi(x')}{kT_e}\right\} H(v'^2) \ , \end{aligned} \tag{5.22}$$

$$f_i^-(x,v) = B\frac{n_0}{L}\int_x^L dx' \frac{1}{\sqrt{v'^2}}\exp\left\{\frac{e\Phi(x')}{kT_e}\right\} H(v'^2) F_n\left(-\frac{\sqrt{v'^2}}{v_{T_i}}\right) \ . \tag{5.23}$$

In (5.22) and (5.23) the velocity v' is defined by (5.17). Here we have to mention that similar solutions are found by K.-U. Riemann [57] using the different from (a) boundary condition. For the ion number density and the ion flux from (5.22) and (5.23) there are

$$\begin{aligned} n_i(x) &= \int_0^\infty dv \{f_i^+ + f_i^-\} \\ &= 2B\frac{n_0}{L}\int_0^\infty dv \left\{\int_0^L \frac{dx'}{\sqrt{v'^2}} F_n\left(-\frac{\sqrt{v'^2}}{v_{T_i}}\right) H(v'^2)\exp\left\{\frac{e\Phi(x')}{kT_e}\right\}\right. \\ &\quad \left. + \int_0^x \frac{dx'}{\sqrt{v'^2}}\left[F_n\left(\frac{\sqrt{v'^2}}{v_{T_i}}\right) - F_n\left(-\frac{\sqrt{v'^2}}{v_{T_i}}\right)\right] H(v'^2)\exp\left\{\frac{e\Phi(x')}{kT_e}\right\}\right\} \ , \end{aligned} \tag{5.24}$$

$$\begin{aligned} J_i(x) =& \int_0^\infty dvv\{f_i^+ - f_i^-\} \\ =& B\frac{n_0}{L}\int_0^\infty dvv \int_0^x dx' \frac{1}{\sqrt{v'^2}} \exp\left\{\frac{e\Phi(x')}{kT_e}\right\} H(v'^2) \\ & \times \left\{F_n\left(\frac{\sqrt{v'^2}}{v_{T_i}}\right) + F_n\left(-\frac{\sqrt{v'^2}}{v_{T_i}}\right)\right\} \end{aligned} \tag{5.25}$$

In order to find the floating potential by comparing the ion and the electron fluxes onto the wall, we further analyze the expression of ion flux $J_i(L)$ from (5.25) at $x = L$.

In the present work we pay our attention to the case of Maxwellian ion source velocity distribution. It is a relatively simple task to formulate the problem but a rather demanding one to perform numerical calculations from many points of view like e.g., numerical reliability and stability up to the CPU cost per simulation case. It seems to be a logical path to be pursued here to first pursue previous works and to extend previously well established results to the extent possible via employing Maxwellian ion-source velocity distribution of arbitrary T_n and without any limit of the system length, i.e., any restriction of ε.

Analogous solutions with other types of ion velocity distribution function sources as the so-called “waterbag” or a “shifted Maxwellian” distribution function under the same assumptions of the finite ion source and finite ε will be elaborated in the future as the CPU price will decrease. The waterbag model is in this thesis tackled roughly in Appendix A, to illustrate that such a simple velocity distribution is in fact equally difficult as a more complex one if one wants to obtain a solution. The main investigation here is devoted to the Maxwellian shaped ion source VDF. This is a very plausible idea, i.e., that the neutrals (or ions) come from the core to the SOL (Scrape-off Layer) region in Tokamak devices with such a velocity distribution, starting their “new life” with a “new identity”. Our task is to reconstruct this new identity based on an initial one. It turns out that the new identity surprisingly differs from the original one. For example, the final temperature differs for an order of magnitude from the temperature of originally ”injected” i.e., generated particles. Other features, like moments of final velocity distribution and their shapes over the system follows from the solution for function Ψ and consecutive solutions for the final local ion-velocity distribution. This method is pursued as follows in the next Section based on the reference assumption of the Maxwellian velocity distribution of ions as generated or injected in the system.

5.3 Maxwellian distribution of neutrals

For the Maxwellian source the auxiliary functions (5.11) is

$$F_n\left(\frac{v}{v_{T_i}}\right) = \exp\left(-\frac{v^2}{2v_{T_i}^2}\right) \ . \tag{5.26}$$

Introducing the dimensionless quantities

$$\begin{aligned} &u = \frac{v}{\sqrt{2}c_s} \ , \quad \frac{e\Phi(x)}{kT_e} \longrightarrow \Phi(x) \ , \quad \frac{x}{L} \longrightarrow x \ , \\ &n = \frac{n_i}{n_0} \ , \quad j = \frac{J_i}{n_0 c_s} \ , \quad \tau = \frac{T_e}{T_i} \ , \quad c_s = \sqrt{\frac{kT_e}{m_i}} \ . \end{aligned} \tag{5.27}$$

The expressions for the ion density and the ion flux (5.24), (5.25) can be simplified to

$$\begin{aligned} n(x) = 2B &\int_0^\infty du \int_0^1 dx' \exp(\Phi(x')) \\ &\times \frac{\exp\left(-\tau\{u^2 - \Phi(x') + \Phi(x)\}\right)}{\sqrt{u^2 - \Phi(x') + \Phi(x)}} H(u^2 - \Phi(x') + \Phi(x)) \ , \end{aligned} \tag{5.28}$$

$$\begin{aligned} j(L) = 2\sqrt{2}B &\int_0^\infty duu \int_0^1 dx' \exp(\Phi(x')) \\ &\times \frac{\exp\left(-\tau\{u^2 - \Phi(x') + \Phi(x)\}\right)}{\sqrt{u^2 - \Phi(x') + \Phi(x)}} H(u^2 - \Phi(x') + \Phi(x)) \ . \end{aligned} \tag{5.29}$$

The integral over x' in (5.28) can be split into two parts

$$\int_0^1 dx'(\dots) = \int_0^x dx'(\dots) + \int_x^1 dx'(\dots) \ . \tag{5.30}$$

In the first interval $(0, x)$ of the integration

$$\Phi(x') - \Phi(x) \geq 0 \tag{5.31}$$

and in the second

$$\Phi(x') - \Phi(x) \leq 0 \ . \tag{5.32}$$

This allows us to use the cut-off property of the H-function and finally we find

$$\begin{aligned} n(x) = B\int_0^L dx' \exp[\Phi(x')] \\ \times \exp\left[\frac{\tau}{2}\{\Phi(x') - \Phi(x)\}\right] \mathrm{K}_0\left\{\frac{\tau}{2}|\Phi(x') - \Phi(x)|\right\} \ , \end{aligned} \tag{5.33}$$

$$j(1) = \sqrt{\frac{2\pi}{\tau}} B\int_0^L dx' \exp[\Phi(x')] \ . \tag{5.34}$$

In obtaining (5.33) also the relation

$$2\int_0^\infty \frac{\exp(-\tau x^2)}{\sqrt{x^2+a^2}} = \exp\left(\frac{\tau}{2}a^2\right)\mathrm{K}_0\left(\frac{\tau a^2}{2}\right) \tag{5.35}$$

is used. Here $\mathrm{K}_0(z)$ is the modified Bessel function of zeroth order. Eq. (5.33) coincides wit the expression for the ion density used in Ref. [10] and Ref. [61]. In the limit of the cold source, $T_i \to 0$ and the auxiliary function reads

$$F_n\left(\frac{v}{v_{T_i}}\right) = \sqrt{2\pi} v_{T_i}\delta(v) \ , \tag{5.36}$$

($\delta(z)$ is the Dirac δ-function) and for the ion density we find expression

$$n(x) = \frac{1}{\sqrt{2}}\int_0^x \frac{dx'}{\lambda_i}\frac{\exp[\Phi(x')]}{\sqrt{\Phi(x') - \Phi(x)}} \tag{5.37}$$

discussed previously in detail in [49, 53]. In (5.37) λ_i is defined by (5.15). In notation (5.27) Poisson's Eq. (5.3) acquires the form

$$\begin{aligned} &B\int_0^1 dx' \exp[\Phi(x') - \Phi(x)] \exp\left[\frac{\tau}{2}\{\Phi(x') - \Phi(x)\}\right] \mathrm{K}_0\left\{\frac{\tau}{2}|\Phi(x') - \Phi(x)|\right\} \\ &= 1 - \varepsilon^2 \exp(-\Phi)\frac{d^2\Phi}{dx^2} \end{aligned} \ , \tag{5.38}$$

where $\varepsilon = \lambda_D/L$ it the arbitrary parameter and $\lambda_D = \sqrt{\epsilon_0 k T_e/e^2 n_0}$ is the electron Debye length. Eq. (5.38) describes the potential profile for the arbitrary temperature of the source. Using (5.10) and (5.34) for finding the floating potential of the wall we obtain the relation

$$\exp(\Phi_w) = 2\pi\sqrt{\frac{m_e}{m_i}}\sqrt{\frac{T_n}{T_e}} B\int_0^1 dx' \exp[\Phi(x')] \ . \tag{5.39}$$

for determining the wall potential.

5.4 Numerical method

We performed a number of simulations for various T_n, each with varied ε taking values 0.0001, 0.003, 0.006, 0.001, 0.003, 0.006, 0.01, 0.01, 0.03, 0.006 and 0.1. It turns out that a numerical solving of the integro-differential equation of type Eq. (5.38) is an extremely difficult problem primarily due to the non-uniform grid employed in the plasma sheath problem solving via the S&E method. The problem arises due to the second derivative of the electric field for which we did not find an optimum numerical algorithm with a well-defined accuracy. However, we found some rules which show that as the ion temperature increases the results become more and more insensitive on ε.

For calculation of the second derivative we implemented piecewise Lagrangian polynomial interpolation [19] of order 2, 3 in subintervals with small Φ gradients. For the second derivative 5 point Lagrangian interpolation is used as a basis for derivative. For the last point 4 point second derivative of Lagrangian interpolation is used. Although such approximation is often considered to be too expensive for numerical computation, it possesses beautiful symmetry and with a modified (weighted) form is comparable in speed to other approximations.

The main difference from $\varepsilon = 0$ case is that wall potential Φ_w is now a free parameter that can be arbitrary. For a gases like Hydrogen used in fusion the Φ_w can be approximated from floating wall condition in Eq. (5.39) for $\varepsilon = 0$ case. Integro-differential equation (5.38) becomes with specified $\Phi(1) = \Phi_w$ boundary condition a relaxation problem in a numerical sense although the whole system is still floating. For initialization we implemented the following function that assures monotonous initial "shot" to the endpoint

$$\Phi[i] = \frac{\Phi_w}{1 - \exp(1)} \left[1 - \exp\left(\frac{i}{\mathrm{N}} \right) \right] , \tag{5.40}$$

disregarding λ_1 and λ_2. When initial profile is relaxed and converged we employ additional dual iteration of the potential profile and endpoint Phi_w with similar smooth stepping technique to assure correct bounary condition (5.39) for a given gas.

Chapter 6

Results

6.1 The two-scale limit $\varepsilon = 0$

The Fredholm equation with the Bissell & Johnson kernel has a solution for the electric potential lying between the analytic value of the Tonks Langmuir limit ($\Phi > \Phi_s = -0.854$ at the sheath entrance) and zero (at the center plane of symmetry). The particular value of Φ_s depends on the ion-source temperature. In Fig. 6.1 we show the potential profiles as calculated in a wide range of ion temperatures (solid lines) in contrast to B&J (scattered). It can be seen that both sets of B&J and our results closely overlap in the range of temperatures where B&J obtained their results. There is, however, a small discrepancy for $T_i = \{0.5, 1, 2, 4\}$ which may be ascribed to B&J's errors in the kernel as we demonstrated in Fig. 3.2. There is an additional error in the presentation of B&J's results in Fig. 6.1, which originates from the fact that we did not have their exact data available but used scanned data from Fig. 4 from their article [10] instead.

This issue, however, is not of primary importance to the present work, since we are interested in the method without approximation. Our next step is to compare our results for the electric potential with those obtained with a more reliable kernel as employed by Scheuer and Emmert. In Fig. 6.2 we show our potential profile with S&E's result, which was presented with one single curve i.e., obtained for $T_i = 1$. The shape of their single curve differs from our results and thus also from those of B&J.

Our other investigations (to be published) performed via the PIC simulation [9, 76] (in particular with BIT1 [73]) have shown that the S&E curve

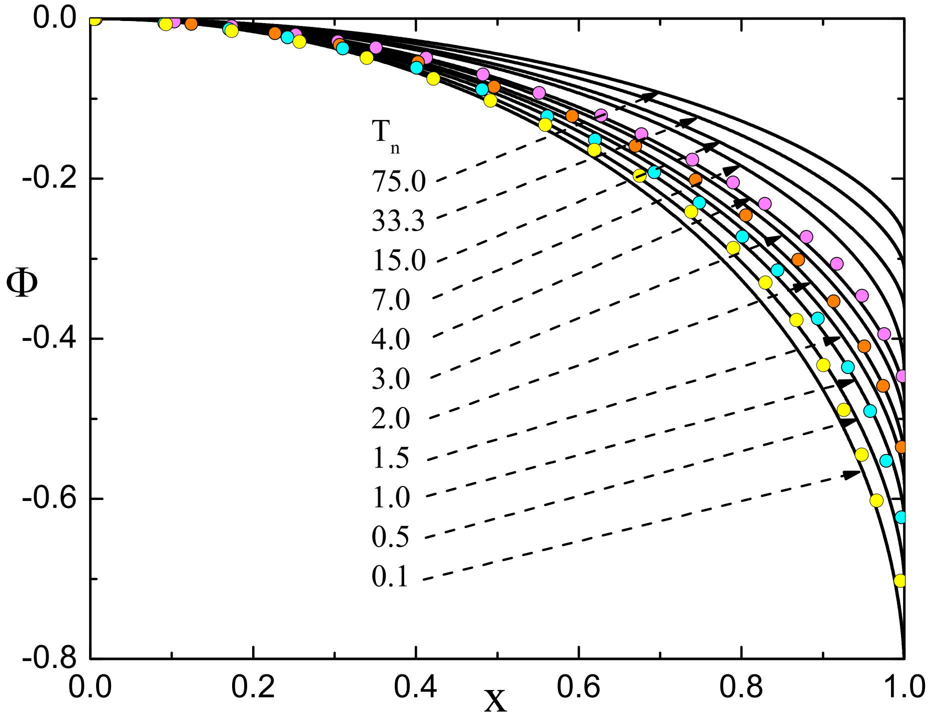

Figure 6.1: (Color) Potential profiles for various ion-source temperatures as obtained by us with the exact kernel (solid lines) and by Bissell and Johnson with their approximate kernel (scattered).

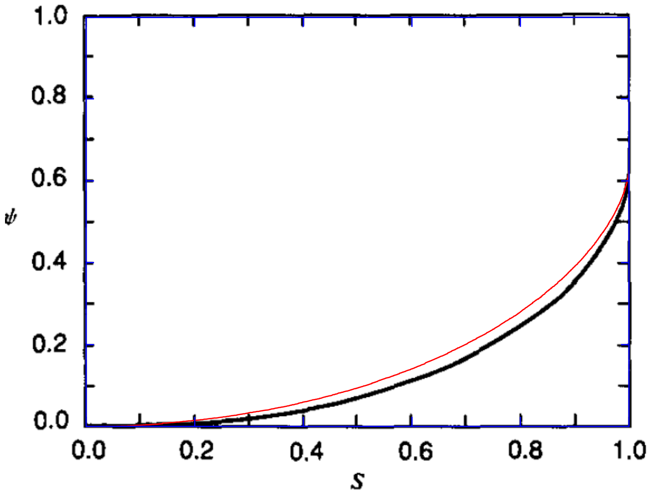

Figure 6.2: Comparison of the potential profile with S&E for $T_i = T_e$. The original scan is overlayed with our potential profile and axis box.

perfectly fits the case with a uniform ion source rather than with one proportional to the electron density.

It turns out definitely that S&E in fact worked with the constant ion source and NOT with the source proportional to the electron density. The question arises why their results at the plasma boundary are in such excellent agreement with B&J and ours. In our article [33] we give a straightforward answer to this question: It turns out that the plasma parameters at the boundary are invariant to the ionization source profile.

The dependence of the potential Φ_s at the quasi-neutral plasma (presheath) boundary on the ion source temperature is shown in Figs. 6.3. The end or the breaking point of the solution i.e., plasma boundary Φ_s, corresponds to the place where the electric field becomes infinite. In Fig. 6.3(a) we show the dependence of the breaking point in a “zoomed-in” range where the S&E results are taken from their article. It is clear that our results overlap with S&E’s results. The small discrepancy can be ascribed to the fact that our method is a very advanced one, i.e., based on at least 1600 cells (whereas S&E used 100 cells) and that we used the exact kernel instead of their approximate one. Our solution in an extremely wide range of ion source temperatures is shown in Fig. 6.3(b).

Once the potential profile is known, it determines the actual velocity distribution at the point of observation, provided the source velocity distribution is exactly specified, as is the case with the B&J model and the present investigation.

Fig. 6.4 illustrates our velocity distributions for the cases of a small and moderately high ion source temperatures in comparison with the cold-ion-source case (Tonks and Langmuir). It can be seen that for small ion source temperatures the shape of the velocity distribution resembles the T&L limit, while with higher ion source temperatures it resembles S&E’s results. In Fig. 6.5 ion velocity distribution is shown at various observing points ($\Phi(x)$ on the right side of the discharge) for two distinct ion-source (neutral gas) temperatures. The first one [Fig. 6.5(a)] corresponds to ”classic” laboratory investigations, while the second one [Fig. 6.5(b)] is applicable to fusion relevant plasmas. In both Figures [(a) and (b)] plasma boundaries $\Phi_s(x_s)$ are marked in bold solid lines. It is evident that ion velocity distribution at those particular points “suddenly” lacks ions with negative ion velocities. This observation should be redefined as a new plasma-sheath criterion. In fact, this

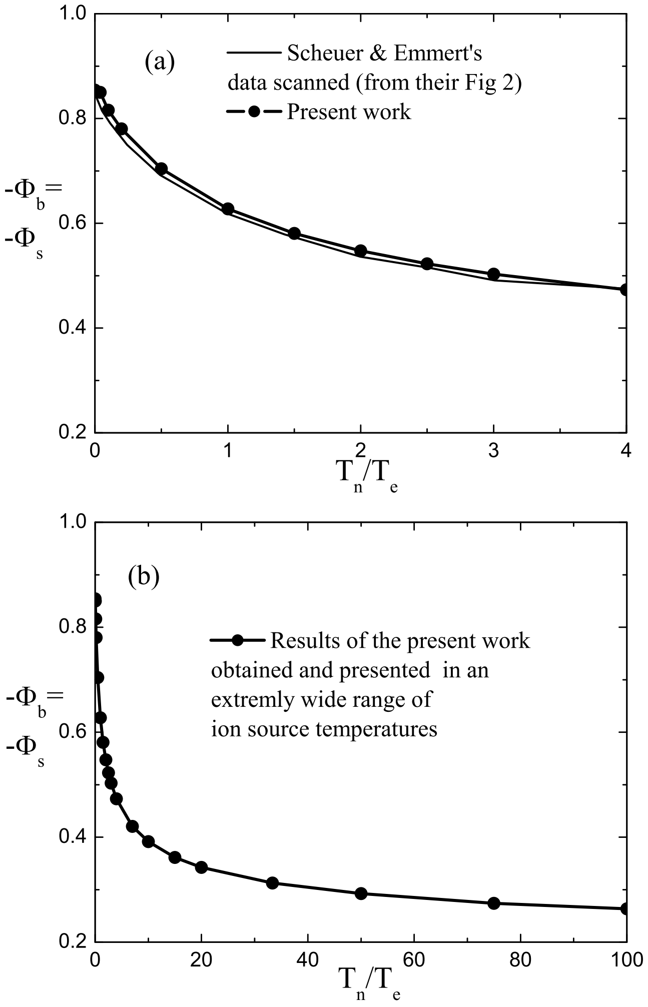

Figure 6.3: The plasma sheath boundary potential in a limited range of ion source temperatures, where the S&E approximate kernel is valid, in comparison with our results (a), and in a wide range of of the ion source temperatures (b), where we employed the exact kernel.

was already been done to some extent by Block and Fälthammar [11] via their criterion for Double Layer formation existence.

Once the ion velocity distribution as a function of position (or equivalently, of the potential corresponding to the latter) has been found, one can calculate from it fluid quantities such as density, particle flux, total energy flux, temperature, and higher moments of velocity distribution like heat flux, etc., as described in section 2.4. While Bissell and Johnson made a step for-

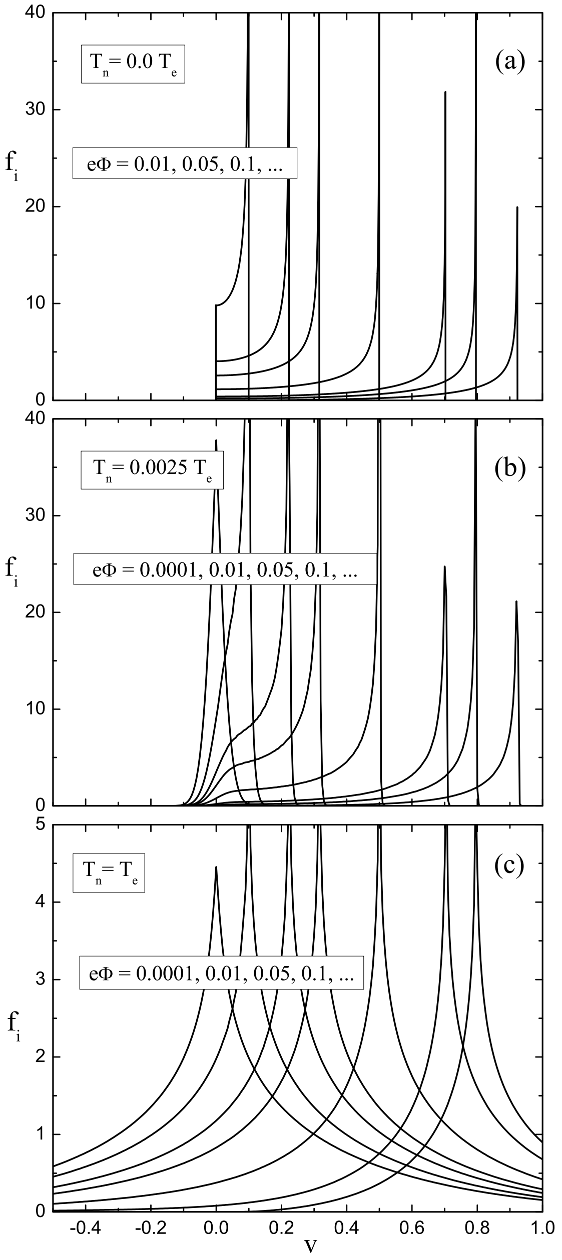

Figure 6.4: The analytic velocity distribution by Tonks and Langmuir in the case of the zero-ion-temperature source in comparison with our results with a finite ion temperature source.

ward by analytically preparing the integrals of the moments of the velocity distribution function for a faster numerical calculation, Scheuer and Em-

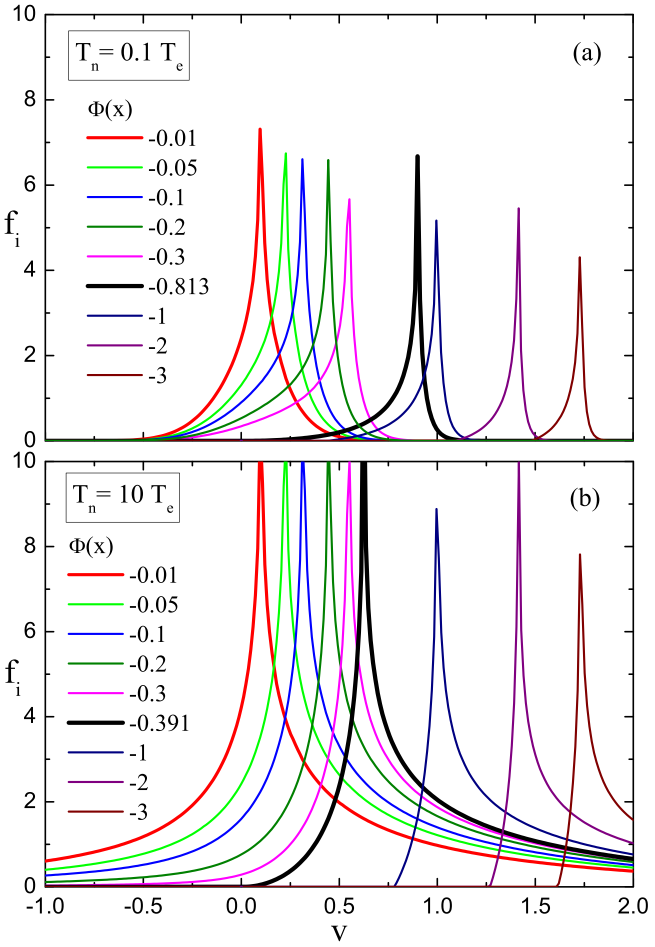

Figure 6.5: (Color online) Velocity distributions for (a) $T_n = 0.1$, and (b) $T_n = 10$.

mert [61], performed direct numerical calculation using some kind of "brute force". The latter is a more expensive, yet more universal method which is applicable to arbitrary analytic and experimental velocity distributions, so we prefer to apply it in our present and future work. In Fig. 6.6(a) we illustrate the ion density profiles in a logarithmic presentation for three particular temperatures (solid lines) in comparison with the electron density, which, by the definition of the model, is Boltzmann-shaped. As expected, the ion densities follow the straight line in the region of quasi-neutrality and more or less sharply change such behavior at the positions of the field singularity (plasma boundary).

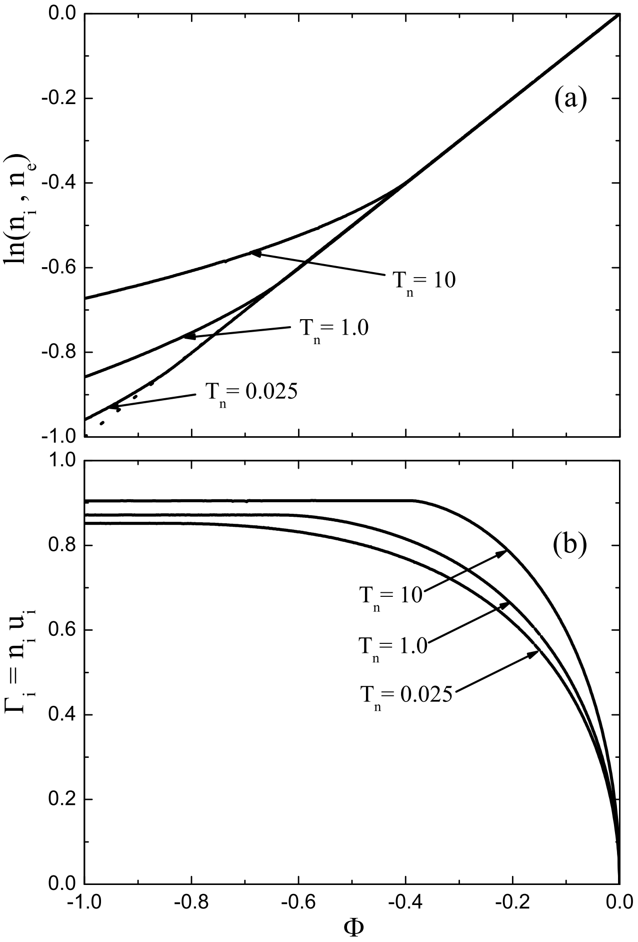

Figure 6.6: (a) Ion and electron densities in a logarithmic presentation as a function of local potential $\Phi(x)$. (b) The ion flux as a function of $\Phi(x)$.

In Fig. 6.6(b) we show the corresponding dimensionless ion fluxes [defined by Eq. (2.28)], also calculated directly from the ion velocity distribution. Ion flux is seen to increase in the plasma region but to become practically independent of the sheath potential to the left of the plasma boundary. In the sheath region, however, relevant assumptions of the model become invalid, so they should be ignored.

As pointed out in the chapter 4, the quantity B is calculated from equality Eq. (4.13) iteratively in a numerical procedure. With the density calculated from the velocity distribution, it turns out a posteriori that the product Bn_i is constant, i.e., with a high degree of accuracy equals unity. The result of calculating B as a function of the source temperature at an arbitrary point (e.g., near the center of the system) is illustrated in Fig. 6.7(a).

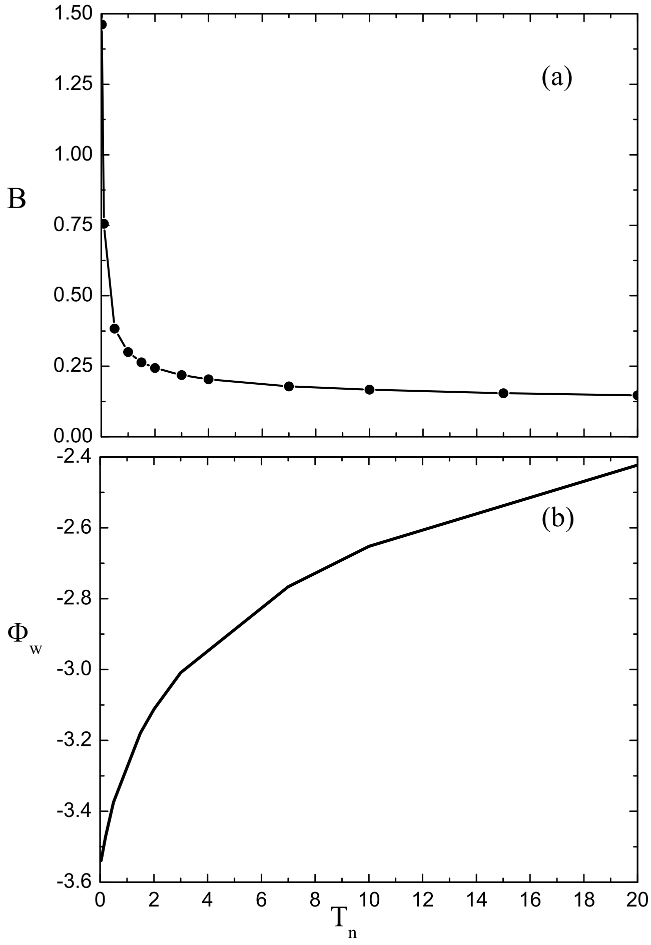

Figure 6.7: The dependence of B (a) and of the wall potential (b) on the ion source temperature.

The next step is to calculate the normalized average plasma density over the system from $\int_0^1 n_e(\phi(s))ds$ and, based on this, to calculate the wall potential with known B. The result is shown in Fig. 6.7(b) for a wide range of ion source temperatures. These results match with those of B&J; however, our results are not limited to the ion source (neutral) temperatures.

Fig. 6.8 shows the effective ion (final) temperature T_i as a function of the local potential for various ion source temperatures T_a. The upper figure shows the distribution of the ion temperature in a wide range of ion source

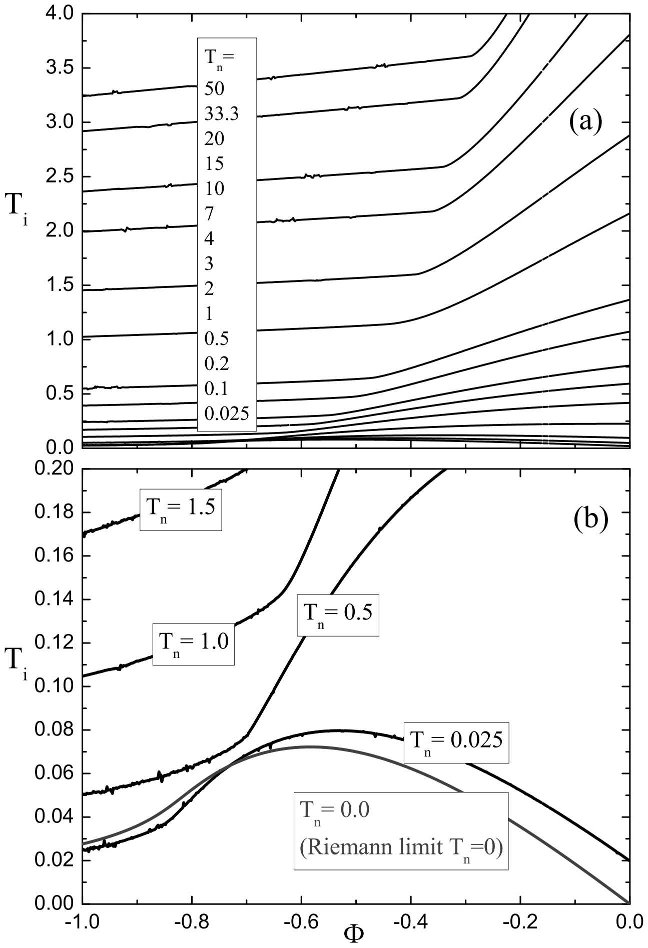

Figure 6.8: Profiles of the ion temperature T_i [defined according to Eq. (2.31)] for various ion source temperatures.

temperatures, while the bottom figure represents a "zoom-in" for a very cold ion source in comparison with a result obtained by using Riemann's software[57] for the limit of the zero ion source temperature. It is evident that high ion source temperatures yield a final temperature which is smaller by an order of magnitude. This fact is of high importance for both general plasma physics and for fusion investigations, where the ions from the core region penetrate the SOL region with rather high temperatures but their temperature might suddenly drop therein.

For a better insight into this effect, Fig. 6.9 shows the dependence of the effective temperature both at the center of the discharge and at the plasma

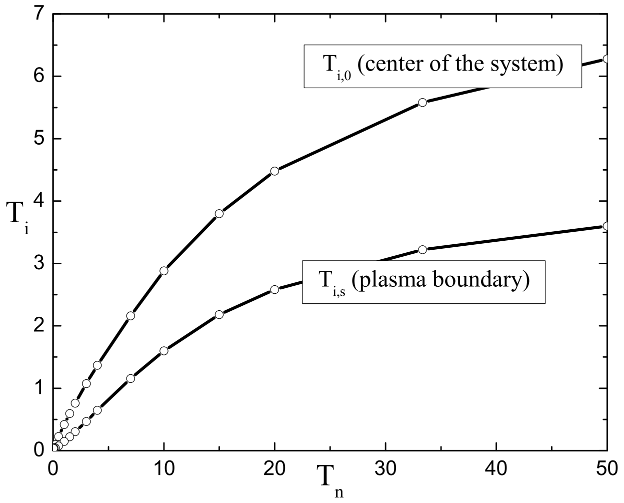

Figure 6.9: the ion temperature at the center and the edge of plasma for various ion source neutral temperatures.

edge as a function of the ion source temperature. It is apparently strange that the final ion temperature is lower by almost an order of magnitude than the ion source temperature. This is a consequence of the ion "cooling" due to energy losses at the boundary. Our result on the final temperature T_i is in good agreement with the results given by B&J for several particular cases.

Some doubts may appear regarding the numerical calculation of the moments from the final velocity distribution due to its singular character. We resolve this dilemma by comparing T_i as calculated with extreme precision via Riemann's software and with our direct integration method. We used our own software, which is based on Eq. (5.38). In the example in Fig. 6.10 this software is applied to the case of an extremely small value of ε ($\varepsilon = 10^{-5}$) for an extremely small ion source temperature ($T_i = 0.002$). The temperature profiles obtained by means of these approaches are illustrated in Fig. 6.10.

Regarding the normalization lengths of plasma, it should be noted that such various lengths can be defined in an arbitrary manner. In fact, it is clear from condition $\int f(v)dv \equiv \int Cf(v)d(v/C) = 1$ that in the Boltzmann equation we can also use any normalization of the velocity distribution with an arbitrary constant C, as well as put any other normalized length x/ℓ, with ℓ an arbitrary constant length, instead of x/L. The "proper" normalization should be decided on the basis of further purposes. While the first normal-

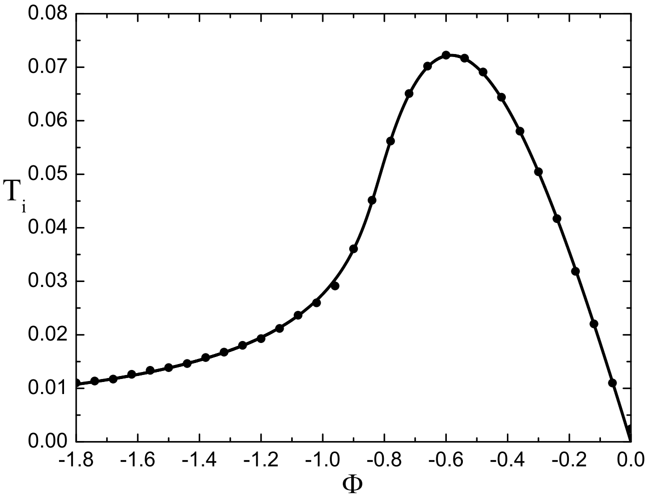

Figure 6.10: Comparison of the results obtained via Riemann's program (solid line) and ours obtained via the direct integration method used in the present work (scattered). For this comparison we used our software based on Eq. (5.38) applied to the case of an extremely small $\varepsilon = 10^{-5}$ for an extremely small ion source temperature ($T_i = 0.002$).

ized length (x/L) just corresponds to a calculation domain extending from 0 to 1, the second one (x/ℓ) is desired to be a physical quantity of interest for particular purposes. According to H&T [29] and Self [62], the proper normalization in the limit of the vanishing ion source temperature and vanishing ε is an analytic value that depends on the ionization mechanism and in the case of ionization proportional to the electron density yields the exact value $x_s = 0.405\ldots$ (plasma boundary, where the electric field becomes singular). Riemann, however, prefers to use a slightly different normalization (see e.g. Ref. [53]) which yields the said value multiplied by $\sqrt{2}$, i.e., $x_s = 0.572\ldots$. Comparing the derivation by B&J with that of Riemann we found that the re-normalization

$$\frac{x}{L} \to \frac{x}{\ell} \equiv B\sqrt{2\pi T_i} \tag{6.1}$$

(where T_i is normalized to T_e) is equivalent to rescaling the system to the ionization length ℓ. The result is shown in Fig. 6.11, however not only for the "classical" case of the vanishing ion source temperature but, instead, for arbitrary values thereof. Our "empirical" extension of Harrison-Thompson's result to an arbitrary ion source temperature is very important for application to the theory of the intermediate plasma-sheath region, which due to lack of

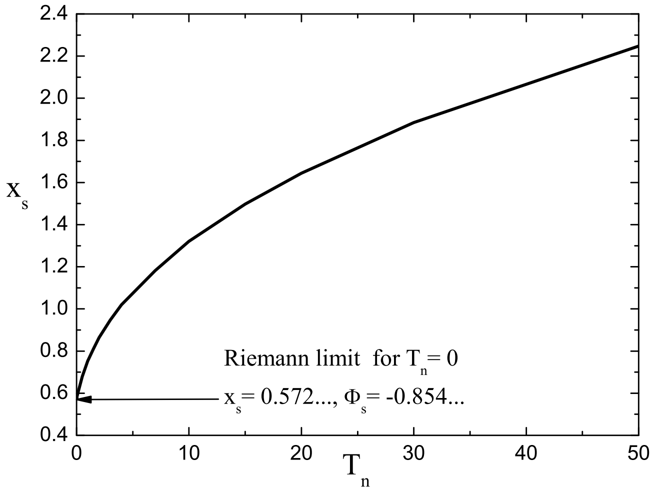

Figure 6.11: Renormalized presheath length x_s as a function of the ion-source temperature.

any data on the ionization length in the case of the finite ion temperature up to now has been limited to the “cold” ion source case only (see e.g., recent works by Riemann [53]).

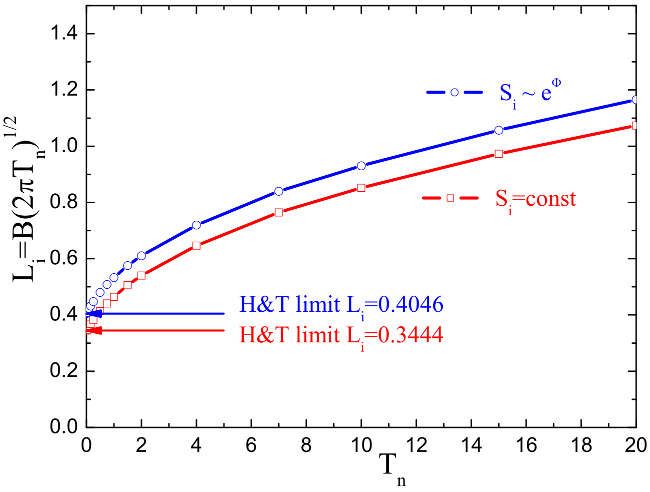

Figure 6.12: Ionization lengths of the Maxwellian-source and flat-source ionization mechanisms as defined by H&T.

Fig. 6.12 represents the dependence of the characteristic ionization length (5.15) on the ion-source temperature. In this we have to keep in mind that the re-normalization is adjusted to “taste” of H&T, but can be converted in a trivial manner to e.g., according to works of Riemann via multiplying by a factor of $\sqrt{2}$.

After obtaining all desired quantities like the ion density and temperature, other derived quantities can be calculated. One such quantity, which has recently been introduced in plasma physics by Kuhn et al.[40] and Jelić et al. [32], is the “local polytropic coefficient”, which is of high importance to plasma sheath determination. In fact, for engineering purposes the definition of the plasma sheath boundary as the point where the ion-sound velocity equals the fluid ion velocity might be of considerable interest. However, determining the ion-sound velocity requires the knowledge of the local ”ion polytropic coefficient”γ. So far there has not been a reliable model to treat this quantity for the regular ion source temperature case. Our solution enables one to further investigate this issue in detail in the near future. Our Fig. 6.13 is just an illustration of the behavior of the polytropic coefficient, which is important in local ion sound velocity calculations. It has been suggested by Kuhn et al. [40] that the maximum of γ may be a possible means of defining the plasma-sheath boundary. Our Fig. 6.13 confirms that this “coincidence” still holds for low ion source temperatures (curve $T_i/T_e = 0.1$). Apparently, the deviation from this rule becomes stronger, as the ion temperature increases.

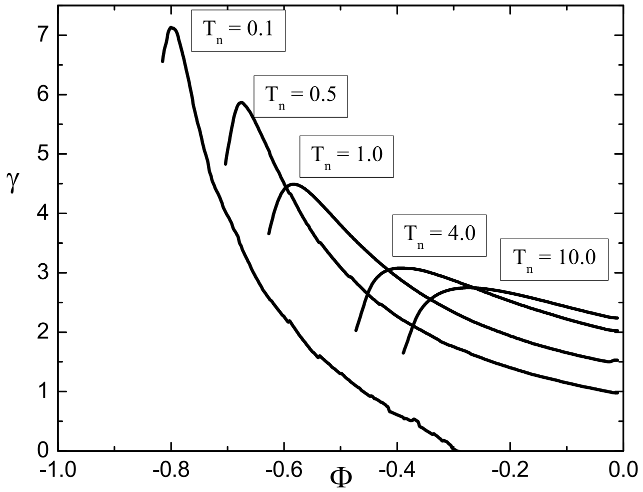

Figure 6.13: Illustration of the local ion polytropic coefficient for several ion source temperatures.

For the characterization of sheath edge singularity we performed numerous simulations with high grid densities in order to obtain sufficiently accurate results from which we could find safely the power α in the formula

$$(\Phi_s - \Phi) \to c(x_s - x)^{\alpha} \; . \tag{6.2}$$

Riemann's analytic solution [57] for $T_n = 0$ is exactly $\alpha = 1/2$. For $T_n > 0$ (that means $T_n = O(1)$) he expects $\alpha = 2/3$ (again exactly, independently on the detailed value of T_n). For α estimation we performed given model fitting with with different number of end-points.

As it was unclear what is the best approximation we initially compared two approximation models: nonlinear and logarithmic non-linear. With logarithmic approximation the logarithm of the exponential model is a linear model for the logarithm of the data and thus better fits points near x_s. It turned out that the question of the sufficient number of points was much larger than initially assumed and this ruled out logarithmic fitting. Usually the width of approximation is under 10^{-4}, depending on the grid and the convergence status of input data. It was observed that even when we reach saturated solution when observing Φ_s and B, additional huge number of iterations can increase $\alpha_{\max}$ and decrease the number of points for optimal approximation.

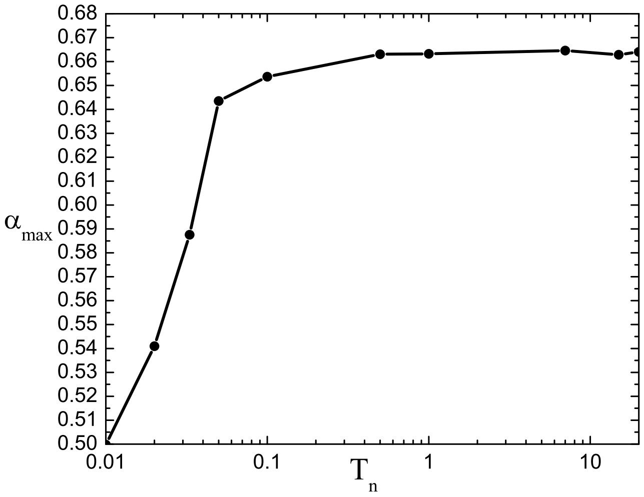

Figure 6.14: Dependence of $\alpha_{\max}$ on the ion-source temperature for logarithmic scale of T_n.

Dependence of $\alpha_{\max}$ on T_n is shown in Fig. 6.14. We used different grids to prove invariance of the $\alpha_{\max}$ on the grid. As pointed before, the optimal number of approximation points is related also to grid setup. For $T_n \geq 1$ we see that approximation came within 1% to the theoretical value of $\alpha = 2/3$. In the area $T_n \leq 0.1$ we observe a gradual drop of α to the theoretical limit for $\alpha_0 = 1/2$.

6.2 Unified plasma and sheath solution $\varepsilon > 0$

The extension of the $\varepsilon = 0$ model to the general case where $\varepsilon > 0$ was described in the previous chapter. The following results were obtained with the unified program code that still maintains both models. The computational grid and almost the entire code remain the same, although numerical models are different. Our results were compared using K.-U. Riemann's software `duo_eps` [57], which is valid only for $T_n = 0$ and $\varepsilon > 0$. It should be noted that the procedure applied by Riemann is a reversal of our method. Our results are obtained with the fixed system length $L = 1$ first. From the engineering point of view this is a natural way to deal with the system of interest. After finding a solution we are able to rescale our results according to any desired coordinates, i.e., in accordance with formula $x_s = \sqrt{2\pi}\sqrt{T_i}B$. Our results of the potential profiles with $L = 1$ are shown in Fig. 6.16. In Fig. 6.17 we show the results after rescaling our results.

High grading of the grid when approaching $x = 1$ enabled us to calculate for even smaller $\varepsilon \leq 0.0006$. A zoomed potential profile in Fig. 6.18 shows such case along with $\varepsilon = 0$ result that appears like straight line. Even higher zoom would show high (infinite) electric field at the endpoint.

Fig. 6.19 shows dependence of potential profiles for a given ε. It should be noted that our cases use hydrogen as a basis for determining wall potential Φ_w, while Riemann prefers argon. To give some comparison within “cold” case we show in Fig. 6.20 results our program for $T_n = 0.01$ and compare it with $T_n = 0$ for different ε. Curves align each other well except for the $\varepsilon = 0.1$ case where we observe “undershoot” similar to $\varepsilon = 0.1$ case in Fig. 6.17. Such discrepancy can be prescribed to low grid used in this cases and to numerical difficulties with low T_n. In any case $\varepsilon = 0.1$ can hardly be considered as a plasma.

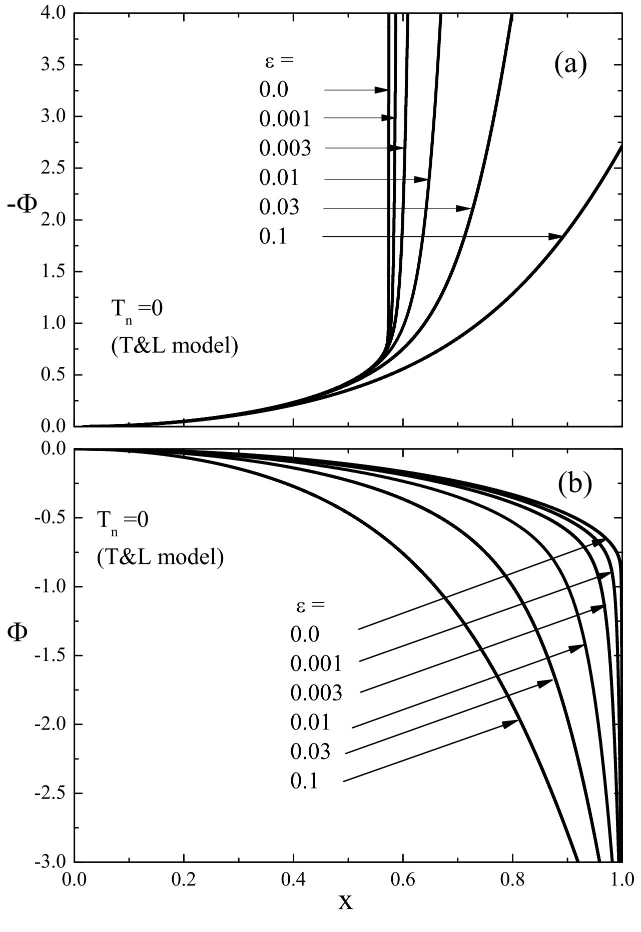

Figure 6.15: Potential profiles obtained by using Riemann's software (a) for an infinitely small ion source (neutral) temperature with varied ε. profiles for various ϵ. In Figure (b) we show the same results rescaled to the system length $L = 1$, based on an arbitrarily chosen wall potential.

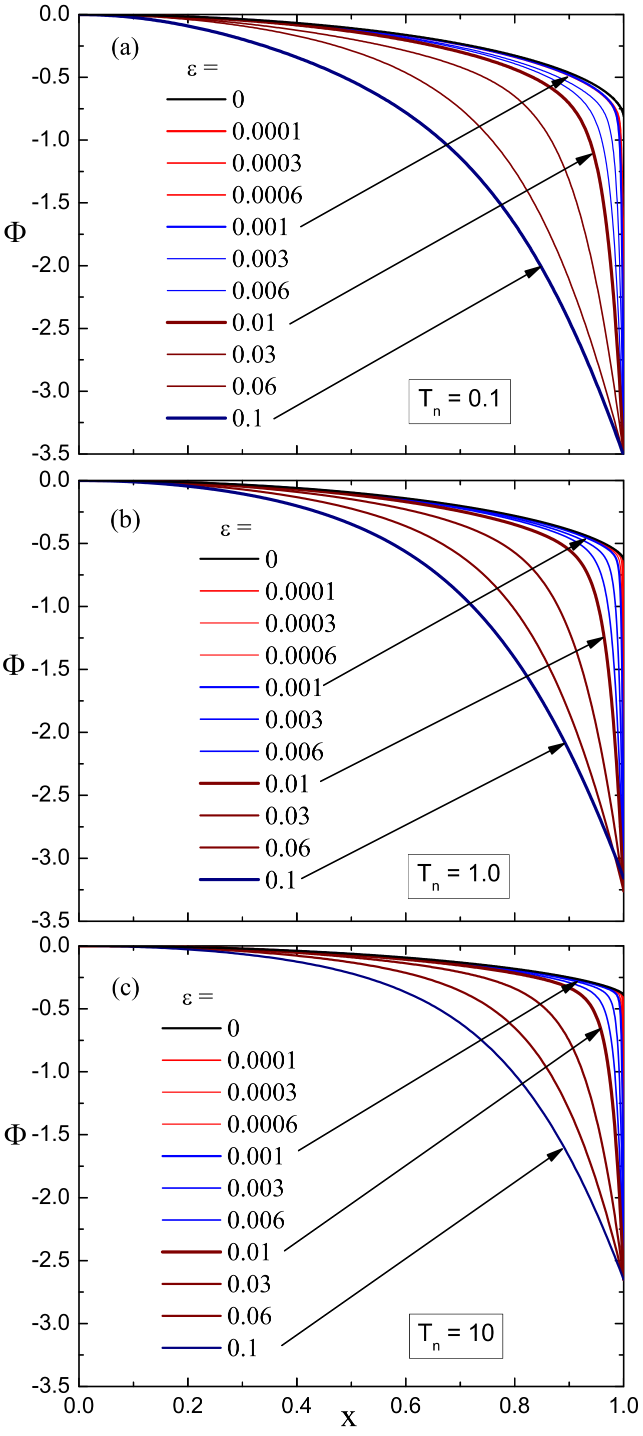

Figure 6.16: Potential profiles for various ε and (a) $T_n = 0.1$, (b) $T_n = 1.0$, (c) $T_n = 10.0$. Our results obtained with the fixed system length $L = 1$. Wall potential Φ_w is dependent on T_n. Hydrogen was used for this simulation.

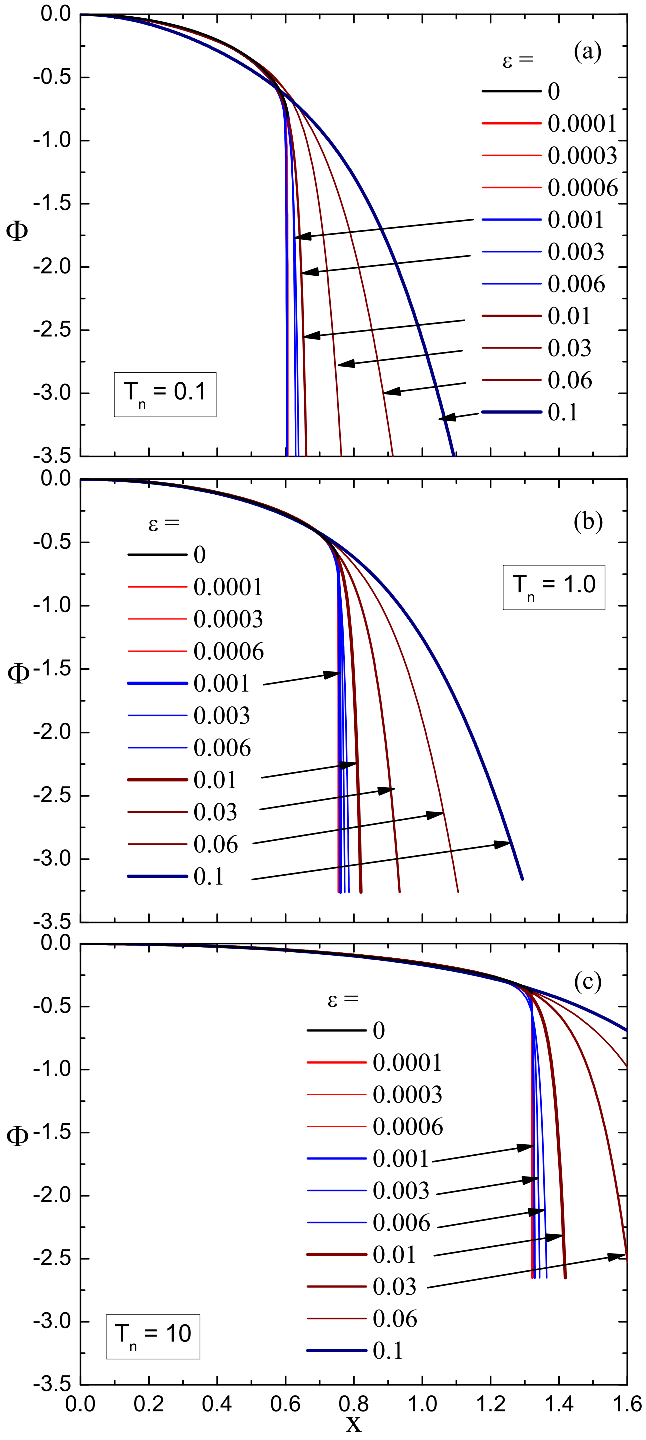

Figure 6.17: Potential profiles for various ε and (a) $T_n = 0.1$, (b) $T_n = 1.0$, (c) $T_n = 10.0$. Rescaled results according to $x_s = \sqrt{2\pi}\sqrt{T_i}B$. From (b) it can be observed that wall potential Φ_w also changes with ε.

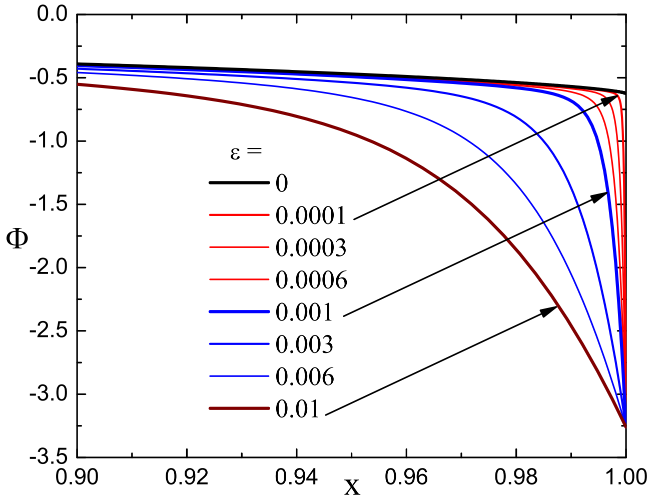

Figure 6.18: Potential profiles for various ε and $T_n = 1$ with a zoomed x range shows high precision results with $\varepsilon \leq 0.0006$.

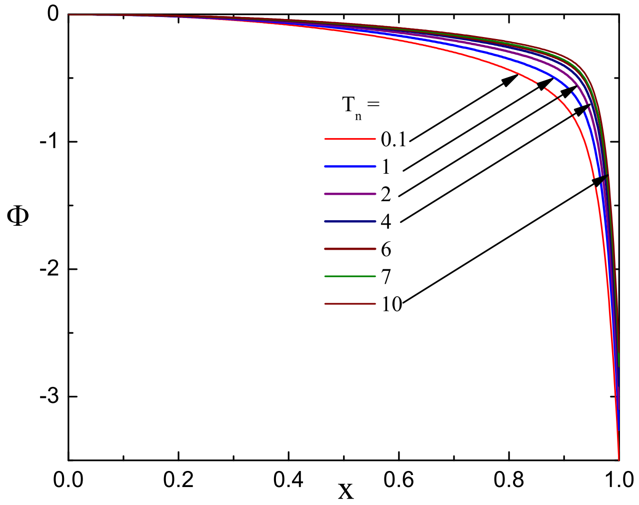

Figure 6.19: Potential profiles for various ion-source temperatures and fixed $\varepsilon = 0.01$.

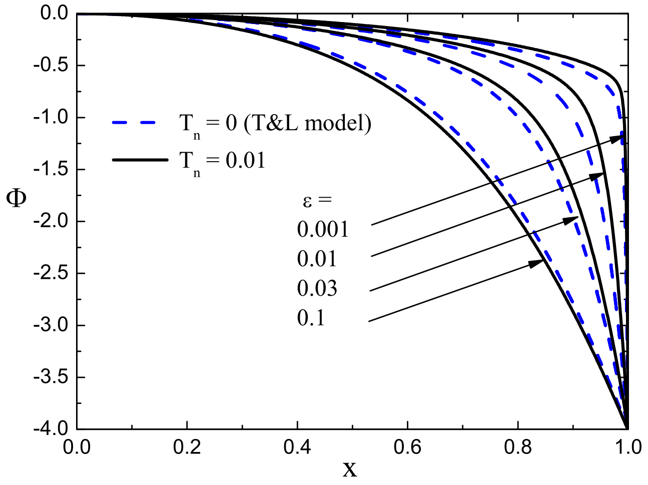

Figure 6.20: Comparison of potential profiles for $T_n = 0$ obtained with Riemann's program (dashed), and $T_n = 0.01$ obtained with our program (solid). Wall potential $\Phi_w = -4.0$ corresponds to argon.

As pointed before the generalized Bohm criterion holds strictly only in the two-scale approach which requires that the smallness parameter ε tends to become infinitely small. In real plasmas this requirement is just a qualitative statement without any practical significance. Since we need to define the plasma-sheath boundary in real plasmas (with finite-ε) we look for a universal way to fit the potential profiles in the intermediate region independently of plasma parameters, i.e., on ε. The rescaling is given in coordinates ζ and ω (instead of x and Φ) and the rules are as follows. In fluid model, appropriate scaling is

$$\zeta = \varepsilon^{-4/5}(x - x_s) \quad \text{and} \quad \omega = \varepsilon^{-2/5}(\Phi - \Phi_s). \tag{6.3}$$

In the kinetic approach with a singular (cold) ion source the transformation of coordinates obey the rule

$$\zeta = \varepsilon^{-8/9}(x - x_s) \quad \text{and} \quad \omega = \varepsilon^{-4/9}(\Phi - \Phi_s) \tag{6.4}$$

In the kinetic approach with a regular (warm) ion source the transformation of coordinates was predicted in the form

$$\zeta = \varepsilon^{-6/7}(x - x_s) \quad \text{and} \quad \omega = \varepsilon^{-4/7}(\Phi - \Phi_s). \tag{6.5}$$

In the above expressions x_s and Φ_s are the position and the corresponding potential of the (unknown) plasma-sheath boundary. The x_s and Φ_s quantities are explicitly found for the fluid model and the kinetic model with a singular ion source. However, these quantities had been unknown for the model with regular (warm) ion source until the work by Kos et al. [39]. This results from mathematical difficulties arising from ion source velocity distribution near the zero velocity. Without knowing these quantities the scaling (6.5) cannot be confirmed or applied. The problem of simultaneously finding x_s and Φ_s is widely discussed by Riemann, who, in fact, inspired our work [39]. However, the knowledge of x_s and Φ_s is just a necessary but not sufficient prerequisite for investigating the scaling rules in normalized coordinates in analogy to the case of a cold ion source (Riemann 2006 [53]). The present work amends this missing link. However, it turns out from our work that at least regarding high ion temperature plasmas we obtained a sufficient number of results to make a legitimate hypothesis on the results to be obtained in the future.

For an increasing ion source temperature (e.g., above $T_i, src \equiv T_a \sim 1$) the potential profiles in normalized and renormalized coordinates are very weakly dependent on ε. Therefore for high enough ion temperatures the problem of the intermediate region between the sheath and plasma as given by the above-stated rules seems to become rather meaningless. The results regarding the dependence of the electric field is shown in Fig. 6.21, where

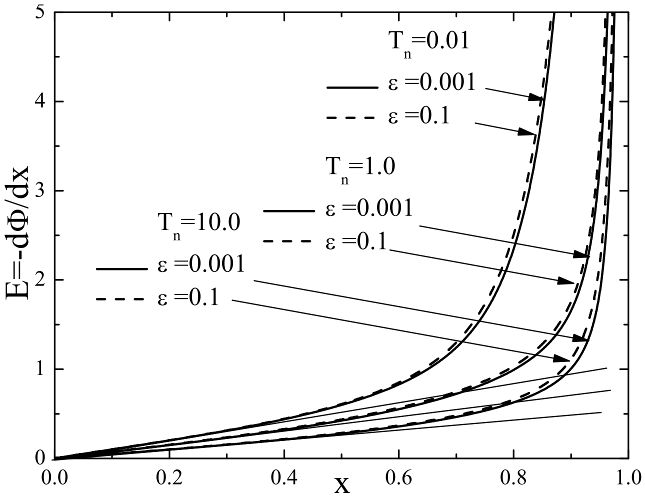

Figure 6.21: Electric fields obtained numerically in a wide range of ion source temperatures ($T_n = 0.01$, 1.00 and 10.0), each for a rather small and rather high choices of ε's ($\varepsilon = 0.001$ and $\varepsilon = 0.1$, respectively

we show the electric field in a wide range each for a rather small and rather

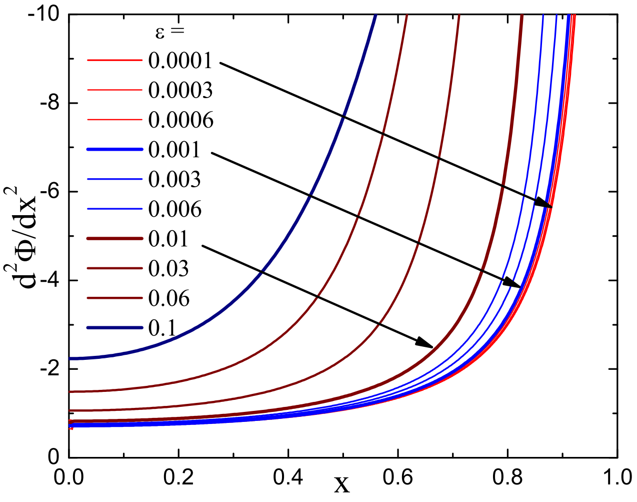

Figure 6.22: Second derivative of the potential for $T_n = 1$ and various ε.

high choices of ε's ($\varepsilon = 0.0001$ and $\varepsilon = 0.1$, respectively). In this figure we also present the tangents to the electric field which show that in a wide range of the discharge the electric field is a linear function of the position. In figure 6.22 we show some "intermediate" results, i.e., the second derivatives of the potential. This can be expected in details for confirming that the second derivative is a 'regular quantity' despite of the fact that in particular codes like Mathematica and C-libraries problems appear with the second derivative, especially for non-uniform grids.

In Fig. 6.23 we finally show the charge imbalances for the two ion-source temperatures and for a whole range of ε's (0.0001 and 0.1). While in the first case ($\varepsilon \leq 0.01$) the plasma condition $n_i - n_e \approx 0$ is well satisfied, in the second case ($\varepsilon > 0.01$) this is highly violated. Notwithstanding, Riemann has found that even in the last case his similarity rules still hold with a surprisingly high accuracy. We may conclude that in the case of the finite ion source temperature the rule holds even more strongly, since with an increased ion temperature, the results in general merge with each other so as to become insensitive to ε.

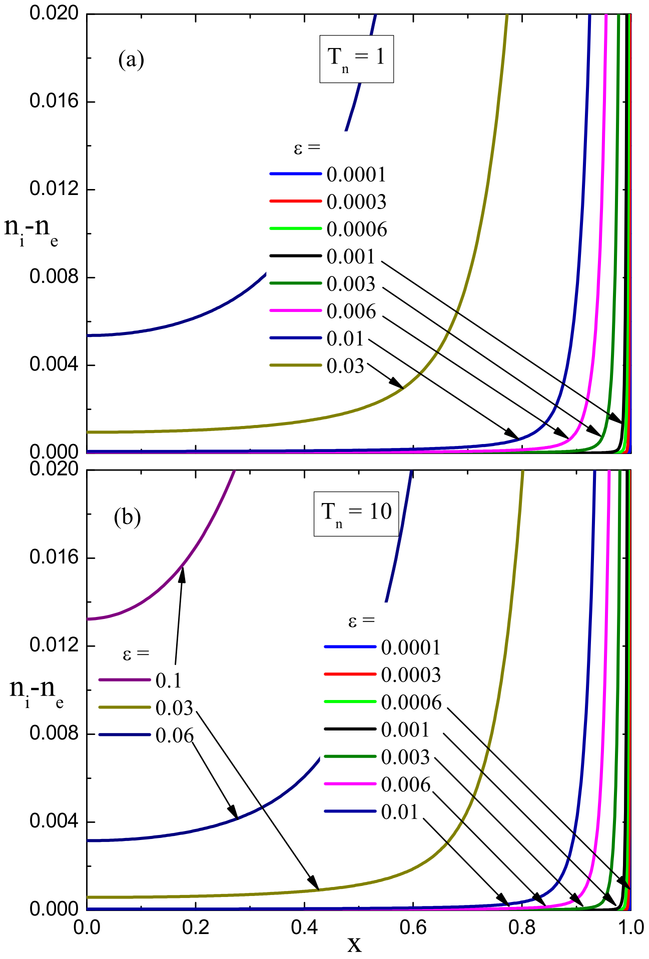

Figure 6.23: Charge imbalance for $T_n = 1$ (a), $T_n = 10$ (b) taken for a comparison with Riemann's results.

6.2.1 Particle In Cell method

For *quasi-neutral* models ($\varepsilon = 0$) solutions can be obtained analytically only in some special cases. Solving the above problem for finite T_i and $\varepsilon > 0$ is a rather non-trivial one, even via the numerical-computation method and still is a considerable challenge which is waiting for a reliable algorithm to be used. Fortunately, we can instead use the Particle-in-Cell numerical simulation (PIC) method [9, 73], which is fully kinetic and inherently requires $\varepsilon > 0$, while the ion temperature is arbitrary.

In PIC simulation the particle motion is entirely defined via its position in so-called phase space. In Fig. 6.24 we see data of particle positions in the two-dimensional phase-space obtained with PIC simulations by Jelić [32] in the one-dimensional plasma-wall transition layer.

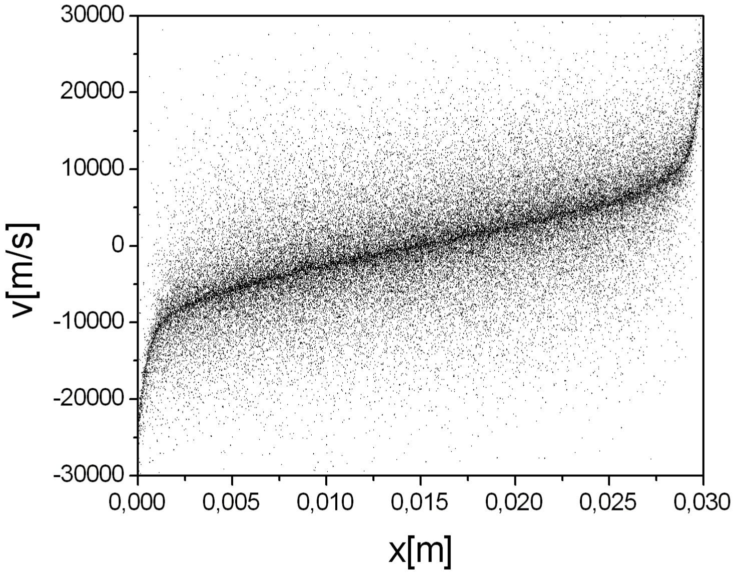

Figure 6.24: Particles (ions) in x-v phase space. The density of points is proportional to the particle distribution function.

Extracting velocity distribution from such an experimental kind of data requires discretization in both x- and v-directions as shown in Fig. 6.25. A convenient method is to choose fixed place "x" and to count the number of particles (each point in Fig. 6.24 represents a particle) with particular velocities along the vertical axis.

Fig. 6.26 presents the velocity distribution at several places (note that the potential and physical coordinate are well related via univalued relation $\Phi = \Phi(x)$), emerging from the requirement of the monotonic potential profile.

Finite x-v grid, i.e., the choice of finite x-v windows, involves a spread of velocity distribution. In the analytic-numerical method, however, we work with infinitely small windows. Thus we have a Maxwell daemon which sits at a place and counts the number of particles which pass to the left and right hand side of the system and measures at the observation point the velocity of each particle. So the velocity distribution that he observes is the exact one. This is equivalent to our method.

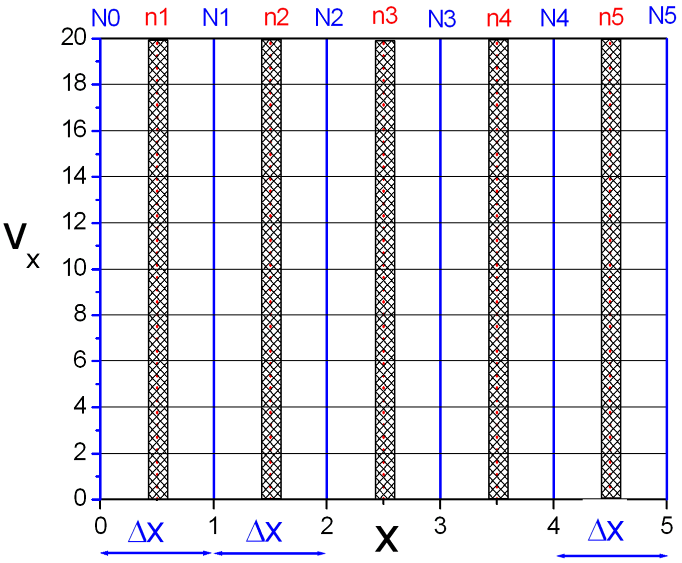
N0
n1
N1
n2
N2
n3
N3
n4
N4
n5
N5
V
x
20
18
16
14
12
10
8
6
4
2
0
0
1
2
3
4
5
ΔX
ΔX
ΔX
X

Figure 6.25: Discretization method of x-v phase-space.

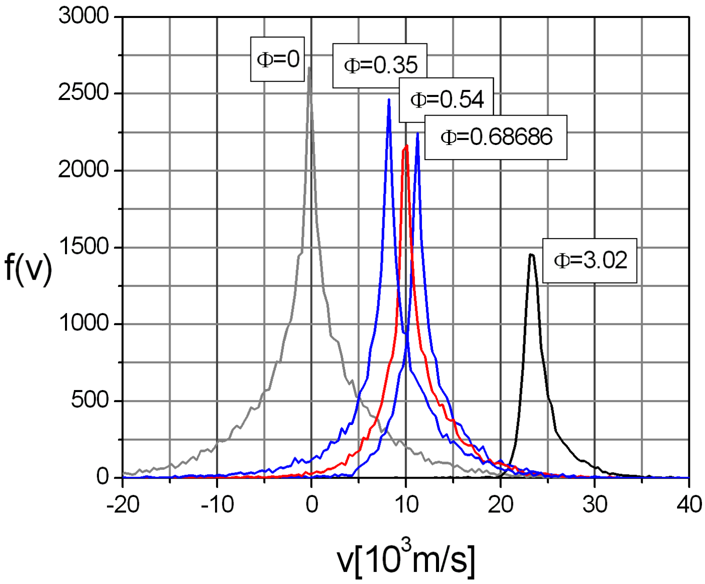

Figure 6.26: Ion velocity distributions as obtained at various places using PIC simulation experiments. Note that the potential corresponds to coordinate x.

On the other hand, the fluid quantities in PIC simulations must not be calculated a posteriori from such velocity distribution but, instead, the number of particles with certain properties (density, directional velocity, temperature, heat and energy fluxes) are "counted" within each discretization cell during the simulation.

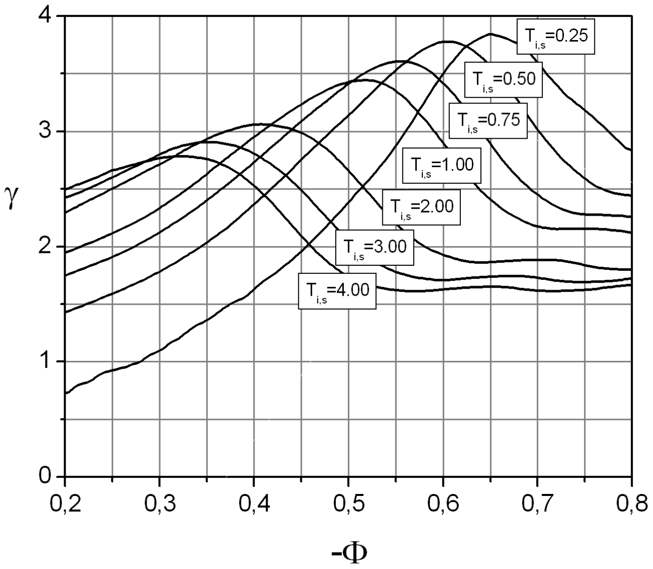

Figure 6.27: Ion polytropic coefficients as obtained from PIC simulations.

In Fig. 6.27 we last show the ion polytropic coefficient obtained in our PIC simulations as a function on the local potential. Simulations were performed with care using huge computer resources and can be considered as highly reliable regarding ion velocity distribution ever done for the Tonks-Langmuir model with finite ion temperatures.

However, a major problem of performing PIC simulations is the high cost of a simulation. In addition, the shape of our velocity distributions from PIC simulations is just a result of a very demanding "experiment". The results from such experiments are characterized by experimental or numerical noise which can be removed with a highly increased cost. Finally, it is difficult to derive some possible semi-empiric physical laws from the simulation results.

Chapter 7

Discussion and Conclusion

In thesis we used Scheuer and Emmert's [61] (S&E) numerical approach to extended the Bissell and Johnson (B&J) model [10] to arbitrary ion source temperatures. However, due to their approximation of the kernel, the S&E approach is still limited to plasmas with low ion temperatures. Thus we employed an exact kernel and at the same time refined the approach of S&E, i.e., applied a high-density and a high-resolution grid with additional convergence stabilization approaches. In order to confirm numerical stability and precision, our results were obtained in both Mathematica and in our own package, yielding an excellent agreement in all numerical figures. From the physical point of view we found that the final ion temperature is much lower than the ion source temperature. This is quite important in fusion devices, where ions penetrate from the core to the SOL region and then, moving towards the divertor plate, become rapidly cooled. Most significantly, we found the plasma edge x_s as a function of the ion source temperature. We have shown that in finite-temperature plasmas the maximum of the polytropic coefficient in fact does not coincide with the edge of the plasma sheath as this is the rule in plasmas with negligible ion-source temperatures, but still can be considered as a good estimation of the plasma-sheath boundary. This fact might be of considerable importance to linking fluid and kinetic plasma parameters in fusion fluid codes like e.g., SOLPS-B2 (e.g. Ref. [15]).

It should be pointed out that our results are strictly valid only up to the breaking point of quasi-neutrality. For a solution which is valid for the whole system it was necessary to involve the effect of the electric field, i.e., to start from the full Poisson equation instead of using the quasi-neutrality condition. Such an approach lead to the integro-differential equation which we obtained in the form

$$\frac{1}{B} = \frac{1}{1-\exp(-\Phi)\varepsilon^2 \dfrac{d^2\Phi}{dx^2}} \int\limits_0^1 \exp\left[(1+\frac{1}{2T_n}(\Phi'-\Phi)\right] \mathrm{K}_0\left[\frac{1}{2T_n}|\Phi'-\Phi|\right] dx' \, . \tag{7.1}$$

In order to solve this equation we employed a new code that extended our model for $\varepsilon = 0$ to arbitrary Debye lengths.

Considering the case when $\varepsilon > 0$, our investigation covers a wide range of ion source temperatures for a wide range of ε. In fact this is the first investigation of the kind to use the analytic-numerical method. Other methods assume employment of the PIC method (see e.g., Krek. et al. [34]). Our principal result for $\varepsilon > 0$ shows that for an increasing ion source temperature (e.g., above $T_i, src \equiv T_n \sim 1$) the potential profiles in normalized and renormalized coordinates are very weakly dependent on ε. The problem of intermediate region between sheath and plasma is provided by Riemann's rules for the finite ion source temperature in Eq. (6.5) turns out to be rather unavailing at least in fusion plasmas.

On the other hand, for low enough ion source temperatures, there is another type of scaling [Eq. (6.4)], which was excellently elaborated by Riemann. In any case, our assumption about the relevance of ε for high ion source temperatures will be investigated in details in subsequent works with both Maxwellian and Water-Bag distributions employed. For the second derivative of the potential we conclude that as the ion temperature increases, the results become more and more insensitive on ε. This is a starting point for further investigations on the proper plasma-sheath definition via either method available.

Our approach is novel in many aspects. As first by using the PIC simulation method we obtained highly reliable potential profiles and the ion velocity distribution ever done for the Tonks-Langmuir model with a finite ion temperature and with finite ε. The quantitative comparison of the basic quantity, i.e., the potential profile obtained with our method shows a nice agreement with the results of Bissell and Johnson in the range of validity of their results. New results, obtained by us outside this range along with derived results, are presented as well.

7.1 Contributions to science

We can summarize the results of the thesis as follows:

1. The model of Bissell and Johnson is extended to the so-called "finite-$\varepsilon \equiv \lambda_D/L$" case. That means that strict quasi-neutrality is not strictly satisfied unless ε is strictly zero. The kernel in our approach is not approximated but calculated exactly. The degree of "exactness" is, of course, dependent on the program package used in this work which is, however, dependent on the libraries used)). The grid for calculating potential profile is refined not only at the wall of the system but also in the center of symmetry.

2. The basic hydrodynamic quantities like ion density, ion outflux, directional energy and temperature are derived directly from velocity distribution on a grid which is self-adaptive near singularities of the kernel of integral as well as near singularities of the electric field, i.e., its inverse value.

3. We extended our analytic-numerical calculations to the case of finite ε, for comparing with PIC simulations, which are applicable to real system without dividing the problem into plasma and sheath scale a-priori. Two types of result are obtained, namely for a wide spectrum of ion temperatures ($0.01 < T_n/T_e < 100$) with $\varepsilon = 0$ and for several temperatures ($T_n/T_e = \{0.1, 1.0, 10\}$) with ε finite ($\varepsilon = \{10^{-5}, 10^{-3}, 0.01, 0.1\}$).

4. It appears that with an increasing ion temperature the dependence of the potential profile on ε becomes more and more insensitive.

Thesis contributions were also published in [39, 38, 37, 42, 28, 33].

Bibliography

[1] Milton Abramovitz and Irene A. Stegun. *Handbook of Mathematical Functions with Formulas, Graphs and Mathematical Tables*, page 379. Dover, New York, 1972.

[2] Milton Abramovitz and Irene A. Stegun. *Handbook of Mathematical Functions with Formulas, Graphs and Mathematical Tables.* Dover, New York, 1974.

[3] Hiroshi Akima. A new method of interpolation and smooth curve fitting based on local procedures. *J. ACM*, 17(4):589–602, 1970.

[4] J. E. Allen. A note on the generalized sheath criterion. *Journal of Physics D: Applied Physics*, 9(16):2331–2332, 1976.

[5] J. E. Allen. Some researches on double layers. *Plasma Phys. Controlled Fusion*, 27:1343, 1985.

[6] J. E. Allen. The plasma–sheath boundary: its history and langmuir's definition of the sheath edge. *Plasma Sources Science and Technology*, 18(1):014004, 2009.

[7] J. G. Andrews and J. E. Allen. Theory of a double sheath between two plasmas. *Proceedings of the Royal Society of London. Series A, Mathematical and Physical Sciences*, 320(1543):459–472, 1971.

[8] J. G. Andrews and R. H. Varey. The sheath at an electrode close to the plasma potential. *Journal of Physics A: Mathematical and General*, 3:413, 1970.

[9] Charles K. Birdsall and Bruce A. Langdon. *Plasma Physics Via Computer Simulation.* McGraw-Hill, 1985.

[10] R. C. Bissell and P. C. Johnson. The solution of the plasma equation in plane parallel geometry with a Maxwellian source. *Physics of Fluids*, 30(2):779–786, 3 1987.

[11] L. P. Block and C.-G. Fälthammar. Mechanisms that may support magnetic-field-aligned electric field in the magnetosphere. *Ann. Geophys.*, 32:161, 1976.

[12] David Böhm. *The Characteristics of Electrical Discharges in Magnetic Fields*, chapter 2.5, pages 49–86. National Nuclear Energy series, Div. 1, v. 5. McGraw-Hill, New York, first edition, 1949. Edited by A. Guthrie and R.K. Wakerling.

[13] T. J. M. Boyd and J. J. Sanderson. *The Physics of Plasmas.* Cambridge University Press, 2003.

[14] A. Caruso and A. Cavaliere. The structure of the collisionless plasma-sheath transition. *Il Nuovo Cimento (1955-1965)*, 26(6):1389–1404, 1962.

[15] A. V. Chankin, D. P. Coster, R. Dux, Ch. Fuchs, G. Haas, A. Herrmann, L. D. Horton, A. Kallenbach, M. Kaufmann, A. S. Kukushkin, K. Lackner, H. W. Müller, J. Neuhauser, R. Pugno, and M. Tsalas. Comparison between measured divertor parameters in ASDEX upgrade and SOLPS code solutions. *Journal of Nuclear Materials*, 363-365:335–340, 2007.

[16] Barbara Chapman, Gabriele Jost, and Ruud van der Pas. *Using OpenMP: Portable Shared Memory Parallel Programming (Scientific and Engineering Computation).* The MIT Press, October 2007.

[17] Francis F. Chen. *Introduction to plasma physics and controlled fusion.* Plenum Press, New York and London, 1984.

[18] D. P. Coster. Time dependent SOL modelling with SOLPS. In R. et al. Koch, editor, *Europhysics Conference Abstracts (CD-ROM, Proc. of the 30th EPS Conference on Controlled Fusion and Plasma Physics, St. Petersburg, 2003)*, volume 27A, page P–1.169, Geneva, 2003.

[19] Germund Dahlquist and Ake Björck. *Numerical Methods in Scientific Computing.* SIAM, 2008.

[20] R. C. Davidson. *Methods in Nonlinear Plasma Theory.* Academic Press, New York and London, 1972.

[21] E.Kuffel, W. S. Zaengl, and J. Kuffel. *High Voltage Engineering Fundamentals.* Butterworth-Heinemann, second edition edition, 2004.

[22] A. Emmert, R. M. Wieland, A. T. Mense, and J. N. Davidson. Electric sheath and presheath in a collisionless, finite ion temperature plasma. *Physics of Fluids*, 23(4):803–812, 1980.

[23] Paola Favati, Grazia Lotti, Gaspare Di Marco, and Francesco Romani. Asymptotic behavior of automatic quadrature. *J. Complex.*, 10(3):296–340, 1994.

[24] Paola Favati, Grazia Lotti, and Francesco Romani. Algorithm 691: Improving QUADPACK automatic integration routines. *ACM Trans. Math. Softw.*, 17(2):218–232, 1991.

[25] Mark Galassi, Jim Davies, James Theiler, Brian Gough, Gerard Jungman, Michael Booth, and Fabrice Rossi. *Gnu Scientific Library: Reference Manual.* Network Theory Ltd., February 2009.

[26] Donald A. Gurnett and Amitava Bhattacharjee. *Introduction to Plasma Physics with Space and Laboratory Applications.* Cambridge University Press, 2005.

[27] J. Guy, B. Mangeot, and A Salè. Solutions for fredholm equations through nonlinear iterative processes. *J. Phys. A: Math. Gen.*, 17:1403–1413, 1984.

[28] Matthieu Haefele, Leon Kos, Pierre Navaro, and Eric Sonnendrücker. Euforia integrated visualization. In *PDP 2010 - The 18th Euromicro International Conference on Parallel, Distributed and Network-Based Computing*, Pisa, Italy, 2010. accepted.

[29] E. R. Harrison and W. B. Thompson. The low pressure plane symmetric discharge. *Proceedings of the Physical Society*, 74(2):145–152, 1959.

[30] R. W. Hockney and J. W. Eastwood. *Computer Simulation Using Particles.* Adam Hilger, 1988.

[31] I. H. Hutchinson. *Principles of Plasma Diagnostics.* Cambridge University Press, Cambridge, 2 edition, 2002.

[32] N. Jelić, K.-U. Riemann, T. Gyergyek, S. Kuhn, M. Stanojević, and J. Duhovnik. Fluid and kinetic parameters near the plasma-sheath boundary for finite debye lengths. *Physics of Plasmas*, 14(10):103506, 2007.

[33] Nikola Jelić, Leon Kos, and D. D. Tskhakaya (sr.). The ionization length in plasmas with finite temperature ion sources. *Physics of Plasmas*, 2009. (submitted).

[34] Nikola Jelić, Janez Krek, Siegbert Kuhn, and Jože Duhovnik. Particle-in-cell (PIC) simulations of the plasma-sheath boundary in finite-ε plasmas with warm ion source of constant temperature. *Physics of Plasmas*, 2009. (to be submitted).

[35] L. Jones, J. Duhovnik, M. Ginola, J. Huttunen, K. Ioki, L. Junek, T. Loewer, U. Luconi, M. Pick, G.-P. Sanguinetti, M. Slovacek, and Y. Utin. Results from ITER vacuum vessel sector manufacturing development in europe. *Fusion Engineering and Design*, 82(15-24):1942–1947, oct 2007.

[36] Igor D. Kaganovich. How to patch active plasma and collisionless sheath: A practical guide. *Physics of Plasmas*, 9(11):4788–4793, 2002.

[37] Leon Kos, Jože Duhovnik, and Nikola Jelić. Extension of collisionless discharge models for application to fusion-relevant and general plasmas. In *Proceedings of the International Conference Nuclear Energy for New Europe 2009*, pages 820.1–820.10. Nuclear society of Slovenia, 2009. http://www.djs.si/bled2009/.

[38] Leon Kos, Nikola Jelić, and Jože Duhovnik. Modelling the plasma-sheath boundary for plasmas with warm-ion sources. In *Proceedings of the International Conference Nuclear Energy for New Europe*, pages 807(1)–807(8), Portorož, Slovenia, 2008. Nuclear society of Slovenia. http://www.nss.si/port2008/.

[39] Leon Kos, Nikola Jelić, Siegbert Kuhn, and Jože Duhovnik. Extension of the Bissel-Johnson plasma-sheath model for application to fusion-relevant and general plasmas. *Physics of Plasmas*, 16(9):093503, 9 2009.

[40] Siegbert Kuhn, K.-U. Riemann, Nikola Jelić, D. D. Tskhakaya, Sr., D. Tskhakaya, Jr., and Mladen Stanojević. Link between fluid and kinetic parameters near the plasma boundary. *Physics of Plasmas*, 13(1):013503, 2006.

[41] Michael A. Lieberman and J. Licthenberg Allan. *Principles of Plasma Discharges and Materials Processing.* John Wiley & Sons, 2 edition, 2005.

[42] Francisco Castejón Maga na, Miguel Cárdenas Montes, Antonio Gómez-Iglesias, Enrique Morales-Ramos, Bernard Guillerminet, David P. Coster, Eric Sonnendrücker, Isabel Campos-Plasencia, Jan Åström, Jan Westerholm, José M. Cela, Leon Kos, Lorna Smith, Marcin Plociennik, Marcus Hardt, Mats Aspnäs, Pär Strand, and Rainer Stotzka. EUFORIA: Grid and high performance computing at the service of fusion modelling. In Silva et al. [63], pages 115–126.

[43] Verboncoeurm J. P., A. B. Langdon, and N. T. Gladd. An object-oriented electromagnetic PIC code. *Computer Physics Communications 87*, pages 199–211, 1995.

[44] Suhas V. Patankar. *Numerical Heat Transfer And Fluid Flow.* Taylor&Francis, 1980.

[45] R. Piessens, E. de Doncker-Kapenga, C. W. Uberhuber, and D. K. Kahaner. *Quadpack. A Subroutine Package for Automatic Integration.* Series in Computational Mathematics 1. Springer-Verlag, 1983.

[46] Andrei D. Polyanin and Alexander V. Manzhirov. *Handbook of Integral Equations.* Chapman & Hall/CRC, 2 edition, February 2008.

[47] Michael J. Quinn. *Parallel Programming in C with MPI and OpenMP.* McGraw-Hill Education (ISE Editions), September 2003.

[48] K.-U. Riemann. Kinetic theory of the plasma sheath transition in a weakly ionized plasma. *Physics of Fluids*, 24(12):2163–2172, 1981.

[49] K.-U. Riemann. The Bohm criterion and sheath formation. *Journal of Physics D: Applied Physics*, 24(4):493–518, 1991.

[50] K.-U. Riemann. Theory of the plasma–sheath transition. *J. Tech. Physics*, 41(1, Special Issue):89–121, 2000. General invited lecture, XXIV, Warshaw.

[51] K.-U. Riemann. Kinetic analysis of the collisional plasma–sheath transition. *Journal of Physics D: Applied Physics*, 36(22):2811–2820, 2003.

[52] K.-U. Riemann. Kinetic analysis of the collisional plasma–sheath transition. *Journal of Physics D: Applied Physics*, 36:2811–2820, 2003.

[53] K.-U. Riemann. Plasma-sheath transition in the kinetic Tonks-Langmuir model. *Physics of Plasmas*, 13(6):063508, 2006.

[54] K.-U. Riemann. Polytropic coefficient γ in the fluid simulation of the plasma-sheath transition. In *28th ICPIG*, pages 479–482, Prague, Chech Republic, 2007. ICPIG.

[55] K.-U Riemann. Plasma and sheath. *Plasma Sources Science and Technology*, 18(1):014006, 2009.

[56] K.-U. Riemann. The plasma-sheath transition. Seminar held at Institute of Theoretics Physics, Innsbruck, 1 2009.

[57] K.-U. Riemann, private communication, 2009.

[58] K.-U. Riemann, J. Seebacher, D. D. Tskhakaya, Sr., and S. Kuhn. The plasma–sheath matching problem. *Plasma Physics and Controlled Fusion*, 47(11):1949–1970, 2005.

[59] Scott Robertson. Sheath and presheath in plasma with warm ions. *Physics of Plasmas*, 16, 2009. (to appear).

[60] I.M. Ryshik and I.S. Gradstein. *Tables of series, products, and integrals.* VEB verlag, Berlin, 1957.

[61] J. T. Scheuer and G. A. Emmert. Sheath and presheath in a collisionless plasma with a maxwellian source. *Physics of Fluids*, 31(12):3645–3648, 1988.

[62] S. A. Self. Exact solution of the collisionless plasma-sheath equation. *Physics of Fluids*, 6:1762, 1963.

[63] Fernando Silva, Gaspar Barreira, and Lígia Ribeiro, editors. *Ibergrid. 2th Iberian Grid Infrastructure Conference Proceedings, 12-14 May 2008, Porto, Portugal*, Porto. Portugal, May 2008. Netbiblo.

[64] P. C. Stangeby. *The Plasma Boundary of Magnetic Fusion Devices.* Institute of Physics Publishing Ltd, Bristol, 2000.

[65] P. C. Stangeby and J. E. Allen. Plasma boundary as a mach surface. *Journal of Physics A: Mathematical and General*, 3:304, 1970.

[66] M. Stanojević, J. Duhovnik, N. Jelić, A. Kendl, and S. Kuhn. Fluid model of the magnetic presheath in a turbulent plasma. *Plasma Physics and Controlled Fusion*, 47(5):685–712, may 2005.

[67] Mladen Stanojević, Jože Duhovnik, Nikola Jelić, and Siegbert Kuhn. Magnetic presheath in a weakly turbulent multicomponent plasma. *Physics of Plasmas*, 14(1):013504, jan 2007.

[68] Z. Sternovsky, K. Downum, and S. Robertson. Numerical solutions to a kinetic model for the plasma-sheath problem with charge exchange collisions of ions. *Phys. Rev. E*, 70(2):026408, Aug 2004.

[69] Zoltan Sternovsky. The effect of ion-neutral collisions on the weakly collisional plasma-sheath and the reduction of the ion flux to the wall. *Plasma Sources Science and Technology*, 14(1):32–35, 2005.

[70] Lewi Tonks and Irving Langmuir. A general theory of the plasma of an arc. *Phys. Rev.*, 34(6):876–922, Sep 1929.

[71] D. Tskhakaya and S. Kuhn. Effect of exb drift on the plasma flow at the magnetic presheath entrance. *Contrib. Phys. Fluids*, 42:3002, 2002.

[72] D. Tskhakaya and S. Kuhn. Kinetic (PIC) simulations of the magnetized plasma–wall transition. *Plasma Phys. Control. Fusion*, 47(5A):A327–A337, 2005.

[73] D. Tskhakaya, S. Kuhn, Y. Tomita, K. Matyash, R. Schneider, and F. Taccogna. Self-consistent simulations of the plasma-wall transition layer. *Contrib. Plasma Phys.*, 48(1-3):121–125, 2008.

[74] D. Tskhakaya and R. Schneider. Optimization of pic codes by improved memory management. *Journal of Computational Physics*, 225:829–839, 2007.

[75] D. D. Tskhakaya, P. K. Shukla, F. Subba, and S. Kuhn. Behaviour of a dust cloud in the plasma sheath adjacent to a conducting wall. *Physics Letters*, A 303:190–195, 2002.

[76] J. P. Verboncoeur, M. V. Alves, V. Vahedi, and C. K. Birdsall. Simultaneous potential and circuit solution for 1D bounded plasma particle simulation codes. *Journal of Computational Physics*, 104(2):321–328, 1993.

[77] J. P. Verboncoeur and V. Vahedi. WinGraphics: An optimized windowing environment for plasma simulation. In *Proceedings of* 13^{th} *Numerical Simulation Conference*, Sante Fe, NM, 1989.

[78] E. Zawaideh, F. Najmabadi, and R. W. Conn. Generalized fluid equations for parallel transport in collisional to weakly collisional plasmas. *Physics of Fluids*, 29:463–474, 1986.

Appendix A

Ion source of the ,,Water bag" type

In this case the velocity distribution of the neutrals has the form

$$f_n\left(\frac{v}{v_{T_i}}\right) = \frac{1}{\sqrt{12}v_{T_i}}\left\{\Theta\left(\frac{v-v_-}{v_{T_i}}\right) - \Theta\left(\frac{v-v_+}{v_{T_i}}\right)\right\} \ , \tag{A.1}$$

where v_- and v_+ are cut-off velocities, $v_+ > v_-$. The fluid velocity and the temperature for the "water bag" distribution are respectively

$$V = \frac{1}{2}\{v_+ + v_-\} \ , \tag{A.2}$$

$$kT_i = \frac{m_i}{12}\{v_+ - v_-\}^2 \tag{A.3}$$

(on further properties of such distributions see [20]). Unlike the Maxwellian source this distribution can be of considerable interest to analytic derivation in the kinetic approach. For simplicity's sake, we consider the symmetric "water bag" below, when

$$v_- = -v_+ \tag{A.4}$$

and the auxiliary function (5.11) has the form

$$F_n\left(\frac{v}{v_{T_i}}\right) = \sqrt{\frac{\pi}{6}}\left\{\Theta\left(\frac{v+v_+}{v_{T_i}}\right) - \Theta\left(\frac{v-v_+}{v_{T_i}}\right)\right\} \ . \tag{A.5}$$

We also assume the "water bag" to be enough broad

$$\frac{m_i v_+^2}{2} \gg e\Phi_w \ . \tag{A.6}$$

This condition implies that not all ions will move after their birth in the positive direction of x-axis towards the wall. The negative wall potential will not be able to turn those ions which have acquired large kinetic energy (A.6) at their birth and move in the negative direction. The calculations quite analogous to those carried out in the previous section lead to the following expressions for the ion density and the ion flux.

$$n(x) = \sqrt{\frac{2\pi}{3}} B \int_0^1 dx' \exp[\Phi(x')] \operatorname{arcsinh}\left(\frac{v_+}{c_s\sqrt{2|\Phi(x') - \Phi(x)|}} \right) , \tag{A.7}$$

$$j(1) = \sqrt{\frac{2\pi}{3}} \frac{v_+}{c_s} B \int_0^1 dx' \exp[\Phi(x')] \ . \tag{A.8}$$

The Poisson equation acquires then the for

$$\begin{aligned} 1 - \varepsilon^2 \exp(-\Phi) \frac{d^2\Phi}{dx^2} =& B\sqrt{\frac{2\pi}{3}} \int_0^1 dx' \exp[\Phi(x') - \Phi(x)] \\ & \times \operatorname{arcsinh}\left(\frac{v_+}{c_s\sqrt{2|\Phi(x') - \Phi(x)|}} \right) \ . \end{aligned} \tag{A.9}$$

Comparing (A.8) with the electron flux onto the wall, the floating potential should be found from the equation

$$\exp(\Phi_w) = \pi\sqrt{\frac{2}{3}\frac{m_e}{m_i}} \ \frac{v_+}{c_s} B \int_0^1 dx' \exp[\Phi(x')] \ . \tag{A.10}$$

Appendix B

Code description

Here we describe the basic parameters and usage cases of our code written in standard C language with the extension of the GSL, OpenMP and MiniXML libraries. The `ppgplasma` code calculates potential profile for a given normalized ion source temperature that is assumed to be Maxwellian. Generalization to arbitrary $\varepsilon = \lambda_D/L$ and to a different discharge scenario with the ϑ is also possible. For reference on the parameters one should consult Chapters 4 and 5 in the present thesis. XML definition describes source code version `r858` available through Subversion repository.

B.1 XML definition

The XML definition of the input parameters for the program were included with the intention to minimize parameter confusion and still provide easy checking through XSLT support readily available by many XML libraries. The input file contains all code specific parameters grouped into thematic groups, namely *global parameters*, *numerical parameters*, *grid parameters*, *code parameters* and *diagnostic parameters*. Default values of parameters are also adopted in the code. Such approach gives a possibility to easily maintain the old code even when adding new features to the code. The decision on the default value is normally based on the influence of new features to the possibility of a rerun of the old simulations. The default input `ppgplasma.xml` file looks as follows:

```
<?xml version="1.0"?>
```

```
<?xml-stylesheet type="text/xsl" href="./input_ppgplasma.xsl"
charset="ISO-8859-1"?>

<parameters>

  <!-- global parameters -->

  <global_parameters>
    <Tn> 1.0 </Tn>
    <epsilon> 0.01 </epsilon>
    <B> 0.3 </B>
    <vartheta> 1.0 </vartheta>
    <mass_ratio> 1836.1527 </mass_ratio>
  </global_parameters>

  <!-- numerical parameters -->

  <numerical_parameters>
    <soft_step> 0.001 </soft_step>
    <parabolic_range> 0.01 </parabolic_range>
    <smooth_step> 1.0 </smooth_step> <!-- range [0,1] -->
    <B_step> 0.0001 </B_step>
    <niter> 200000 </niter>
    <zone_epsrel> 1.0e-7 </zone_epsrel>
    <shift_to_origin_rate> 2500 </shift_to_origin_rate>
    <phi_wall_step>0.001</phi_wall_step>
  </numerical_parameters>

  <!-- grid parameters -->

  <grid_parameters>
   <np> 1601 </np>
   <lambda1> 1.4 </lambda1>
   <lambda2> 2.4 </lambda2>
   <phi_1> -0.8 </phi_1>
  </grid_parameters>

  <!-- code parameters -->

  <code_parameters>
    <use_finite_epsilon> 0 </use_finite_epsilon>
    <use_parabolic_rewrite> 1 </use_parabolic_rewrite>
    <use_average_smoothing> 0 </use_average_smoothing>
    <use_fix_right_side> 1 </use_fix_right_side>
    <use_adjust_B> 1 </use_adjust_B>
    <use_regrid> 1 </use_regrid>
    <use_shift_to_origin> 1 </use_shift_to_origin>
    <use_adjust_phi_wall> 0 </use_adjust_phi_wall>
  </code_parameters>

  <!-- diagnostics parameters -->

  <diagnostics_parameters>
    <iter_dat> 100 </iter_dat>
    <psi_dat> 20 </psi_dat>
    <psi1_dat> 1 </psi1_dat>
    <pot_dat> 0 </pot_dat>
    <ds_dpsi_dat> 0 </ds_dpsi_dat>
    <dpsi_ds_dat> 0 </dpsi_ds_dat>
    <ddpsi_ds2_dat> 1 </ddpsi_ds2_dat>
  </diagnostics_parameters>

</parameters>
```

B.2 Parameters

B.2.1 Global Parameters

This group of parameters is used to prescribe physical parameters of the problem. The parameters are considered at the startup for a specific case of investigation. This means that it is up to the code and its *code parameters* how these parameters are considered in calculation. For some cases these parameters are not considered at all as they are not influential, but they can be left in the XML file or can be even left out and rely on the default value.

- **Tn :** is the normalized temperature of the neutral gas $T_n = 1/\tau$. This parameter is always considered and is the most influential for a given investigation. Practical ranges are [0.002, 1000]. Although used in many places in the code, the most influential is part is within the arguments of the modified Bessel function

  $$\mathrm{K}_0\left\{\frac{1}{2T_n}\left|\Phi(x') - \Phi(x)\right|\right\} \, , \qquad \text{(B.1)}$$

  where T_n plays a major role that limits the practical range.

- **epsilon :** is a relatively small but finite $\varepsilon = \lambda_D/\ell$, with λ_D the electron Debye length and ℓ being the relevant characteristic length of the problem and is considered only if **use_finite_epsilon = 1**. Practical values are in the range [0, 0.1]. Following Riemann [53], we limit our investigation to $\varepsilon = \{0.0, 0.001, 0.003, 0.01, 0.03, 0.1\}$

- **B :** is the initial value of the constant B, which is considered to be the eigenvalue of the problem and is related to the source strength. This value is used only if there is no **psi.dat** in the current directory available, to be read from. If **psi.dat** is available, the value is not considered at all.

- **vartheta :** defaults to 1.0 for Maxwellian-shaped ion sources. The parameter ϑ characterizes the rate of ion generation per unit volume: when $\vartheta = 0$ the rate is uniform; when $\vartheta = 1$ the rate is proportional to the electron density. The values of ϑ greater than unity correspond to those cases where ion generation due to ionization is multiple stage process dependent upon the electron density. As a constant source **vartheta = 0.0** should be used. The influence of ϑ is shown in the following generalized equation

  $$\frac{1}{B} = \frac{1}{1 - \exp(-\Phi)\varepsilon^2 \dfrac{d^2\Phi}{dx^2}} \times \int\limits_0^1 dx' \exp\left[(\vartheta + \frac{\tau}{2})\Phi(x') - (1 + \frac{\tau}{2})\Phi(x)\right] \mathrm{K}_0 \left\{\frac{\tau}{2}|\Phi(x') - \Phi(x)|\right\} . \tag{B.2}$$

  With explicit source distribution and ϑ the non-dimensional form of ion velocity distribution function is

  $$f_i(\Phi(x), v) = B \times \int_0^1 dx' \exp(\vartheta\Phi') \frac{\exp\left[-(v^2 - (\Phi' - \Phi))/T_n\right]}{\sqrt{v^2 - (\Phi' - \Phi)}} . \tag{B.3}$$

- **mass_ratio :** is the mass ratio between ion and electron and is related to wall potential Φ_w with equation

  $$\exp(\Phi_w) = 2\pi\sqrt{\frac{m_e}{m_i}}\sqrt{\frac{T_n}{T_e}} B \int_0^1 dx' \exp[\Phi(x')] . \tag{B.4}$$

Default value of **mass_ratio = 1836.1527** is for Hydrogen that is of central interest in fusion. When **use_finite_epsilon = 0** this value is not used in iterations. With combination **use_adjust_phi_wall = 1** and **use_finite_epsilon = 0** the wall potential Φ_w is calculated and printed during each iteration. If **use_finite_epsilon = 1** the Φ_w is always printed out.

B.2.2 Numerical Parameters

This group holds the parameters that set up and control the convergence behavior during the iterative process of solving Eq. (B.2).

- **soft_step :** controls the step size for each potential grid point. This parameter equals to α in Eq. (4.11) and can be associated to the time-step when solving some differential equations. Practical values are in the range [0.00001, 0.1]. As with fixed-point iterative methods, larger values can increase convergence, causing at the same time oscillatory behavior or even divergence. The default value of 0.01 can be used for most cases.

- **parabolic_range :** specifies the length of the parabolic rewrite or interpolation that can be used to stabilize oscillations at starting grid points. The number of grid points that are rewritten with parabolic interpolation is calculated at the first iteration and is used for the successive iterations. This range as formulated in Eq. (4.12) should be used for $\varepsilon = 0$ only, as they can cause the second order derivative to be non-continuous when $\varepsilon \neq 0$ at the point of the rewrite start. The practical range [0, 0.1] can be used when quick convergence is desired, gradually lowered when approaching the final solution and then completely disabled with **use_parabolic_rewrite = 0**.

- **smooth_step :** controls the degree of Laplacian smoothing as defined by Eq. (4.11). Smoothing in the direction from $x = 1$ to $x = 0$ is performed at every iteration and has impact on the smoothness of the higher order derivatives of $\Phi(x)$ (see e.g. Fig. 6.22). The practical value range is [0, 1], whereas it should be as low as possible and completely disabled when approaching the final solution. Smoothing during iterations especially helps stabilizing convergence when $T_n < 0.1$. Low frequency oscilations can be observed in such cases. Lowering this value should be done with extreme care when approaching zero. For $T_n = 0.001$ this parameter cannot be completely disabled. As average smoothing is executed in-place the complete solution is undershoted. This is a reason that **use_smooth_step = 0** should be considered as final step of every exact solution.

- **B_step :** step size the adjustment of the system eigenvalue B ad described by Eq. (4.13). Empirically it was found that within our analytic-numerical approach the influence of B has little or no dependence on the potential profile. Its influence can be mainly described as a solution shift as described in Eq. 4.4. As B behaves as a true eigenvalue of the system, this made us possible to compensate the shift through calculation of B at each iteration with `B_step` that ranges $[0, 1]$. Default value can be used. For range $T_n = [0, 0.1]$ it is recommended that **B_step $\leq$ 0.0001** to prevent interference oscilations caused by high **soft_step**.

- **niter :** maximum number of iterations. The default value is set to a high value due to the possibility to stop the iteration at any time and to continue later on. The `niter` is only useful for batch computing on clusters or GRID where no interactive investigation is possible.

- **zone_epsrel :** specifies QAGS relative accuracy for integration in each interval. For rough results or when having difficulties with precision this value can be changed to **zone_epsrel = 1.0e-6** or even larger. When GSL library is compiled with `long double` precision then **zone_epsrel = 1.0e-8** can be used.

- **shift_to_origin_rate :** Specifies how oftenly the whole solution is shifted to origin. This is related to calculation of B and its convergence. Normally, default value can be used for all cases. For more details consult [37].

- **phi_wall_step :** Adjusting the last point of the system when both **use_finite_epsilon = 1** and **use_adjust_phi_wall = 1** are set. Floating wall condition (B.4) is gradually assured with continuous relaxation of the system.

B.2.3 Grid Parameters

Examining the nature of the solution of Eq. (B.2) and post-calculation of the VDF in Eq. (B.3) and its moments the computational grid is established with high refinements at both sides of the computational domain that is normalized in the range $[0, 1]$. Equation (4.5) specifies the location of the grid points. Changing the grid density is possible during the restart, as the code includes a possibility to re-grid from one grid to another if any of the following parameters are changed.

- **np :** number of grid points N. Practical values are in the range $[300, 3000]$ and are related to the grid density parameters. Besides its precision, this is the most influential parameter to the computational time in each iteration. In each iteration step $N(N-1)$ integration subintervals are evaluated. For the default value of **np = 1601** roughly 2.5×10^6 integrals are evaluated.
- **lambda1 :** grid density λ_1 when approaching $x = 0$. A higher density at this point is mainly required due to the derived quantities in post-calculations.
- **lambda2 :** grid density λ_2 at the end of the calculation domain when approaching the last point at $x = 1$.
- **phi_1 :** Boundary potential Φ_b initial value of the last point at $x = 1$. When **use_finite_epsilon = 1** then this should be set to the value of Φ_w calculated with limiting case **use_finite_epsilon = 0** from Eq. (B.4). Potential profile is initialized in such way that it is monotonous and ends at the **phi_1**. This value is (as initial value for B) used only at initialization when **psi.dat** does not exist. Potential values are initialized using

$$\Phi[i] = \frac{\mathrm{phi\_1}}{1-\exp(1)}\left[1-\exp\left(\frac{i}{\mathrm{np}}\right)\right] . \tag{B.5}$$

B.2.4 Code Parameters

Although separate codes for each type of investigation can be more appropriate and tailored with `#pragma` code inclusion statements, during our tests we found that such approach lead to an unmanageable code and confusion in the final results, which required to store the entire source code as a reference for each investigation. *Code parameters* overcomes such scenario with a conditional inclusion of each piece of code in the investigation. This also means that there is only one executable that behaves differently on the basis of the code included. With prefix `use_` we clearly state the boolean expression for each portion of the code.

- **use_finite_epsilon :** specifies if generalized equation (B.2) is used. When **use_finite_epsilon = 0** simplified equation where $\varepsilon = 0$ is used. This rules out calculation of the second derivative of a potential profile and consequently speeds up the computing.
- **use_parabolic_rewrite :** code for parabolic interpolation from $x = 0$ to the length of profile specified by parameter `parabolic_range`.
- **use_average_smoothing :** inclusion of smoothing code with the influential parameter `smooth_step`.
- **use_fix_right_side :** Sometimes we encounter `-inf` values for Φ with a high density grid when approaching $x = 1$. Extrapolation algorithm is employed when such case is detected and when **use_fix_right_side = 1**. The cause of such behavior is too high density at the "right side" of the domain. When such case is detected in some of the last grid points, they are corrected and normally this case does not repeat frequently. Setting **use_fix_right_side = 0** can thus be set only when examining the case when this condition occurs, otherwise it can be safely included in th code at the negligible expense of CPU time.
- **use_adjust_B :** Adjustment of the B with `B_step` can be disabled with **use_adjust_B = 0**. This is normally not desired, except for investigations of the potential profile shift and influence of the prescribed B. It should be noted that parameter `B` in *global parameters* is only an initial value when no solution is written in **psi.dat**. When B is to be fixed, **psi.dat** should be changed and not **ppgplasma.xml**.
- **use_regrid :** The change of the current grid from the previous to a new one is controlled by this parameter. Change of any *Grid parameter* can

cause interpolation of existing grid to a new grid at the startup with a lower or higher number of grid points.

- **use_shift_to_origin :** Shifting of the initial solution at the startup is controlled by this parameter. There are, so to speak, no problems setting either value if using **use_adjust_B = 1**.

- **use_adjust_phi_wall :** As a last step of assuring floating wall condition (B.4) when **use_finite_epsilon = 1** the last point is moved towards calculated Φ_w with a soft step specified with `phi_wall_step`. For initial relaxation with finite ε **use_adjust_phi_wall = 0** should be used. After converged state is reached **use_adjust_phi_wall = 1** shoul be set for final convergence of the **use_finite_epsilon = 1** case. For more details consult **mass_ratio**.

B.2.5 Diagnostic Parameters

Various intermediate results can be written during iterations and at the end of the program. The text format is textual and compatible with diagnostic tools like `gnuplot`, which is available at every computing cluster as a standard tool.

- **iter_dat :** dumps the whole potential profile into **iter.dat** at every n-th iteration. The file is appended at each restart to preserve history. Normally this file can become rather large as it requires manual deletion. Examining profile history within `gnuplot` is done with *every* clause where the start and the increment of the plots are specified. Dumping is disabled with **iter_dat = 0**.

- **psi_dat :** rate of **psi.dat** stamping. This file consists of all intermediate variables required for restart or to evaluate the potential profile that is written with a zero shift and a shift variable separately. The writing of the file cannot be disabled as it is always written at the end of the program.

- **psi1_dat :** The writing of the last boundary Φ_s and B into **psi1.dat** can be disabled with **psi_dat = 0**. The last point of observation can be an excellent stopping criterion for the case $\varepsilon = 0$. As it dumps only two values at each iteration it can be considered as a standard file that is appended like **iter.dat**. Normally **psi1_dat = 1** is used and can grow substantially in size if numerous (over 200000) iterations are required.

- **pot_dat :** can be written at the end and contains just the potential profile without restart variables as **psi.dat**.
- **ds_dpsi_dat :** Inverse derivative $dx/d\Phi$ related to the inverse electric field is written into **ds_dpsi.dat** at the end of the program for debugging purposes and evaluation of potential profile smoothness.
- **dpsi_ds_dat :** derivative $d\Phi/dx$ is written into **dpsi_ds.dat** at the end of the program for debugging purposes and evaluation of the potential profile smoothness.
- **ddpsi_ds2_dat :** The second derivative is written when using $\varepsilon \neq 0$ with additional columns for debugging Poisson's equation.

Dodatek C

Slovenski povzetek

C.1 Uvod

Zaradi enostavnosti se prehod med plazmo in steno običajno razdeli na dve plasti: plašč s širino v rangu velikosti Debyjeve dolžine λ_D in predplašč z značilno dolžino v rangu velikosti relevantne kolizijske oziroma ionizacijske dolžine L. Običajno je

$$\lambda_D \ll L \, , \tag{C.1}$$

kar omogoča ločeno obravnavanje obeh plasti. Taka poenostavitev je znana kot dvodelna aproksimacija (*two-scale approximation*). Pod pogojem (C.1) lahko za predplašč predpostavimo kvazi-nevtralnost, medtem ko za Debyjev plašč predpostavimo razlikovanje naboja delcev.

Postavitev roba kvazi-nevtralne plazme, tj. meje (ali roba) plašča, je star, vendar še vedno nezadostno rešen problem, ki je pomemben za fuzijo kot tudi za laboratorijske plazme in plazme v vesolju. Meja plašča je površina, do katere lahko predpostavimo kvazi-nevtralnost. Predplašč lahko modeliramo z uporabo fluidnih aproksimacij (namesto vpeljave računsko zahtevnih kinetičnih modelov) z relevantnimi mejnimi pogoji na začetku plašča. Vendar je mejno površino še vedno nemogoče določiti z zadostno natančnostjo. Meja plašča se lahko dovolj natančno določi le v asimptoti dvodelne limite. Pri taki aproksimaciji se lahko meja plašča veže na stran plazme (neskončno tanek plašč) kot mesto singularnosti električnega polja (znameniti Tonksov in Langmuirov model [70] iz leta 1929) ali na stran plašča (neskončno velik plašč) kot mesto izginjanja električnega polja (znameniti Bohmov model [12] iz leta 1949). Oba modela sta bila prvotno izpeljana za primer “mrzlega” vira ionov (ioni, ki so narejeni v plazmi z *zanemarljivimi hitrostmi* v primerjavi s hitrostmi elektronov) in sta bila kasneje razširjena v splošno sprejeti izraz, ki pravi, da je rob plašča mesto, na katerem povprečna ionska hitrost v smeri x (pravokotni na steno) večja ali enaka lokalni ionski zvočni hitrosti.

$$u_i \geq \sqrt{k(T_e^* + \gamma T_i)/m_i}\ , \tag{C.2}$$

kjer je k Boltzmannova konstanta, m_i masa ionov, T_e^* je t.i. “screening” (”izločilna”) temperatura elektronov ($T_e^* = en_e/(kdn_e/d\Phi)$), T_i končna temperatura ionov, Φ je lokalni potencial plazme in γ je ionski politropični koeficient (definiran z $dp_i/dx = \gamma kT_i dn_i/dx$), z vsemi količinami na meji plazme in plašča. Prav zaprav je izraz (C.2) dobljen s hidro-dinamično aproksimacijo ioniziranega plina.

Zadnjih petdeset let so predpostavljali, da je γ konstantna v vseh fluidnih modelih plazme, šele pred kratkim pa so ugotovili, da je γ prostorsko spremenljiva količina (odvisna od koordinate x v enodimenzionalnem primeru) in ne le globalna konstanta. Kuhn et al. (2006) [40] so predvsem z analitičnim pristopom pokazali, da asimptotična dvodelna limita γ_i (podpisano i pomeni ione) izkazuje oster vrh prav na meji plazme in plašča. Jelić at al. (2007) [32] so izvedli tako analitične kot numerične simulacije “particle-in-cell”(PIC) (”delec v celici”) s plazmami končne $\varepsilon (= \lambda_D/L)$, ki so potrdile rezultate Kuhna et al. za “mrzlo” porazdelitev hitrosti ionov ($T_i \ll T_e$). Vendar so analitični rezultati, dobljeni za mrzle vire ionov, le omejene pomembnosti za fuzijske plazme.

Z namenom, da se razširi veljavnost Tonksovega in Langmuirovega modela na primer končne temperature ionskega vira, sta Bissell in Johnson [10] leta 1987 razvila primernejši model. Vendar njuna rešitev v modelu ni dovolj zanesljiva, saj preneha veljati za majhne temperature ionski virov, kar je posledica aproksimacije jedra v integralni enačbi. Dodatno sta Bissell in Johnson predpostavila robni pogoj *v naprej* in temelji na t.i. “posplošenem robnem Bohmovem kriteriju”. Ta predpostavka je bila pred kratkim eksplicitno ovržena za vse primere (glej Riemann [53] in sklicevanja v članku).

Po drugi strani sta Scheuer in Emmert [61] leta 1988 uporabila boljši približek jedra, ki je razširil veljavnost Bissllovega in Johnsonovega modela za nižje temperature ionskih virov, in tako dosegla dobro ujemanje prvotnega Tonksovega in Langmuirovega modela. Dodatno pa nista vnaprej predpostavila meje predplašča, temveč sta ga določila ’a posteriori.’

Vendar zaradi *aproksimacij jedra* obe rešitvi ostajata omejeni na nizke ali visoke temperature. V pričujočem delu predstavljamo način, kako dobiti rezultate za poljubno T_n/T_e v širokem območju temperatur. To je izvedeno z vpeljavo točnega jedra v integralni enačbi in numeričnim reševanjem. Dodatno prikazujemo naše PIC simulacije kot visoko zanesljiv referenčni vir naših raziskav.

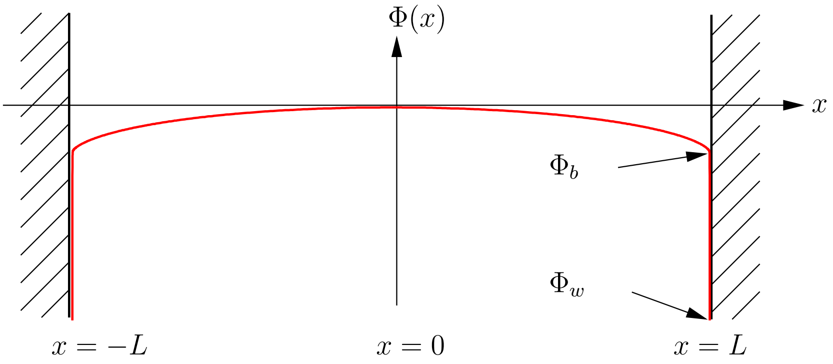

Slika C.1: Shematski prikaz nekolizijske razelektritvene analize v enodimenzionalno (ravninski) geometriji s potencialom $\Phi(x)$ po vzpostavitvi plaščev. Center plazme je na $x=0$, steni na $x=\pm L$.

Geometrija problema je simetrična enodimenzionalna planarno-vzporedna, kakor je prikazano na sliki C.1.

Za primer *"porazdelitve hitrosti mrzlega ionskega vira"* je bila končna temperatura izračunana analitično. Kot že omenjeno poprej, se izraz "mrzel" nanaša na primer, ko se ioni v plazmi "rojevajo" z zanemarljivo temperaturo v primerjavi s temperaturo elektronov. Ko se enkrat v modelu reši enačba predplašča plazme (v plašču se lokalizira močno električno polje), se reši tudi enačba v plašču z uporabo robnega pogoja, ki izhaja iz rešitve enačbe plazme.

Ob koncu prejšnjega stoletja so bili poskusi reševanja dvodelnega problema za primer *"porazdelitve hitrosti toplega vira ionov"*, tj. za primer, ko je temperatura vira ionov primerljiva s temperaturo pripadajočih elektronov. V takem primeru Fredholmove enačbe modela ni možno analitično rešiti, razen v primeru, da vnaprej predpišemo posebno obliko porazdelitve ionskega vira, za katerega je možen analitičen rezultat. Prvotna izpeljava fizikalnega problema v Bissllovem in Johnsonovem modelu [10] vodi v enačbo tipa

$$\exp\left((1+\frac{\tau}{2})\Phi\right) = B\int_0^{\Phi_b} \Psi(\Phi')\exp\left((1+\frac{\tau}{2})\Phi'\right)\mathrm{K}_0\left(\frac{\tau}{2}|\Phi-\Phi'|\right)d\Phi' \ , \tag{C.3}$$

kjer je $\Psi(\Phi)$ neznana funkcija, Φ_b potencial na robu predplašča in $\mathrm{K}_0(z)$ modificirana Besselova funkcija. To je integral Fredholmovega tipa prve vrste. Vendar celo v dvodelni aproksimaciji končne porazdelitve ionov ni bilo moč izračunati za poljubno temperaturo vira ionov, saj je bilo singularno jedro integralne enačbe neprimerno za numerične izračune. V doktorskem delu nameravamo rešiti to enačbo natančno, poleg tega pa rešiti razširjeni problem, ki smo ga formulirali, torej bolj “težaven” problem integro-diferencialne enačbe v obliki

$$\begin{aligned}\exp\left((1+\frac{\tau}{2})\Phi\right)&\left[1+\varepsilon^2\frac{\exp(-\Phi)}{\Psi^3(\Phi)}\frac{d^2\Psi(\Phi)}{d^2\Phi}\right]\\ = B\int_0^{\Phi_b} &\Psi(\Phi')\exp\left((1+\frac{\tau}{2})\Phi'\right)\mathrm{K}_0\left(\frac{\tau}{2}|\Phi'-\Phi|\right)d\Phi' \ ,\end{aligned} \tag{C.4}$$

ki je zasnovana na polni Poissonovi enačbi namesto na pogoju kvazi-nevtralnosti. Ta integro-diferencialna enačba se lahko šteje kot posplošitev enačb Fredholmovega tipa, ki ni ne prve ne druge vrste, marveč je očitno nelinearna in v literaturi ni klasificirana.

V zgornjih enačbah je B lastna vrednost problema, medtem ko sta ε in τ prosta parametra.

C.1.1 Motivacija in namen disertacije

Avtor je bil dolgo časa vključen v izkoriščanje paralelnih računalniških kapacitet povezanih s fuzijskimi raziskavami z namenom optimizacije Evropskih računalniških virov. Njegovo sodelovanje v projektu EUFORIA [42, 28] je zahtevalo poglobljeno vključevanje pri preizkušanju nekaterih zahtevnih problemov v plazmi. Ker je bila Bissllova in Johnsonova enačba [10] za ta namen velik izziv, je začel razvijati svoje programske pakete za rešitev problema. Tako pričakujemo, da bo pričujoča disertacija pomembno prispevala k fuzijski skupnosti z nadgradnjo obstoječih rezultatov.

Rešitev zgoraj predstavljenega problema ima velik pomen za fuzijo in splošno plazmo. Pri uporabi fluidnih kod, kot sta npr. SOLPS [15] in EDGE-

2D, namenjena za simulacije v področju *Scrape-Off Layer* (SOL) [18] TOKAMAK [64] naprav, je namreč potrebno določiti meje računskega območja. Robnih pogojev se na osnovi teorije fluidov ne da določiti natančno, saj je potrebno uporabiti še kinetično teorijo. Rezultati iz kinetične teorije, ki predpostavlja toplo ionsko populacijo, pa zahtevajo obsežne računske vire.

Raziskava problemov na obstoječih modelih je pokazala, da vpeljane aproksimacije niso dovolj natančne in da modeli izkazujejo nekoliko različne rezultate.

Raziskave v disertaciji so usmerjene na dosego naslednjih ciljev:

- Jedro ne sme biti aproksimirano, temveč računano neposredno z uporabo splošnih programskih paketov.
- Mreža za izračun profila potenciala mora biti zgoščena ne samo ob steni, temveč tudi v središču simetrije tako, da se bo uporabila adaptivna metoda integracije.
- Osnovne hidrodinamične količine, kot so ionska gostota, ionski fluks, ionska energija in temperatura, se morajo izpeljati neposredno iz porazdelitve hitrosti na mreži, ki mora biti samoadaptivna v bližini singularnosti jedra integrala kot tudi v bližini singularnosti električnega polja oz. inverzne vrednosti.
- Obstoječi modeli bodo razširjeni s t.i. končnim "finite-$\varepsilon \equiv \lambda_D/L$", da kvazinevtralnost ni striktno zagotovljena, temveč se uporablja kompletna Poissonova enačba namesto pogoja kvazinevtralnosti.
- Za dokaz se bosta izvedla dva izračuna, in sicer v širokem spektru ionskih temperatur z upoštevanjem končne vrednosti ε in $\varepsilon = 0$

Hipoteza. Problem specialnega tipa Fredholmove integralno diferencialne enačbe je potrebno reševati numerično, brez aproksimacij, da bi lahko dobili razširjeno območje rešitev, ki so primerne za aplikacijo v fuzijsko in splošno relevantnih plazmah za poljubno ionsko temperaturo in poljubne širine plazemskega plašča.

C.1.2 Pregled disertacije

V disertaciji so predstavljene raziskave in rešitve, ki temeljijo na naslednjih predpostavkah:

- Poissonova enačba je postavljena za celotno območje razelektritve.
- Dvodelna aproksimacija je dosežena v limiti neskončno majhne Debyjeve dolžine v primerjavi z dolžino sistema, temperatura vira ionov ima lahko poljubno vrednost.
- Temperatura vira ionov ima lahko poljubno vrednost.
- Ionizacijski mehanizem je lahko poljuben.

Poglavje 2 predstavlja fizikalne in teoretične osnove plazme in njeno modeliranje. Relevantni nekolizijski modeli in njihove omejitve so razloženi v poglavju 3. Razširitev temperaturnega območja za vroče vire ionov z našo analitično–numerično metodo je predstavljena v poglavju 4. Posplošitev obstoječih teoretičnih modelov na končne Debyjeve dolžine in razširitev naše analitično-numerične metode je razdelana v poglavju 5. Rezultati dobljeni z našo analitično-numerično metodo in naše referenčne PIC simulacije so predstavljene v poglavju 6. Zaključki z diskusijo so podani v poglavju 7. Pomožni podatki, ki pomagajo bralcu ali uporabniku naše kode, so podani v dodatkih.

C.2 Izvleček vsebine

C.2.1 Fizikalno ozadje problema

Plazma je kvazinevtralen plin z nabitimi in nevtralnimi delci, ki izkazujejo kolektivno vedenje [17]. Plazmo lahko predstavimo z različnimi teoretičnimi pristopi, ki karakterizirajo različne pojave v plazmi. Takšni modeli so:

- Aproksimacija gibanja posameznih delcev.
- Fluidne aproksimacije.
- Kinetični popisi plazme.

Gibanje posameznih delcev lahko aproksimiramo v redko ioniziranih plinih, tako da spremljamo posamezne delce brez medsebojne interakcije. Kinetična aproksimacija se lahko uporablja v računalniških simulacijah (PIC), ki iterativno izračunavajo položaj vseh delcev v konsistentnem električnem ali magnetnem polju, izhajajoč iz položaja in hitrosti delcev. Tak pristop je zelo drag, saj vključuje mnoge tehnične omejitve, ki izhajajo iz simultanega reševanja mnogih Newtonovih enačb skupaj z Maxwellovimi enačbami. Zato je razvoj analitično-numerične metode, ki rešuje problem brez poglabljanja v gibanje posameznega delca, zelo pomembna.

Kinetična Boltzmannova enačba je podana kot

$$v\frac{\partial f_i}{\partial x} - \frac{e}{m_i}\frac{d\Phi}{dx}\frac{\partial f_i}{\partial v} = S_i(x,v) \ , \tag{C.5}$$

kjer je vir ionov $S_i(x,v)$ na desni strani zapletena funkcija, ki popisuje relevantno mikroskopsko fiziko v modelu s koordinato x, hitrostjo v, elementarnim pozitivnim nabojem e, maso iona m_i in elektrostatičnim nabojem $\Phi(x)$ v odvisnosti od položaja x. Formalno rešitev Boltzmannove diferencialne enačbe lahko najdemo z metodo karakteristik. Ko je po rešitvi enačbe (C.5) profil potenciala $\Phi(x)$ znan, lahko s t.i.metodo trajektorij (razdelek 2.4), določimo porazdelitev hitrosti ionov f_i (VDF) in izpeljane višje momente kot so: ionska gostota

$$n_i(\Phi(x)) = \int_{-\infty}^{\infty} f_i(v)dv \ , \tag{C.6}$$

ionski tok

$$\Gamma_i(\Phi(x)) = \int_{-\infty}^{\infty} vf_i(v)dv \ , \tag{C.7}$$

skupna energija ionov

$$K_i(\Phi(x))) = \frac{1}{n_i(\Phi)}\int_{-\infty}^{\infty} v^2 f_i(v)dv \ , \tag{C.8}$$

smerna hitrost ionov

$$u_i(\Phi(x)) = \frac{1}{n_i(\Phi)}\Gamma_i(\Phi) \ , \tag{C.9}$$

in temperatura

$$T_i(\Phi(x)) = K_i(\Phi) - u_i^2(\Phi) \ , \tag{C.10}$$

kot ena najpomembnejših količin na katerem koli mestu $x(\Phi)$.

Po drugi strani pa Poissonova enačba podaja

$$-\frac{d^2\Phi}{dx^2} = \frac{e}{\varepsilon_0}(n_i - n_e) \ , \tag{C.11}$$

kjer je ε_0 dielektrična konstanta vakuuma, in n_i je gostota ionov ter n_e gostota elektronov. Ob pogoju kvazinevtralnosti, ko sta gostoti $n_i \simeq n_e$ enaki lahko Poissonovo enačbo zanemarimo, kar je bilo upoštevano kot poenostavitev v večini dosedanjih analtično-numeričnih modelih.

C.2.2 Pregled stanja in obstoječih modelov

Problem nekolizijskih razelektritev je bil formuliran kot kvazinevtralen plazemski pogoj z znano maxwellovsko obliko porazdelitve hitrosti vira ionov pri neznani končni ionski porazdelitvi hitrosti. Osnovna naloga je iskanje ionske porazdelitve hitrosti v področju kvazinevtralne plazme ob predpostavki infinitezimalno tankega plašča na meji plazme. Razširjena naloga, ki doslej še ni bila rešena, je analogni problem. Osnovni pogoj je, da ima plazemski plašč končno debelino.

To pomeni podrobno reševanje Poissonove enačbe namesto uporabe pogoja kvazinevtralnosti. Matematična formulacija fizikalnega problema se prevede v reševanje integro-diferencialne enačbe Fredholmovega tipa. Za primer "porazdelitve hitrosti hladnega ionskega vira" je bila porazdelitev hitrosti izračunana analitično [70]. Izraz "hladen" se nanaša na primer, ko se ioni v plazmi rojevajo z zanemarljivo temperaturo v primerjavi s temperaturo elektronov. Za primer "porazdelitve hitrosti toplega ionskega vira" pa Fredholmova enačba ni rešljiva razen v primeru, da se vnaprej predpostavi posebna oblika porazdelitve ionskega vira (jedro), ki vodi v analitični rezultat.

Aproksimacijo jedra in enačbe plazme s polinomsko vrsto sta prva izvedla Bissell in Johnson [10], katerih rešitev je bila dobljena v omejenem rangu temperatur ionskega vira. Sheuer in Emmert [61] (S&E) sta uporabila diskretizacijski pristop z aproksimacijo jedra, ki ga je mogoče analitično integrirati po conah in nato uporabiti iterativno numerični postpek. Vseeno S&E rešitev ostaja znotraj omejenega ranga temperatur ionskega vira. Obe metodi z različnima pristopoma izkazujeta (v nasprotju s svojo trditvijo) različne rezultate, iz katerih ni mogoče z gotovostjo postaviti zaključkov v bližini plašča.

Kuhn et al. [40] in Jelić et al. [32] so nedavno razvili koncept politropičnega koeficienta in pokazali, da je njegova maksimalna vrednost povezana z mejo plazme v primeru plazem hladnega ionskega vira. Njihovi rezultati še niso bili aplicirani za primer toplega ionskega vira, ker za zdaj še ne obstaja zadovoljiva rešitev plašča plazme za ta primer.

Riemann [48, 49, 50, 52, 53] razvija teorijo vmesnega področja z namenom povezave med plaščem in plazmo. Prav tako je ta pristop omejen na modele hladnih ionov z željo razširitve na polno rešitev s končnimi Debyjevimi dolžinami oz. s podrobnim reševanjem Poissonove enačbe namesto uporabe pogoja kvazinevtralnosti.

Skupina raziskovalcev na Berkeleyju se ukvarja z reševanjem plazemskih problemov v različnih geometrijah z uporabo njihovih PIC ("Particle In Cell") simulacijskih kod [77, 43, 76]. Skupina v Innsbrucku prav tako uporablja svoje verzije berkeleyjskih kod, ki se aplicirajo v bližini divertorja z zahtevno fiziko, izvedeno v njihovi kodi BIT1 [73, 74, 71]. Tako primerjajo PIC simulacije z numeričnimi rezultati, da s tem dobijo ustrezno povezavo med simulacijskim eksperimentom in numerično računskimi napovedmi. Primerjava bo torej možna takrat, ko bodo sploh na voljo zadovoljive računske napovedi, kar je bil tudi namen te disertacije.

C.2.3 Analitično numerična metoda

V našem delu smo sledili pristopu S&E, vendar smo ga še dodatno izpolnili z

- vpeljavo točnega jedra,
- z boljšo ločljivostjo računske mreže,
- z vpeljavo zgoščevanja mreže v centru in na mestu neskončnega potencial električnega polja,
- z vpeljavo dodatnih stabilizacijski pristopov za izboljšavo konvergence.

C.2.4 Razširitev teoretičnega modela

Osnovni analitični model, zasnovan na Bissllovem in Johnsonovem modelu smo z novim pristopom razširili z upoštevanjem Poissonove enačbe (C.11), ki v normaliziranih koordinatah vpeljuje relativno debelino plazemskega plašča $\varepsilon = \lambda_D/L$ in razširjeno enačbo

$$\begin{aligned} &B\int_0^1 dx' \exp\left[\Phi(x')-\Phi(x)\right]\exp\left[\frac{\mathcal{T}}{2}\{\Phi(x')-\Phi(x)\}\right]\mathrm{K}_0\left\{\frac{\mathcal{T}}{2}|\Phi(x')-\Phi(x)|\right\} \\ &= 1-\varepsilon^2\exp(-\Phi)\frac{d^2\Phi}{dx^2} \end{aligned}, \tag{C.12}$$

ki je ne moremo več okarakterizirati kot Fredholmovo ali Hammesteinovo integro-diferencialno enačbo. Reševanje te enačbe smo se lotili s posplošitvijo naše analitično-numerične metode, ki je bila najprej razvita za $\varepsilon = 0$.

C.2.5 Rezultati

V poglavju 5 in 6 so predstavljeni rezultati, ki so bili izpeljani iz rešitve enačbe plazme (C.12) tako za $\varepsilon = 0$ kot za posplošeno rešitev $\varepsilon > 0$.

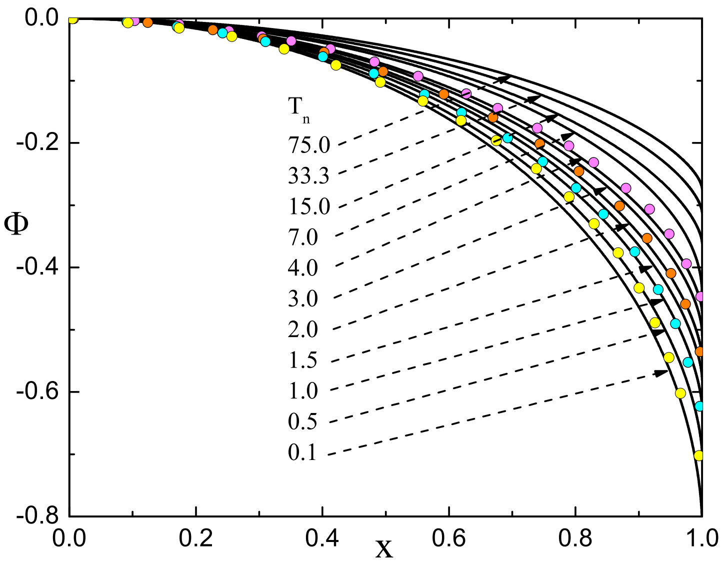

Slika C.2: Profili potencialov v razširjenem območju temperatur ionskih virov, kot smo jih izračunali z našo analitično-numerično metodo (polne črte) v primerjavi z ozkim območjem Bissllovega in Johnsonovega modela (pikčasto).

Rešitev enačbe (C.12) za primer $\varepsilon = 0$ prikazuje slika C.2. Primerjave profilov potencialov z B&J in S&E modelom so pokazale dobro ujemanje v območjih, kjer so le-ti veljavni. Profil potenciala predstavlja "prstni odtis" za vse nadaljnje izračune pomembnih količin v fiziki plazme.

Za limitni primer $T_n = 0$ je na voljo analitična rešitev v točki $\Phi_s = -0.854$. S primerjavo z Riemannovnim programom smo na primeru občutljive izpeljane količine, kot je temperatura ionov, pokazali, da je mogoče z našo metodo trajektorij iz profila potenciala izračunati singularne porazdelitve hitrosti ionov (slika 6.4), ki z integracijo vodijo v dovolj točne izpeljane količine na poljubnem mestu $x(\Phi)$.

S primerjavo rezultatov Riemannovega programa, ki je omejen na $T_n = 0$, vendar omogoča $\varepsilon \geq 0$, smo našli povezavo med lastno vrednostjo sistema B in dolžino predplašča x_s. V poglavju 5 renormalizirane profile potencialov za različne ε tudi primerjali (slika 6.16 in 6.17). Empirično smo razširili Harrisonov in Thompsonov model na poljubne temperature ionskih virov, kar je pomembno za aplikacijo teorije vmesne plasti med plazmo in plaščem, ki je bila zaradi nepoznavanja ionizacijske dolžine doslej omejena le na primer "mrzlih" virov ionov.

C.3 Sklepi

V disertaciji smo uporabili numerični pristop Scheuerja in Emmerta [61] za razširitev Bissllovega in Johnsonovega modela [10] na poljubne temperature ionskega vira. S&E pristop je še vedno omejen na nizke temperature ionskih virov zaradi omejitev v aproksimaciji jedra. Zato smo vpeljali natančno jedro in hkrati povečali ločljivost in gostoto mreže in z dodatnimi stabilizacijskimi ukrepi izboljšali konvergenco. Za potrditev numerične stabilnosti in natančnosti so bili rezultati preverjeni v Mathematici in v naši programski kodi, ki so izkazali odlično ujemanje v vseh numeričnih rezultatih. S fizikalnega stališča smo ugotovili, da je končna ionska temperatura veliko manjša od temperature ionskega vira. Ta ugotovitev je zelo pomembna v fuzijskih napravah, kjer ioni prehajajo iz jedra (CORE) v področje SOL, kjer se ob približevanju divertorjem na hitro ohladijo. Kot najpomembnejše smo našli mejo plazme x_s kot funkcijo temperature ionskih virov. Pokazali smo, da v plazmah s končno temperaturo ionskih virov maksimum politropičnega koeficienta ne sovpada z robom plašča plazme, kot je to praviloma pri plazmah z zanemarljivo majhnimi temeraturami ionskih virov, vendar jih lahko še vedno obravnavamo kot dober približek za mejo med plazmo in plaščem. To dejstvo je lahko pomembno pri povezovanju fluidnih in kinetičnih parametrov plazme v fluidnih kodah, kot je npr. SOLPS-B2 (glej npr. Lit. [15]).

Potrebno je poudariti, da so naši rezultati striktno veljavni samo do prelomne točke kvazinevtralnosti. Za rešitev, ki velja za celoten sistem, je bilo treba vpeljati vpliv električnega polja, tj.polno Poissonovo enačbo namesto predpostavke o kvazinevtralnosti. Tak pristop vodi do integro-diferencialne enačbe, ki smo jo izpeljali v naslednji obliki

$$\frac{1}{B} = \frac{1}{1 - \exp(-\Phi)\varepsilon^2 \dfrac{d^2\Phi}{dx^2}} \int\limits_0^1 \exp\left[(1 + \frac{1}{2T_n}(\Phi' - \Phi)\right] \mathrm{K}_0 \left[\frac{1}{2T_n}|\Phi' - \Phi|\right] dx' \ . \tag{C.13}$$

Za reševanje le-te smo izdelali novo kodo, ki razširja naš prvotni model za $\varepsilon = 0$ na poljubne Debyjeve dolžine.

Za primer, ko je $\varepsilon > 0$, naše raziskave obsegajo široko območje temperatur ionskih virov in za široko območje ε. To je prva taka raziskava z uporabo analitično-numerične metode. Druge metode predpostavljajo vključevanje PIC metod (glej npr. Krek. et al. [34]). Naš glavni rezultat za $\varepsilon > 0$ kaže, da z rastočo temperaturo (npr. nad $T_i, src \equiv T_n \sim 1$) profili potenciala v normaliziranih in renormaliziranih koordinatah niso izrazito odvisni od ε. Problem vmesnega področja med plaščem in plazmo, kot je to podano z Riemannovimi pravili za končne temperature ionskih virov v enačbi (6.5), se zdi v tem, da postaja nepomemben vsaj v fuzijskih plazmah.

Po drugi strani pa je za dovolj nizke temperature ionskih virov tudi sicer na voljo drugačno skaliranje [Enačba (6.4)], ki ga je Riemann temeljito razdelal. Naše predpostavke o pomembnosti ε za visoke temperature ionskih virov bodo podrobneje razdelane v našem nadaljnjem delu tako za maxwellovske kot tudi za *Water-Bag* porazdelitve. Glede vpliva drugega odvoda potenciala sklepamo, da z naraščajočo temperaturo ionskega vira rezultati postajajo vse bolj neobčutljivi na ε. To je lahko tudi osnova nadaljnjih raziskav za pravilno definicijo plazemskega plašča ne glede na izbrano metodo.

Naš pristop je nov z več pogledov. Najprej smo s PIC simulacijami pridobili visoko zanesljive profile potencialov in porazdelitve hitrosti ionov, ki doslej še niso bile narejene za Tonksov in Langmuirov model s končnimi temperaturami ionskih virov in končnimi ε. Kvantitativna primerjava osnovne količine, tj. profila potencialov, kaže dobro ujemanje z rezultati Bisslla in Johnsona v območju veljavnosti njunega modela. Novi rezultati, dobljeni zunaj ranga, so prav tako predstavljeni skupaj z izpeljanimi količinami.

C.3.1 Prispevki k znanosti

Prispevke disertacije lahko strnemo v:

1. Bissllov in Johnsonov model je razširjen v t.i. “končni-$\varepsilon \equiv \lambda_D/L$” primer. To pomeni, da striktna kvazinevtralnost ni striktno zagotovljena, razen za primer, ko je ε natančno nič. Jedro v našem pristopu ni aproksimirano, marveč natančno računano. Stopnja “natančnosti” je seveda odvisna od uporabljene programske knjižnice. Mreža za izračun profila potenciala je zgoščena na steni kot tudi v središču simetrije problema.

2. Osnovne hidrodinamične količine, kot so ionska gostota, iztok, smerna energija in temperatura, so izračunane neposredno iz porazdelitve hitrosti na mreži, ki je samoadaptivna v bližini singularnosti električnega polja oz. njegove inverzne vrednosti.

3. Našo analitično-numerično metodo smo razširili na primer končnega ε za primerjavo s simulacijami PIC, ki so primerne za simulacijo realnih sistemov brez predhodne delitve problema na plazmo in plašč. Prikazali smo dve vrsti rezultatov: za širok spekter temperatur ionskih virov $(0.01 < T_n/T_e < 100)$ z $\varepsilon = 0$ in za več temperatur $(0.01 < T_n/T_e < 100)$ s končnim ε $(\varepsilon = \{10^{-5}, 10^{-3}, 0.01, 0.1\})$.

4. Z naraščajočo temperaturo ionov postaja odvisnost profila potenciala od ε vse manjša.

Prispevki disertacije so bili objavljeni tudi v [39, 38, 37, 42, 28, 33].

Vita

Leon Kos was born in Postojna, Slovenia, on June 9, 1966. He graduated from Ljubljana University in 1991 with a Bachelor degree in Mechanical Engineering. He earned a Master of Science degree in Mechanical Engineering at Ljubljana University in 1995. During his graduate program he worked as an assistant and researcher at the CAD laboratory at the Ljubljana Faculty of Mechanical Engineering, where he participated in many research and industrial projects.

Leon Kos se je rodil 9.6.1966 v Postojni. Diplomiral je leta 1991 na Fakulteti za strojništvo Univerze v Ljubljani. Po končani diplomi se je zaposlil na Fakulteti za strojništvo Univerze v Ljubljani, v laboratoriju za računalniško podprto konstruiranje, kjer je leta 1995 pridobil magisterij. Med podiplomskim študijem na fakulteti je sodeloval v mnogih raziskovalnih in industrijskih projektih.

Author's statement

The present Doctoral Thesis, or Dissertation, is an extended written treatise that presents original results and interpretations of a unique investigation by the degree candidate under the supervision of his mentor prof. dr. Jožef Duhovnik and his co-mentor prof. dr. Siegbert Kuhn.

Izjava

Doktorsko delo predstavlja rezultate lastnega znanstveno-raziskovalnega dela na osnovi sodelovanja z mentorjem prof. dr. Jožefom Duhovnikom in somentorjem prof. dr. Siegbertom Kuhnom.

Leon Kos